THE REGULATION OF MICROTUBULE DYNAMICS BY +TIPS AND CROSS-LINKING PROTEINS

Rebecca Cressey Adikes

A dissertation submitted to the faculty at the University of North Carolina at Chapel Hill in partial fulfillment of the requirements for the degree of Doctor of Philosophy in the Biology Department.

Chapel Hill
2018

Approved by:

Kerry Bloom

Bob Goldstein

Paul Maddox

Elizabeth Shank

Kevin C. Slep

ABSTRACT

Rebecca Cressey Adikes: The regulation of microtubule dynamics by
+TIPs and cross-linking proteins
(Under the supervision of Kevin C. Slep)

The dynamic cytoskeleton is composed of distinct filamentous polymer networks. These polymers create highly dynamic scaffolds for many cellular processes in eukaryotes. The polymers provide tracks for cargo transport, mechanically stabilize the cell, establish cell polarity, and are central components of the force-generating machinery required for cell division. In order to perform these various cellular tasks the polymers undergo spatially and temporally regulated assembly and disassembly. Understanding the spatial and temporal regulation of these cellular polymers is essential to understanding cell function.

Here, we investigate the spatial and temporal regulation of two polymer networks in cells, the microtubule (MT) and F-actin networks. We developed and employed methods to alter protein targeting and localization using a novel optogenetic approach and a classical structural/functional approach to understand how the recruitment of effectors of these networks alters network dynamics.

We developed and employed an optogenetic tool to gain insight into the msec/sec resolution time regime of MT-F-actin cross-linking. This allowed us to uncover key immediate downstream cellular events of cross-linking including decreased MT comet velocities on the sec time scale and an exclusion of MT from the cell periphery on the min-hr time scale. Additionally, using more classical structure/function based experiments, we were able to alter

protein targeting using protein domains and through mutation of the protein sequence by just 1-amino acids. This enabled us to uncover that the XMAP215 family member Msps contains a very specific mechanism to allow for MT plus end targeting and thus proper function of the full-length molecule. These results highlight the importance of precise protein positioning and interactions with binding partners to regulate cytoskeletal dynamic.

ACKNOWLEDGMENTS

My years as a graduate student have been a journey and I have learned a lot! I would like to thank everyone who made it possible for me to get to where I am today.

First, I would like to thank my advisor, Kevin Slep, who provided me with some challenging and very exciting projects. Thank you for believing that I could be successful with them especially when I thought I was not making progress. Thank you for giving me so much freedom to find my way.

Thank you to the all the Slep lab members past and present. To Jamie Fox who helped me get started. To Karen Plevock Haase for being an amazing friend; late nights in lab with music blaring, drinking hazelnut lattés and discussing all things cell biology while trying to do four experiments simultaneously will always be some of my favorite grad school memories. To Alka Das for sharing all your cloning *magic*, answering so many questions, and being such a hard working, patient and positive person. To Tom Lane for being a wonderful listener and always willing to help in any way you could. To all the Slep lab undergrads, for your dedication, hard work, positive energy and excitement, I would never have made it without you! To Tanner Fadero, for being the best first undergraduate a grad student could have. To Brian Saway for kicking the TOG6 project into gear! To Angela Xue for working so hard, always with a huge smile on your face. To Sofia Corella, for your dedication and persistence. To both Sofia and Angela, for our talks in lab and over dinner. To Sofia and April for a day neither of you probably remember but helped me to keep going when it was hard.

Thank you to my committee members for your support and insightful ideas. To the

Maddox labs for allowing me to be a part of lab meetings and lab events, I learned so much from all of you and made wonderful friends! I would like to acknowledge the larger Cytoskeleton Community (UNC, The Triangle and ASCB) for your inspiration, wonderful science, amazing conversations and advice.

I would like to thank all my previous mentors, especially Omar Quintero my first research advisor. Thank you for being there for me every step of the way.

Thank you to all my friends who I met over the past six years (UNC and embryo2017) who made grad school a bit more fun, and bit less serious and who let me just be me.

Thank you to all my family, for being so supportive even though you sometimes didn't get why I was still in school. To my parents who always reminded me of my deadlines, and that I could get the things that I wanted to get done done, despite what I perceived as obstacles.

PREFACE

The second chapter of this thesis was published in the Journal of Cell Biology in January 2018 with Dr. Ryan Hallett as second author. Dr. Hallett helped with the original design concept for the SxIP-iLID system. Brian Saway, the third author, was a UNC undergraduate research under my supervision who performed some of the original SxIP-iLID imaging experiments (Figure 2.1C) and performed much of the eGFP comet tracking data reported in Figure 2.1F.

The third chapter is currently in preparation for submission. This chapter was a collaborative effort with two UNC undergraduate researchers under my supervision. Brian Saway, became interested in this project and asked 'What will happen if we delete the predicted TOG 6 domain?' He cloned FL Msps lacking the predicted TOG 6 and performed the experiments and some of the data analysis for Figure 3.1, Figure 3.4, and Figure 3.6. Angela Xue was interested in understanding the structure of TOG6 and what residues conferred localization of the FL molecule and how this domain regulated localization. Angela purified TOG6 and all mutant forms of TOG6; she assisted in the experiments and analyzing the data presented in Figure 3.5. Angela performed the experiments, collected and analyzed the data and generated the figures for Figure 3.8, Figure 3.9, Supplemental Figure 3.1, Supplemental Figure 3.3 and Supplemental Figure 3.4.

TABLE OF CONTENTS

LIST OF TABLES

LIST OF FIGURES

LIST OF ABBREVIATIONS AND SYMBOLS

°C	Celsius degree
α	alpha
β	beta
βME	2-Mercaptoethanol
aa	amino acid
ACF7	Actin Cross-linking Factor 7
AMP	Ampicillin
bp	base pair
BSA	Bovine Serum Albumin
CAP	cytoskeleton-associated protein
CH	Calponin Homology
ch-TOG	colonic, hepatic tumor overexpressed gene
CD	Circular Dichrosim
CLASP	Cytoplasmic linker associated protein
ConA	conconavlin A
CTD	C-terminal Domain
DAPI	4',6-diamidino-2-phénylindole
DNA	DeoxyriboNucleic Acid
DTACC	Drosophila Transforming Acidic Coiled Coil
dsRNA	double stranded RiboNucleic Acid

EB	End Binding
EBH	EB-homology
GAR	Gas2-related
GCN4	General control protein 4
GDP	Guanosine DiPhosphate
GDP.P_i	Guanosine DiPhosphate.Phosphate
GFP	Green Fluorescent Protein
GSR	Glycine-Serine-Arginine rich
GTP	Guanosine TriPhosphate
GTPases	Guanosine TriPhosphate enzymes
HEAT	Huntington, elongation factor 2, phosphate A2, and TOR PI-3 kinase
iLID	improved Light Inducible Dimer
IPTG	Isopropyl β-D-1-thiogalactopyranoside
KAN	Kanamycin
kDa	kiloDalton
L	Liter
LID	Light Inducible Dimer
LOV	Light Oxygen Voltage
LZ	Leucine Zipper
MACF2	microtubule actin crosslinking factor 2
MAPs	microtubule associated protein
msps	minispindles
MT	microtubules

mg/ml	milligram per milliliter
ml	milliliters
mW	milliWatts
MW	Molecular Weight
NA	Numerical Aperture
NES	Nuclear Exclusion Signal
ng	nanogram
nm	nanometer
+TIPs	plus end interacting proteins
P	P value
PACT	pericentrin-AKAP-450 centrosomal targeting
PBS	Phosphate Buffer Saline
PBST	Phosphate Buffer Saline Tween
PCR	Polymerase Chain Reaction
PDZ	post synaptic density protein (PSD95), Drosophila disc large tumor suppressor (Dlg1), and zonula occludens-1 protein (zo-1)
RT	Room Temperature
SxIP	Serine-x-Isolecuine-Proline
TACC	Transforming Acidic Coiled Coil
tgRFP	tag Red Fluorescent Protein
TIRF	Total Internal Reflection Fluoresence
TOG	Tumor Overexpressed Gene
TULIP	TUnable Light-controlled Interacting Protein

XKCM1	Xenopus Kinesin
XMAP215	Xenopus Microtubule Assocoited Protein of 215 kDa
Zyg-9	Zygote
μg/ml	micrograms per milliliter
µm	micron
μm^2	micro meter squared

CHAPTER 1: INTRODUCTION

1.1 The dynamic cytoskeleton

The dynamic cytoskeleton is composed of multiple distinct filamentous polymer networks. These polymers create highly dynamic scaffolds for many cellular processes in eukaryotes. The dynamics of polymer assembly and disassembly are under tight spatial and temporal regulation, facilitating their involvement in many cellular processes. The polymers provide tracks for cargo transport, mechanically stabilize the cell, establish cell polarity, and are central components of the force-generating machinery required for cell division. The coordination of these dynamic networks is fundamental to orchestrating cellular functions such as cell migration, invasion, adhesion, and division. Cells divide, migrate, adhere, and invade many times throughout organismal development as well as in disease states. Understanding the spatial and temporal regulation of these the cytoskeleton polymers is essential to understanding cell function.

Actin and MTs are the two components of the dynamic cytoskeleton. Actin is composed of G-actin monomers that assemble to create helical F-actin filaments (Holmes et al., 1990; Oda et al., 2009; Fujii et al., 2010). Microtubules are composed of αβ-tubulin heterodimers. Approximately thirteen protofilaments interact laterally, assembling to create a hollow tube-like structure (Kirschner and Williams, 1974, Li et al., 2002). Both systems can undergo spontaneously assemble into filaments in the presence of nucleotide. This process is kinetically restrained and its efficiency increases with increase monomer concentration

(Voter and Erickson, 1984; Pollard et al., 1986; Pollard et al., 1990; Carlier et al., 1991; Fygenson et al., 1994, Sept and McCammon, 2001).

Assembly of the monomers of both actin and MTs in a head to tail fashion generates structurally polar filaments, and the difference in polymerization kinetics at each end of the filament results in structures that are polar with respect to assembly/disassembly dynamics. Inside the cell there are numerous proteins that regulate polymer assembly. Actin-biding proteins are key regulators of the assembly of actin monomers into filaments, while microtubule associated proteins (MAPs) regulate MT formation and dynamics.

1.1.1 Microtubules exhibit dynamic instability

Since the αβ-tubulin heterodimer is polar the MT is a polar filament, the β-subunit is exposed at the MT plus end, which is more dynamic and usually oriented toward the cell periphery whereas the α-subunit is exposed at the less dynamic minus end oriented toward the cells center and can be imbedded in the centrosome (Walker et al., 1988, Desai and Mitchison, 1997; Howard and Hyman, 2003). MTs undergo dynamic instability, the repaid switching between phases of polymerization and depolymerization at their ends. The switch from polymerization to depolymerization is termed catastrophe while the switch from depolymerization to polymerization is termed rescue. A MT end can also exist in a metastable pause state, where no addition or loss of tubulin heterodimers occurs (Mitchison and Kirschner, 1984, Cassimeris et al., 1988). During interphase dynamic instability is essential for the generation of a network to efficiently transport cargo and properly polarize the cell (Tanaka and Kirschner, 1991; Li and Gundersen, 2008). During mitosis dynamic instability allows for search and capture of chromosomes and their proper segregation (McIntosh et al., 2002). Although initially described in microtubules, other filament systems

also display dynamic instability, such as the bacterial actin ParM system (van den Ent et al., 2002). Rather than being a property of a particular type of filament (i.e. actin versus microtubules), instability dynamics are a property that emerges from the relative probabilities of assembly and disassembly.

Tubulin heterodimers are GTPases with two GTP binding sites, a non-exchange site on α –tubulin and an exchangeable site on β-tubulin (Weisenberg and Deery et al., 1976, Spiegelman et al., 1977, David-Pfeuty et al., 1977, MacNeal and Purich, 1978). MT polymerization-dependent GTP hydrolysis occurs as tubulin heterodimers are incorporated at the MT plus end. As subunits are added to the polymer, GTP bound at the β-tubulin site undergoes a stepwise transition from GTP to GDP.P_i to GDP, resulting in zones of tubulin bound to different nucleotide states along the MT lattice with the majority of the MT containing GDP-bound tubulin. GDP-bound tubulin is highly unstable, and thus if this region of the MT becomes exposed to the free ends of the filament, the MT will undergo rapid depolymerization (Carlier and Pantaloni, 1981; Mitchison and Kirschner, 1984; Chen and Hill, 1985; Kirschner and Mitchison, 1986; Carlier et al., 1989; Caplow, 1992; Caplow and Shanks, 1995; Walker et al., 1989).

While dynamic instability is an inherent property of microtubules, a host of cytoplasmic MAPs regulate MT dynamics in space and time. MAPs can alter the rates of MT nucleation, polymerization, depolymerization and transition between these states. MAPs also regulate filament length through MT severing, the availability of new free ends through severing, filament stability though binding, and introduction of post-translational modifications that further alter the properties of tubulin (Olmstead, 1986; Belmont and Mitchison, 1996; Sousa et al., 2007). MAPs can specifically bind to and alter dynamics the

MT minus end, lattice, or plus end. MAPs that interact specifically with the plus end are known as MT plus end tracking proteins (+TIPs) (Schuyler and Pellman, 2001; Akhmanova and Hoogenraad, 2005; Akhmanova and Steinmetz, 2008).

1.1.2 MT plus end protein complex: +TIP recruitment and interactions

+TIPs include the end binding protein (EB) family, EB interacting proteins such as Sentin/SLAIN1/2 and Spectraplakins, some kinesin family members, several kinetochore proteins, TOG domain containing protein families including Crescerin, CLASP and XMAP215, and most recently the TACC family. (Gard and Kirschner, 1987; Vasquez et al., 1994, Akhmanova et al., 2001; Mimori-Kiysoue et al., 2005; Slep et al., 2005; Varga et al., 2006; Slep and Vale, 2007, Lampert et al., 2010; van der Vaart et al., 2011; Li et al., 2011; van der Vaart et al., 2012; Gudimchuk et al., 2013; Nwagbara et al., 2014; Chen and Hancock, 2015, Gutiérrez-Caballero et al., 2015; Das et al., 2015; Lucaj et al., 2016; Rutherford et al., 2016). The impact that these proteins have alone and in concert on MT dynamics is an active area of investigation.

EB proteins can autonomously bind to the MT plus end, acting as major sites for the recruitment of a majority of other +TIPs to the MT plus end, and are required for generating dynamic MTs in vitro and in vivo (Rogers et al., 2002; Slep and Vale, 2007, Zhang et al., 2015). EB proteins contain an N-terminal calponin-homology (CH) tubulin-binding domain, central linker and a C-terminal globular domain (Gimona et al., 2002; Buey et al., 2001, Slep and Vale, 2007). The C-terminal domain contains the EB-homology domain (EBH) comprised of a coiled-coil dimerization domain and a four-helix bundle and an acidic EEY/F tail (Slep et al., 2005; Slep and Vale, 2007; Akhmanova et al., 2008). EB proteins usually exist as dimers, and can homo- and heterodimerize through EBH domain interactions

(Honnappa et al., 2005; Slep et al., 2005; De Groot et al., 2010; Sen et al., 2013).

The CH domains of EB proteins specifically bind at the intersection of four tubulin heterodimers and recognize the GTP hydrolysis transition state / post-hydrolysis state of the MT lattice (Zanic et al., 2009: Maurer et al., 2011; Maurer et al., 2012; Guesdon et al., 2016). EB proteins recruit a host of other +TIPs to the MT plus end. Proteins containing cytoskeleton-associated protein (CAP) -Gly domains interact with the EEY/F residue of the tail of EB proteins (Honnappa et al., 2006; Weisbrich et al., 2007; Bjelic et al., 2012). The hydrophobic cavity of the EBH domain binds proteins containing a short linear Ser-X-Ile-Pro (SxIP) motif (Slep et al., 2007, Honnappa et al., 2009). SxIP motif containing proteins include the spectraplakin microtubule actin crosslinking factor 2 (MACF2) and Sentin/SLAIN1/2 (Slep et al., 2005; van der Vaart et al., 2011).

Proteins of the spectraplakin family, such as MACF2, typically contain two N-terminal calponin-homology (CH)-type F-actin binding domains, and a C-terminal MT-binding module consisting of an EF-Hand-Gas2-related (GAR) region, Gly-Ser-Arg rich (GSR) motifs, and an EB-binding Sx(I/L)P motif (Lee et al., 2000; Slep et al., 2005, Wu et al., 2008; Applewhite et al., 2010, Lane et al., 2017). This domain architecture allows proteins of the spectraplakin family to cross-link the F-actin and MT cytoskeletal networks through binding F-actin filaments at one end and the MT lattice or plus end at the other. Previous studies have shown that coordination between F-actin and MTs is important for cell migration, mitosis, and tissue morphogenesis. Spectraplakin loss of function leads to severe axon shortening and MT disorganization (Sanchez-Soriano et al., 2009). Mutations in the *Drosophila* actin-MT cross-linking protein Shot cause a variety of cellular and tissue defects including changes in actin-MT organization, cell-cell adhesion, and integrin mediated

epidermal attachments to muscle (Gregory and Brown, 1998; Walsh and Brown, 1998; Prokop et al., 1998; Strumpf and Volk 1998; Röper and Brown, 2003). Conditional knock out of the spectraplakin Actin Cross-linking Factor 7 (ACF7) in mice yields defects in cell migration (Wu et al., 2008, Goryunov et al., 2010). Although recent studies have proposed mechanisms for the regulation of spectraplakins (Wu et al., 2011; Kapur et al., 2012; Applewhite et al., 2013; Takács et al., 2017), the direct downstream cellular outputs of regulated cross-linking remain poorly understood.

Sentin/SLAIN are EB binding, SxIP motif containing +TIPs. Sentin has been shown to be specific to *Drosophlia,* contains a single SxIP-like motifs (TIGP) that binds EB proteins, and recruits XMAP215 to MT plus ends (Li et al., 2011). SLAIN is the functional mammalian homologue of Sentin, it contains four SxIP-like motifs and one distantly related motif, RSLP. These motifs are required for robust MT plus end binding (van der Vaart et al., 2011). Sentin interacts with the *Drosophila* XMAP215 family member, Msps, and SLAIN2 interacts with CLIP-170, CLASP and the mammalian XMAP215 family member ch-TOG. Furthermore, both Sentin and SLAIN2 recruit their respective XMAP215 family member to the plus end as depletion of Sentin/SLAIN2 EB1/2 comets showed little Msps/ch-TOG while Sentin/SLAIN2 could still be observed in Msps/ch-TOG depleted cells (Li et al., 2011, van der Vaart et al., 2011). Depletion of Sentin and SLAIN both decrease the number and length of EB positive comments and decrease MT growth velocities. The interaction between Sentin/SLAIN and Msps/ch-TOG occurs between the N-terminal region of Sentin/SLAIN and the C-terminal domain of Msps/ch-TOG (Li et al., 2011, van der Vaart et al., 2011).

1.1.3 The XMAP215 family promote MT polymerization

The XMAP215 family of proteins, which contains both Msps and ch-TOG, is highly

conserved and essential. XMAP215 family members localize to MT ends and accelerate MT assembly, promoting MT polymerization by directly binding tubulin dimers under high tubulin concentrations (Charrasse et al., 1998; Al-Bassam et al., 2006; Slep and Vale, 2007; Brouhard et al., 2008; Slep, 2009; Widlund et al., 2011). Additionally, it has been shown that XMAP215 can counter act the MT destabilizing activity of the MT depolymerase XKCM1 (Tournebize et al., 2000; Kinoshita et al., 2001). XMAP215 family members promote polymerization and drive bipolar spindle assembly using an N-terminal array of tumor over expressed gene (TOG) domains that bind to tubulin heterodimers. TOG domains contain tandem Huntington, elongation factor 2, phosphate A2, and TOR PI-3 kinase (HEAT) repeats with highly conserved intra-HEAT loops essential for interacting with tubulin (Al-Bassam et al., 2006; Slep and Vale, 2007; Ayaz et al., 2012). Studies of XMAP215 family members in multiple species (*S. pombe*, *C. elegans*, *Xenopus* egg extracts, *Drosophila* and HeLa cells) have shown that they play an essential role during interphase and mitosis, as their depletion leads to decreased MT growth rates, resulting in short spindles or defects in spindle architecture (Gard and Kirschner, 1987; Vasquez et al, 1994; Matthews et al., 1998; Cullen et al., 1999; Tournebize et al., 2000; Kosco et al., 2001; Gergely et al., 2003, Brittle and Ohkura et al., 2005; Kawamura and Wasteneys, 2008; Kronja et al., 2009; Cassimeris et al., 2009; Zanic et al., 2013). Members of the XMAP215 family contain a varying number of N-terminal TOG domains and the details of the structure and function of these domains has been well characterized (Al-Bassam et al., 2007; Slep and Vale, 2007; Ayaz et al., 2012; Fox et al, 2014; Howard et al., 2015; Byrnes and Slep, 2017). However, the structure and functional role of the C-terminal region (CTD) remains poorly understood. The CTD has been shown to interact with TACC family proteins, Sentin/SLAIN, clathrin, CLASP and in *S.*

Pombe Ndc80. These interactions are required for proper localization of XMAP215, proper interphase MT dynamics and network architecture, as well as proper spindle formation and dynamics (Lee et al., 2001; Bellanger and Gönczy, 2003; Le Bot et al., 2003; Srayko et al., 2003; Gergely et al., 2003; Li et al., 2011; van der Vaart et al., 2011; Hood et al., 2013; Mortuza et al., 2014; Trogden and Rogers 2015; Miller et al., 2016). We hypothesize that the structural elements of the conserved CTD of the XMAP215 family of proteins are responsible for regulating MT dynamics by properly localizing the full-length molecule to MT plus ends during mitosis and interphase.

Overall the field in interested in understanding the following: Is there a specific higher order to generation of plus end protein complexes? How are these complexes built and regulated to ensure the proper output of tubulin dynamics and cross-linking of cytoskeletal networks in different cell types, during different cellular events at different developmental stages?

Our work probes this regulation in two ways 1) through classic structure/function experiments and mutational analysis using minimal proteins domains to assess localization and function of key domains and residues conserved within those domains 2) through development of a novel tool to spatially and temporally target proteins to the MT plus ends allowing us to uncover spatiotemporal role of protein localization on MT dynamics.

Here we show that key conserved residues in the CTD of XMAP215 family member Msps target the protein to the MT plus end which is required to rescue interphase MT dynamics. Furthermore, we propose that these key residues are necessary for Msps:Sentin interaction. We developed a novel tool (SxIP-iLID) to target proteins to MT plus ends using blue light to regulate the interation between iLID domains and SspB motifs (Guntas et al.,

2015). We show that EB-binding SxIP motifs, appended to the iLID N-terminus, confer iLID with MT plus end tracking activity. When exposed to blue light, SxIP-iLID recruits SspB-tagged proteins to MT plus ends. We establish SxIP-iLID as a tool with broad utility that can be used to systematically study the mechanisms of MT regulators and MT associated proteins. Specifically, we show that optogenetically induced cross-linking of MT-plus ends and F-actin decreases MT growth velocities and prevents MTs from entering into the peripheral region of the cell.

REFERENCES

Akhmanova A, Hoogenraad CC. Microtubule plus-end-tracking proteins: mechanisms and functions. Current opinion in cell biology. 2005;17(1):47-54. doi: 10.1016/j.ceb.2004.11.001. PubMed PMID: 15661518.

Akhmanova A, Hoogenraad CC, Drabek K, Stepanova T, Dortland B, Verkerk T, et al. Clasps are CLIP-115 and -170 associating proteins involved in the regional regulation of microtubule dynamics in motile fibroblasts. Cell. 2001;104(6):923-35. PubMed PMID: 11290329.

Akhmanova A, Steinmetz MO. Tracking the ends: a dynamic protein network controls the fate of microtubule tips. Nature reviews Molecular cell biology. 2008;9(4):309-22. doi: 10.1038/nrm2369. PubMed PMID: 18322465.

Al-Bassam J, van Breugel M, Harrison SC, Hyman A. Stu2p binds tubulin and undergoes an open-to-closed conformational change. The Journal of cell biology. 2006;172(7):1009-22. doi: 10.1083/jcb.200511010. PubMed PMID: 16567500; PubMed Central PMCID: PMC2063759.

Applewhite DA, Grode KD, Duncan MC, Rogers SL. The actin-microtubule cross-linking activity of Drosophila Short stop is regulated by intramolecular inhibition. Molecular biology of the cell. 2013;24(18):2885-93. doi: 10.1091/mbc.E12-11-0798. PubMed PMID: 23885120; PubMed Central PMCID: PMC3771950.

Applewhite DA, Grode KD, Keller D, Zadeh AD, Slep KC, Rogers SL. The spectraplakin Short stop is an actin-microtubule cross-linker that contributes to organization of the microtubule network. Molecular biology of the cell. 2010;21(10):1714-24. doi: 10.1091/mbc.E10-01-0011. PubMed PMID: 20335501; PubMed Central PMCID: PMC2869377.

Ayaz P, Ye X, Huddleston P, Brautigam CA, Rice LM. A TOG:alphabeta-tubulin complex structure reveals conformation-based mechanisms for a microtubule polymerase. Science. 2012;337(6096):857-60. doi: 10.1126/science.1221698. PubMed PMID: 22904013; PubMed Central PMCID: PMC3734851.

Bellanger JM, Gonczy P. TAC-1 and ZYG-9 form a complex that promotes microtubule assembly in C. elegans embryos. Current biology : CB. 2003;13(17):1488-98. PubMed PMID: 12956950.

Belmont LD, Mitchison TJ. Identification of a protein that interacts with tubulin dimers and increases the catastrophe rate of microtubules. Cell. 1996;84(4):623-31. PubMed PMID: 8598048.

Bjelic S, De Groot CO, Scharer MA, Jaussi R, Bargsten K, Salzmann M, et al. Interaction of mammalian end binding proteins with CAP-Gly domains of CLIP-170 and p150(glued). Journal of structural biology. 2012;177(1):160-7. doi: 10.1016/j.jsb.2011.11.010. PubMed PMID: 22119847.

Brittle AL, Ohkura H. Mini spindles, the XMAP215 homologue, suppresses pausing of interphase microtubules in Drosophila. The EMBO journal. 2005;24(7):1387-96. doi: 10.1038/sj.emboj.7600629. PubMed PMID: 15775959; PubMed Central PMCID: PMC1142550.

Brouhard GJ, Stear JH, Noetzel TL, Al-Bassam J, Kinoshita K, Harrison SC, et al. XMAP215 is a processive microtubule polymerase. Cell. 2008;132(1):79-88. doi: 10.1016/j.cell.2007.11.043. PubMed PMID: 18191222; PubMed Central PMCID: PMC2311386.

Brown GA, Ginsberg PC, Harkaway RC. Prostatic adenocarcinoma diagnosed by prostate-specific antigen analysis of pleural fluid. Urologia internationalis. 1998;60(3):197-8. PubMed PMID: 9644796.

Buey RM, Sen I, Kortt O, Mohan R, Gfeller D, Veprintsev D, et al. Sequence determinants of a microtubule tip localization signal (MtLS). The Journal of biological chemistry. 2012;287(34):28227-42. doi: 10.1074/jbc.M112.373928. PubMed PMID: 22696216; PubMed Central PMCID: PMC3436528.

Byrnes AE, Slep KC. TOG-tubulin binding specificity promotes microtubule dynamics and mitotic spindle formation. The Journal of cell biology. 2017;216(6):1641-57. doi: 10.1083/jcb.201610090. PubMed PMID: 28512144; PubMed Central PMCID: PMC5461023.

Caplow M. Microtubule dynamics. Current opinion in cell biology. 1992;4(1):58-65. PubMed PMID: 1558755.

16. Caplow M, Shanks J. Induction of microtubule catastrophe by formation of tubulin-GDP and apotubulin subunits at microtubule ends. Biochemistry. 1995;34(48):15732-41. PubMed PMID: 7495804.

Carlier MF. Actin: protein structure and filament dynamics. The Journal of biological chemistry. 1991;266(1):1-4. PubMed PMID: 1985885.

Carlier MF. Actin: protein structure and filament dynamics. The Journal of biological chemistry. 1991;266(1):1-4. PubMed PMID: 1985885.

Carlier MF, Didry D, Simon C, Pantaloni D. Mechanism of GTP hydrolysis in tubulin polymerization: characterization of the kinetic intermediate microtubule-GDP-Pi using phosphate analogues. Biochemistry. 1989;28(4):1783-91. PubMed PMID: 2719934.

Carlier MF, Pantaloni D. Kinetic analysis of guanosine 5'-triphosphate hydrolysis associated with tubulin polymerization. Biochemistry. 1981;20(7):1918-24. PubMed PMID: 7225365.

Cassimeris L, Becker B, Carney B. TOGp regulates microtubule assembly and density during mitosis and contributes to chromosome directional instability. Cell motility and the cytoskeleton. 2009;66(8):535-45. doi: 10.1002/cm.20359. PubMed PMID: 19373773.
Cassimeris L, Pryer NK, Salmon ED. Real-time observations of microtubule dynamic instability in living cells. The Journal of cell biology. 1988;107(6 Pt 1):2223-31. PubMed PMID: 3198684; PubMed Central PMCID: PMC2115680.

Charrasse S, Schroeder M, Gauthier-Rouviere C, Ango F, Cassimeris L, Gard DL, et al. The TOGp protein is a new human microtubule-associated protein homologous to the Xenopus XMAP215. Journal of cell science. 1998;111 (Pt 10):1371-83. PubMed PMID: 9570755.

Chen Y, Hancock WO. Kinesin-5 is a microtubule polymerase. Nature communications. 2015;6:8160. doi: 10.1038/ncomms9160. PubMed PMID: 26437877; PubMed Central PMCID: PMC4600729.

Chen YD, Hill TL. Monte Carlo study of the GTP cap in a five-start helix model of a microtubule. Proceedings of the National Academy of Sciences of the United States of America. 1985;82(4):1131-5. PubMed PMID: 3856250; PubMed Central PMCID: PMC397208.

Cullen CF, Deak P, Glover DM, Ohkura H. mini spindles: A gene encoding a conserved microtubule-associated protein required for the integrity of the mitotic spindle in Drosophila. The Journal of cell biology. 1999;146(5):1005-18. PubMed PMID: 10477755; PubMed Central PMCID: PMC2169485.

Das A, Dickinson DJ, Wood CC, Goldstein B, Slep KC. Crescerin uses a TOG domain array to regulate microtubules in the primary cilium. Molecular biology of the cell. 2015;26(23):4248-64. doi: 10.1091/mbc.E15-08-0603. PubMed PMID: 26378256; PubMed Central PMCID: PMC4642858.

David-Pfeuty T, Erickson HP, Pantaloni D. Guanosinetriphosphatase activity of tubulin associated with microtubule assembly. Proceedings of the National Academy of Sciences of the United States of America. 1977;74(12):5372-6. PubMed PMID: 202954; PubMed Central PMCID: PMC431725.

De Groot CO, Jelesarov I, Damberger FF, Bjelic S, Scharer MA, Bhavesh NS, et al. Molecular insights into mammalian end-binding protein heterodimerization. The Journal of biological chemistry. 2010;285(8):5802-14. doi: 10.1074/jbc.M109.068130. PubMed PMID: 20008324; PubMed Central PMCID: PMC2820806.

Desai A, Mitchison TJ. Microtubule polymerization dynamics. Annual review of cell and developmental biology. 1997;13:83-117. doi: 10.1146/annurev.cellbio.13.1.83. PubMed PMID: 9442869.

Fox JC, Howard AE, Currie JD, Rogers SL, Slep KC. The XMAP215 family drives microtubule polymerization using a structurally diverse TOG array. Molecular biology of the cell. 2014;25(16):2375-92. doi: 10.1091/mbc.E13-08-0501. PubMed PMID: 24966168; PubMed Central PMCID: PMC4142611.

Gard DL, Kirschner MW. A microtubule-associated protein from Xenopus eggs that specifically promotes assembly at the plus-end. The Journal of cell biology. 1987;105(5):2203-15. PubMed PMID: 2890645; PubMed Central PMCID: PMC2114854.

Fujii T, Iwane AH, Yanagida T, Namba K. Direct visualization of secondary structures of F-actin by electron cryomicroscopy. Nature. 2010;467(7316):724-8. doi: 10.1038/nature09372. PubMed PMID: 20844487.

Fygenson DK, Braun E, Libchaber A. Phase diagram of microtubules. Physical review E, Statistical physics, plasmas, fluids, and related interdisciplinary topics. 1994;50(2):1579-88. PubMed PMID: 9962129.

Gergely F, Draviam VM, Raff JW. The ch-TOG/XMAP215 protein is essential for spindle pole organization in human somatic cells. Genes & development. 2003;17(3):336-41. doi: 10.1101/gad.245603. PubMed PMID: 12569123; PubMed Central PMCID: PMC195983.

Gimona M, Djinovic-Carugo K, Kranewitter WJ, Winder SJ. Functional plasticity of CH domains. FEBS letters. 2002;513(1):98-106. PubMed PMID: 11911887.

Goryunov D, He CZ, Lin CS, Leung CL, Liem RK. Nervous-tissue-specific elimination of microtubule-actin crosslinking factor 1a results in multiple developmental defects in the mouse brain. Molecular and cellular neurosciences. 2010;44(1):1-14. doi: 10.1016/j.mcn.2010.01.010. PubMed PMID: 20170731; PubMed Central PMCID: PMC2847646.

Gudimchuk N, Vitre B, Kim Y, Kiyatkin A, Cleveland DW, Ataullakhanov FI, et al. Kinetochore kinesin CENP-E is a processive bi-directional tracker of dynamic microtubule tips. Nature cell biology. 2013;15(9):1079-88. doi: 10.1038/ncb2831. PubMed PMID: 23955301; PubMed Central PMCID: PMC3919686.

Guesdon A, Bazile F, Buey RM, Mohan R, Monier S, Garcia RR, et al. EB1 interacts with outwardly curved and straight regions of the microtubule lattice. Nature cell biology. 2016;18(10):1102-8. doi: 10.1038/ncb3412. PubMed PMID: 27617931.

Gutierrez-Caballero C, Burgess SG, Bayliss R, Royle SJ. TACC3-ch-TOG track the growing tips of microtubules independently of clathrin and Aurora-A phosphorylation. Biology open.

2015;4(2):170-9. doi: 10.1242/bio.201410843. PubMed PMID: 25596274; PubMed Central PMCID: PMC4365485.

Holmes KC, Popp D, Gebhard W, Kabsch W. Atomic model of the actin filament. Nature. 1990;347(6288):44-9. doi: 10.1038/347044a0. PubMed PMID: 2395461.

Honnappa S, Gouveia SM, Weisbrich A, Damberger FF, Bhavesh NS, Jawhari H, et al. An EB1-binding motif acts as a microtubule tip localization signal. Cell. 2009;138(2):366-76. doi: 10.1016/j.cell.2009.04.065. PubMed PMID: 19632184.

Honnappa S, John CM, Kostrewa D, Winkler FK, Steinmetz MO. Structural insights into the EB1-APC interaction. The EMBO journal. 2005;24(2):261-9. doi: 10.1038/sj.emboj.7600529. PubMed PMID: 15616574; PubMed Central PMCID: PMC545816.

Honnappa S, Okhrimenko O, Jaussi R, Jawhari H, Jelesarov I, Winkler FK, et al. Key interaction modes of dynamic +TIP networks. Molecular cell. 2006;23(5):663-71. doi: 10.1016/j.molcel.2006.07.013. PubMed PMID: 16949363.

Hood FE, Williams SJ, Burgess SG, Richards MW, Roth D, Straube A, et al. Coordination of adjacent domains mediates TACC3-ch-TOG-clathrin assembly and mitotic spindle binding. The Journal of cell biology. 2013;202(3):463-78. doi: 10.1083/jcb.201211127. PubMed PMID: 23918938; PubMed Central PMCID: PMC3734082.

Howard AE, Fox JC, Slep KC. Drosophila melanogaster mini spindles TOG3 utilizes unique structural elements to promote domain stability and maintain a TOG1- and TOG2-like tubulin-binding surface. The Journal of biological chemistry. 2015;290(16):10149-62. doi: 10.1074/jbc.M114.633826. PubMed PMID: 25720490; PubMed Central PMCID: PMC4400331.

Howard J, Hyman AA. Dynamics and mechanics of the microtubule plus end. Nature. 2003;422(6933):753-8. doi: 10.1038/nature01600. PubMed PMID: 12700769.

Kabsch W, Mannherz HG, Suck D, Pai EF, Holmes KC. Atomic structure of the actin:DNase I complex. Nature. 1990;347(6288):37-44. doi: 10.1038/347037a0. PubMed PMID: 2395459.

Kapur M, Wang W, Maloney MT, Millan I, Lundin VF, Tran TA, et al. Calcium tips the balance: a microtubule plus end to lattice binding switch operates in the carboxyl terminus of BPAG1n4. EMBO reports. 2012;13(11):1021-9. doi: 10.1038/embor.2012.140. PubMed PMID: 22995871; PubMed Central PMCID: PMC3492708.

Kawamura E, Wasteneys GO. MOR1, the Arabidopsis thaliana homologue of Xenopus MAP215, promotes rapid growth and shrinkage, and suppresses the pausing of microtubules

in vivo. Journal of cell science. 2008;121(Pt 24):4114-23. doi: 10.1242/jcs.039065. PubMed PMID: 19033380.

Kinoshita K, Arnal I, Desai A, Drechsel DN, Hyman AA. Reconstitution of physiological microtubule dynamics using purified components. Science. 2001;294(5545):1340-3. doi: 10.1126/science.1064629. PubMed PMID: 11701928.

Kirschner MW, Williams RC. The mechanism of microtubule assembly in vitro. Journal of supramolecular structure. 1974;2(2-4):412-28. doi: 10.1002/jss.400020229. PubMed PMID: 4474574.

Kosco KA, Pearson CG, Maddox PS, Wang PJ, Adams IR, Salmon ED, et al. Control of microtubule dynamics by Stu2p is essential for spindle orientation and metaphase chromosome alignment in yeast. Molecular biology of the cell. 2001;12(9):2870-80. PubMed PMID: 11553724; PubMed Central PMCID: PMC59720.

Kronja I, Kruljac-Letunic A, Caudron-Herger M, Bieling P, Karsenti E. XMAP215-EB1 interaction is required for proper spindle assembly and chromosome segregation in Xenopus egg extract. Molecular biology of the cell. 2009;20(11):2684-96. doi: 10.1091/mbc.E08-10-1051. PubMed PMID: 19369422; PubMed Central PMCID: PMC2688548.

Lampert F, Hornung P, Westermann S. The Dam1 complex confers microtubule plus end-tracking activity to the Ndc80 kinetochore complex. The Journal of cell biology. 2010;189(4):641-9. doi: 10.1083/jcb.200912021. PubMed PMID: 20479465; PubMed Central PMCID: PMC2872915.

Lane TR, Fuchs E, Slep KC. Structure of the ACF7 EF-Hand-GAR Module and Delineation of Microtubule Binding Determinants. Structure. 2017;25(7):1130-8 e6. doi: 10.1016/j.str.2017.05.006. PubMed PMID: 28602822.

Le Bot N, Tsai MC, Andrews RK, Ahringer J. TAC-1, a regulator of microtubule length in the C. elegans embryo. Current biology : CB. 2003;13(17):1499-505. PubMed PMID: 12956951.

Lee MJ, Gergely F, Jeffers K, Peak-Chew SY, Raff JW. Msps/XMAP215 interacts with the centrosomal protein D-TACC to regulate microtubule behaviour. Nature cell biology. 2001;3(7):643-9. doi: 10.1038/35083033. PubMed PMID: 11433296.

Lee S, Harris KL, Whitington PM, Kolodziej PA. short stop is allelic to kakapo, and encodes rod-like cytoskeletal-associated proteins required for axon extension. The Journal of neuroscience : the official journal of the Society for Neuroscience. 2000;20(3):1096-108. PubMed PMID: 10648715.

Li H, DeRosier DJ, Nicholson WV, Nogales E, Downing KH. Microtubule structure at 8 A resolution. Structure. 2002;10(10):1317-28. PubMed PMID: 12377118.

Li R, Gundersen GG. Beyond polymer polarity: how the cytoskeleton builds a polarized cell. Nature reviews Molecular cell biology. 2008;9(11):860-73. doi: 10.1038/nrm2522. PubMed PMID: 18946475.

Li W, Miki T, Watanabe T, Kakeno M, Sugiyama I, Kaibuchi K, et al. EB1 promotes microtubule dynamics by recruiting Sentin in Drosophila cells. The Journal of cell biology. 2011;193(6):973-83. doi: 10.1083/jcb.201101108. PubMed PMID: 21646401; PubMed Central PMCID: PMC3115803.

Lucaj CM, Evans MF, Nwagbara BU, Ebbert PT, Baker CC, Volk JG, et al. Xenopus TACC1 is a microtubule plus-end tracking protein that can regulate microtubule dynamics during embryonic development. Cytoskeleton. 2015;72(5):225-34. doi: 10.1002/cm.21224. PubMed PMID: 26012630; PubMed Central PMCID: PMC4520305.

MacNeal RK, Purich DL. Stoichiometry and role of GTP hydrolysis in bovine neurotubule assembly. The Journal of biological chemistry. 1978;253(13):4683-7. PubMed PMID: 659441.

Matthews LR, Carter P, Thierry-Mieg D, Kemphues K. ZYG-9, a Caenorhabditis elegans protein required for microtubule organization and function, is a component of meiotic and mitotic spindle poles. The Journal of cell biology. 1998;141(5):1159-68. PubMed PMID: 9606208; PubMed Central PMCID: PMC2137183.

Maurer SP, Bieling P, Cope J, Hoenger A, Surrey T. GTPgammaS microtubules mimic the growing microtubule end structure recognized by end-binding proteins (EBs). Proceedings of the National Academy of Sciences of the United States of America. 2011;108(10):3988-93. doi: 10.1073/pnas.1014758108. PubMed PMID: 21368119; PubMed Central PMCID: PMC3053978.

Maurer SP, Fourniol FJ, Bohner G, Moores CA, Surrey T. EBs recognize a nucleotide-dependent structural cap at growing microtubule ends. Cell. 2012;149(2):371-82. doi: 10.1016/j.cell.2012.02.049. PubMed PMID: 22500803; PubMed Central PMCID: PMC3368265.

McIntosh JR, Grishchuk EL, West RR. Chromosome-microtubule interactions during mitosis. Annual review of cell and developmental biology. 2002;18:193-219. doi: 10.1146/annurev.cellbio.18.032002.132412. PubMed PMID: 12142285.

Miller MP, Asbury CL, Biggins S. A TOG Protein Confers Tension Sensitivity to Kinetochore-Microtubule Attachments. Cell. 2016;165(6):1428-39. doi: 10.1016/j.cell.2016.04.030. PubMed PMID: 27156448; PubMed Central PMCID: PMC4892958.

Mimori-Kiyosue Y, Grigoriev I, Lansbergen G, Sasaki H, Matsui C, Severin F, et al. CLASP1 and CLASP2 bind to EB1 and regulate microtubule plus-end dynamics at the cell

cortex. The Journal of cell biology. 2005;168(1):141-53. doi: 10.1083/jcb.200405094. PubMed PMID: 15631994; PubMed Central PMCID: PMC2171674.

Mitchison T, Evans L, Schulze E, Kirschner M. Sites of microtubule assembly and disassembly in the mitotic spindle. Cell. 1986;45(4):515-27. PubMed PMID: 3708686.

Mitchison T, Kirschner M. Dynamic instability of microtubule growth. Nature. 1984;312(5991):237-42. PubMed PMID: 6504138.

Mitchison T, Kirschner M. Microtubule assembly nucleated by isolated centrosomes. Nature. 1984;312(5991):232-7. PubMed PMID: 6504137.

Mortuza GB, Cavazza T, Garcia-Mayoral MF, Hermida D, Peset I, Pedrero JG, et al. XTACC3-XMAP215 association reveals an asymmetric interaction promoting microtubule elongation. Nature communications. 2014;5:5072. doi: 10.1038/ncomms6072. PubMed PMID: 25262927; PubMed Central PMCID: PMC4200520.

Nwagbara BU, Faris AE, Bearce EA, Erdogan B, Ebbert PT, Evans MF, et al. TACC3 is a microtubule plus end-tracking protein that promotes axon elongation and also regulates microtubule plus end dynamics in multiple embryonic cell types. Molecular biology of the cell. 2014;25(21):3350-62. doi: 10.1091/mbc.E14-06-1121. PubMed PMID: 25187649; PubMed Central PMCID: PMC4214782.

Oda T, Iwasa M, Aihara T, Maeda Y, Narita A. The nature of the globular- to fibrous-actin transition. Nature. 2009;457(7228):441-5. doi: 10.1038/nature07685. PubMed PMID: 19158791.

Olmsted JB. Microtubule-associated proteins. Annual review of cell biology. 1986;2:421-57. doi: 10.1146/annurev.cb.02.110186.002225. PubMed PMID: 3548773.

Pollard TD. Mechanism of actin filament self-assembly and regulation of the process by actin-binding proteins. Biophysical journal. 1986;49(1):149-51. doi: 10.1016/S0006-3495(86)83630-X. PubMed PMID: 19431625; PubMed Central PMCID: PMC1329614.

Pollard TD. Actin. Current opinion in cell biology. 1990;2(1):33-40. PubMed PMID: 2183841.

Prokop A, Uhler J, Roote J, Bate M. The kakapo mutation affects terminal arborization and central dendritic sprouting of Drosophila motorneurons. The Journal of cell biology. 1998;143(5):1283-94. PubMed PMID: 9832556; PubMed Central PMCID: PMC2133088.

Rogers SL, Rogers GC, Sharp DJ, Vale RD. Drosophila EB1 is important for proper assembly, dynamics, and positioning of the mitotic spindle. The Journal of cell biology. 2002;158(5):873-84. doi: 10.1083/jcb.200202032. PubMed PMID: 12213835; PubMed Central PMCID: PMC2173155.

Roper K, Brown NH. Maintaining epithelial integrity: a function for gigantic spectraplakin isoforms in adherens junctions. The Journal of cell biology. 2003;162(7):1305-15. doi: 10.1083/jcb.200307089. PubMed PMID: 14517208; PubMed Central PMCID: PMC2173965.

Rutherford EL, Carandang L, Ebbert PT, Mills AN, Bowers JT, Lowery LA. Xenopus TACC2 is a microtubule plus end-tracking protein that can promote microtubule polymerization during embryonic development. Molecular biology of the cell. 2016;27(20):3013-20. doi: 10.1091/mbc.E16-03-0198. PubMed PMID: 27559128; PubMed Central PMCID: PMC5063610.

Sanchez-Soriano N, Travis M, Dajas-Bailador F, Goncalves-Pimentel C, Whitmarsh AJ, Prokop A. Mouse ACF7 and drosophila short stop modulate filopodia formation and microtubule organisation during neuronal growth. Journal of cell science. 2009;122(Pt 14):2534-42. doi: 10.1242/jcs.046268. PubMed PMID: 19571116; PubMed Central PMCID: PMC2704885.

Schuyler SC, Pellman D. Microtubule "plus-end-tracking proteins": The end is just the beginning. Cell. 2001;105(4):421-4. PubMed PMID: 11371339.

Sen I, Veprintsev D, Akhmanova A, Steinmetz MO. End binding proteins are obligatory dimers. PloS one. 2013;8(9):e74448. doi: 10.1371/journal.pone.0074448. PubMed PMID: 24040250; PubMed Central PMCID: PMC3765442.

Sept D, McCammon JA. Thermodynamics and kinetics of actin filament nucleation. Biophysical journal. 2001;81(2):667-74. doi: 10.1016/S0006-3495(01)75731-1. PubMed PMID: 11463615; PubMed Central PMCID: PMC1301543.

Slep KC, Rogers SL, Elliott SL, Ohkura H, Kolodziej PA, Vale RD. Structural determinants for EB1-mediated recruitment of APC and spectraplakins to the microtubule plus end. The Journal of cell biology. 2005;168(4):587-98. doi: 10.1083/jcb.200410114. PubMed PMID: 15699215; PubMed Central PMCID: PMC2171753.

Slep KC, Vale RD. Structural basis of microtubule plus end tracking by XMAP215, CLIP-170, and EB1. Molecular cell. 2007;27(6):976-91. doi: 10.1016/j.molcel.2007.07.023. PubMed PMID: 17889670; PubMed Central PMCID: PMC2052927.

Strumpf, D., and T Volk. 1998. Kakapo, a novel cytoskeletal-associated protein is essential for the restricted localization of the neuregulin-like factor, vein, at the muscle-tendon junction site. J Cell Biol, 143, 1259-70.

Sousa A, Reis R, Sampaio P, Sunkel CE. The Drosophila CLASP homologue, Mast/Orbit regulates the dynamic behaviour of interphase microtubules by promoting the pause state.

Cell motility and the cytoskeleton. 2007;64(8):605-20. doi: 10.1002/cm.20208. PubMed PMID: 17487886.

Spiegelman BM, Penningroth SM, Kirschner MW. Turnover of tubulin and the N site GTP in Chinese hamster ovary cells. Cell. 1977;12(3):587-600. PubMed PMID: 562716.
Srayko M, Quintin S, Schwager A, Hyman AA. Caenorhabditis elegans TAC-1 and ZYG-9 form a complex that is essential for long astral and spindle microtubules. Current biology : CB. 2003;13(17):1506-11. PubMed PMID: 12956952.

Takacs, Z., F. Jankovics, P. Vilmos, P. Lenart, K. Roper, and M. Erdelyi. 2017. The spectraplakin Short stop is an essential microtubule regulator involved in epithelial closure in Drosophila. J Cell Sci, 130, 712-724. doi: 10.1242/jcs.193003

Tanaka EM, Kirschner MW. Microtubule behavior in the growth cones of living neurons during axon elongation. The Journal of cell biology. 1991;115(2):345-63. PubMed PMID: 1918145; PubMed Central PMCID: PMC2289161.

Tournebize R, Popov A, Kinoshita K, Ashford AJ, Rybina S, Pozniakovsky A, et al. Control of microtubule dynamics by the antagonistic activities of XMAP215 and XKCM1 in Xenopus egg extracts. Nature cell biology. 2000;2(1):13-9. doi: 10.1038/71330. PubMed PMID: 10620801.

van den Ent F, Moller-Jensen J, Amos LA, Gerdes K, Lowe J. F-actin-like filaments formed by plasmid segregation protein ParM. The EMBO journal.
2002;21(24):6935-43. PubMed PMID: 12486014; PubMed Central PMCID: PMC139093.

van der Vaart B, Franker MA, Kuijpers M, Hua S, Bouchet BP, Jiang K, et al. Microtubule plus-end tracking proteins SLAIN1/2 and ch-TOG promote axonal development. The Journal of neuroscience : the official journal of the Society for Neuroscience. 2012;32(42):14722-8. doi: 10.1523/JNEUROSCI.1240-12.2012. PubMed PMID: 23077057.

van der Vaart B, Manatschal C, Grigoriev I, Olieric V, Gouveia SM, Bjelic S, et al. SLAIN2 links microtubule plus end-tracking proteins and controls microtubule growth in interphase. The Journal of cell biology. 2011;193(6):1083-99. doi: 10.1083/jcb.201012179. PubMed PMID: 21646404; PubMed Central PMCID: PMC3115796.

Varga V, Helenius J, Tanaka K, Hyman AA, Tanaka TU, Howard J. Yeast kinesin-8 depolymerizes microtubules in a length-dependent manner. Nature cell biology. 2006;8(9):957-62. doi: 10.1038/ncb1462. PubMed PMID: 16906145.

Vasquez RJ, Gard DL, Cassimeris L. XMAP from Xenopus eggs promotes rapid plus end assembly of microtubules and rapid microtubule polymer turnover. The Journal of cell biology. 1994;127(4):985-93. PubMed PMID: 7962080; PubMed Central PMCID: PMC2200056.

Voter WA, Erickson HP. The kinetics of microtubule assembly. Evidence for a two-stage nucleation mechanism. The Journal of biological chemistry. 1984;259(16):10430-8. PubMed PMID: 6469971.

Walker RA, Inoue S, Salmon ED. Asymmetric behavior of severed microtubule ends after ultraviolet-microbeam irradiation of individual microtubules in vitro. The Journal of cell biology. 1989;108(3):931-7. PubMed PMID: 2921286; PubMed Central PMCID: PMC2115382.

Walker RA, O'Brien ET, Pryer NK, Soboeiro MF, Voter WA, Erickson HP, et al. Dynamic instability of individual microtubules analyzed by video light microscopy: rate constants and transition frequencies. The Journal of cell biology. 1988;107(4):1437-48. PubMed PMID: 3170635; PubMed Central PMCID: PMC2115242.

Walsh EP, Brown NH. A screen to identify Drosophila genes required for integrin-mediated adhesion. Genetics. 1998;150(2):791-805. PubMed PMID: 9755209; PubMed Central PMCID: PMC1460349.

Weisbrich A, Honnappa S, Jaussi R, Okhrimenko O, Frey D, Jelesarov I, et al. Structure-function relationship of CAP-Gly domains. Nature structural & molecular biology. 2007;14(10):959-67. doi: 10.1038/nsmb1291. PubMed PMID: 17828277.

Weisenberg RC, Deery WJ. Role of nucleotide hydrolysis in microtubule assembly. Nature. 1976;263(5580):792-3. PubMed PMID: 995195.

Widlund PO, Stear JH, Pozniakovsky A, Zanic M, Reber S, Brouhard GJ, et al. XMAP215 polymerase activity is built by combining multiple tubulin-binding TOG domains and a basic lattice-binding region. Proceedings of the National Academy of Sciences of the United States of America. 2011;108(7):2741-6. doi: 10.1073/pnas.1016498108. PubMed PMID: 21282620; PubMed Central PMCID: PMC3041093.

Wu X, Kodama A, Fuchs E. ACF7 regulates cytoskeletal-focal adhesion dynamics and migration and has ATPase activity. Cell. 2008;135(1):137-48. doi: 10.1016/j.cell.2008.07.045. PubMed PMID: 18854161; PubMed Central PMCID: PMC2703712.

Wu X, Shen QT, Oristian DS, Lu CP, Zheng Q, Wang HW, et al. Skin stem cells orchestrate directional migration by regulating microtubule-ACF7 connections through GSK3beta. Cell. 2011;144(3):341-52. doi: 10.1016/j.cell.2010.12.033. PubMed PMID: 21295697; PubMed Central PMCID: PMC3050560.

Zanic M, Stear JH, Hyman AA, Howard J. EB1 recognizes the nucleotide state of tubulin in the microtubule lattice. PloS one. 2009;4(10):e7585. doi: 10.1371/journal.pone.0007585. PubMed PMID: 19851462; PubMed Central PMCID: PMC2761489.

Zanic M, Widlund PO, Hyman AA, Howard J. Synergy between XMAP215 and EB1 increases microtubule growth rates to physiological levels. Nature cell biology. 2013;15(6):688-93. doi: 10.1038/ncb2744. PubMed PMID: 23666085.

Zhang R, Alushin GM, Brown A, Nogales E. Mechanistic Origin of Microtubule Dynamic Instability and Its Modulation by EB Proteins. Cell. 2015;162(4):849-59. doi: 10.1016/j.cell.2015.07.012. PubMed PMID: 26234155; PubMed Central PMCID: PMC4537847.

CHAPTER 2: CONTROL OF MICROTUBULE DYNAMICS USING AN OPTOGENETIC MICROTUBULE PLUS END-F-ACTIN CROSSLINKER[1]

2.1 Introduction

Cellular and developmental processes require the temporal control of protein-protein interactions. The cytoskeleton, composed of MTs, F-actin, and intermediate filaments, is tightly regulated and remodeled throughout the cell cycle. How proteins regulate cytoskeletal dynamics and mediate cross-talk between the networks is an active area of research. For example, the dynamic coupling of the actin and MT networks is essential for neuronal growth (Tortosa et al., 2011, Sanchez-Soriano et al., 2009, Lee et al., 2000; Lee and Luo, 1999; Prokop et al., 1998), cell shape changes, migration (Guo et al., 1995, Wu et al., 2008, Wu et al., 2011) and determining the site of the contractile ring (Kunda and Baum, 2009). Historically, probing the role of protein-protein interactions in complex cellular networks with temporal resolution has been difficult. However, recent advances in cellular optogenetic techniques have enabled biologists to dissect the temporal mechanisms that regulate diverse cellular systems. Many inducible protein dimer systems have recently been generated, optimized, and made available to researchers to control protein activity and/or localization within cells and organisms. Currently available dimer systems include both chemically induced dimers, such as the FRB/FKBP12 system that can be heterodimerized

[1] Adikes R.C., Hallett R., Saway B.F., Kuhlman B., Slep K.C. (2017). Control of microtubule dynamics using a microtubule plus end-F-actin cross-linker. Journal of Cell Biology. 217 (2): 779 doi: 10.1083/jcb.201705190

with rapamycin (Rivera et al., 1996), and light inducible dimers (LIDs). LIDs come from photoactivatable systems naturally occurring in plants and allow for regional, reversible activation using light. LIDs include phytochromes, cryptochromes, and Light-Oxygen-Voltage (LOV) domains. LOV domains have been used in engineered homodimer paired systems such as tunable light-controlled interacting protein tags (TULIPs (LOVpep/ePDZb)) (Strickland et al., 2012), improved light-inducible dimer (iLID) (iLID/SspB) (Guntas et al., 2015), and Zdk/LOV2 – a heterodimer that dissociates when photoactivated (Wang and Hahn, 2016). These LOV-based systems rely on a blue light-dependent conformational change in the LOV2 domain that facilitates the release and unfolding of an α-helix termed the Jα helix. The iLID/SspB system contains a short ssrA peptide sequence embedded in the Jα helix of the LOV domain. The ssrA sequence is occluded from binding its partner SspB in the dark. However, upon blue light activation, the ssrA sequence becomes accessible and can bind SspB. Specific advantages of the iLID/SspB system include 1) no off-target effects in non-plant eukaryotes, and 2) the availability of a suite of iLID constructs with different on/off kinetics and SspB binding affinities (Guntas et al., 2015, Hallett et al., 2016, Zimmerman et al., 2016).

iLID as well as other LIDs have been used to perturb pathways involved in cell protrusion (Hallett et al., 2016), and cell migration (Weitzman and Hahn, 2014), to activate formins to control actin architecture (Rao et al., 2013), and regulate organelle transport and positioning (van Berjeijk et al., 2015, Duan et al., 2015). Most recently the Zdk/LOV2 system was used to dissociate the MT plus end protein EB1 with temporal and spatial control. This study revealed that the equilibrium of MT polymerization dynamics changes in under a minute and the MT network rapidly reshapes (van Haren et al., 2017 *Preprint*).

However, a system to recruit selected proteins or protein domains of interest to MT plus ends has not been created.

Here, we develop and validate an optogenetically controlled MT plus end recruitment system, which can be easily adapted to answer a variety of questions pertaining to the regulation of MT dynamics and MT network organization. To create this system we utilized iLID (iLID/SspB). This system is ideal for the reversible recruitment of specific SspB-fusion proteins to MT plus ends. To localize iLID to MT plus ends, we fused the iLID module to a motif that binds to EB proteins. EB proteins specifically bind MT plus ends by recognizing the GTP hydrolysis transition state / post-hydrolysis state of the MT lattice (Zanic et al., 2009: Maurer et al., 2011; Maurer et al., 2012; Guesdon et al., 2016). Many proteins localize to the MT plus end by interacting with EB proteins (Jiang et al., 2012). These proteins engage the EB dimer using a highly conserved motif known as a SxIP motif (Slep et al., 2005; Honnappa et. al., 2005; Honnappa et al., 2009). Here, we show that EB-binding SxIP motifs, appended to the iLID N-terminus, confer iLID with MT plus end tracking activity. When exposed to blue light, SxIP-iLID recruits SspB-tagged proteins to MT plus ends. We establish SxIP-iLID as a tool with broad utility that can be used to systematically study the mechanisms of MT regulators and MT associated proteins.

We then utilized SxIP-iLID to investigate how MT-F-actin cytoskeletal cross-linking affects MT dynamics and cell morphology. Previous studies have shown that coordination between F-actin and MTs is important for cell migration, mitosis, and tissue morphogenesis. One class of cytoskeletal cross-linkers are the spectraplakins. Spectraplakin loss of function leads to severe axon shortening and MT disorganization (Sanchez-Soriano et al., 2009). Mutations in the *Drosophila* actin-MT cross-linking protein Shot cause a variety of cellular

and tissue defects including changes in actin-MT organization, cell-cell adhesion, and integrin mediated epidermal attachments to muscle (Gregory and Brown, 1998; Walsh and Brown, 1998; Propkop et al., 1998; Strumpf and Volk 1998; Röper and Brown, 2003). Conditional knock out of the spectraplakin Actin Cross-linking Factor 7 (ACF7) in mice yields defects in cell migration (Wu et al., 2008, Goryunov et al., 2010). These mutational and knock out experiments provide information on long-term whole tissue depletion of a spectraplakin, however having a subcellular temporal and rapidly reversible way to probe the effects of cross-linking will provide mechanistic details on the direct cellular changes induced by cross-linking. Proteins of the spectraplakin family typically contain two N-terminal calponin-homology (CH)-type F-actin binding domains, and a C-terminal MT-binding module consisting of an EF-Hand-Gas2-related (GAR) region, Gly-Ser-Arg rich (GSR) motifs, and an EB-binding Sx(I/L)P motif (Lee et al., 2000; Slep et al., 2005, Wu et al., 2008; Applewhite et al., 2010, Lane et al., 2017). Although recent studies have proposed mechanisms for the regulation of spectraplakins (Wu et al., 2011; Kapur et al., 2012; Applewhite et al., 2013; Takács et al., 2017), the direct downstream cellular outputs of regulated cross-linking remain poorly understood. To begin to understand how cross-linking affects cytoskeletal dynamics and network organization we utilized the SxIP-iLID system to optogenetically cross-link MTs and F-actin. We show that whole cell light-mediated MT-actin cross-linking decreases MT growth velocities and creates a MT exclusion zone.

2.2 Results

2.2.1 Design of a light-inducible system for MT plus end tracking

Our goal was to control the temporal recruitment of proteins to the MT plus end. To do so we designed a switch that would constitutively track MT plus ends and recruit a protein

or domain of interest upon blue light activation (Fig. 2.1, A and B). To generate a MT plus end recruitment switch we capitalized on the ability of the EB MT plus end tracking protein family to directly bind cellular factors that contain a SxIP motif (Slep et al., 2005; Honnappa et. al., 2005; Honnappa et al., 2009). We fused individual or arrayed EB-binding SxIP motifs to the iLID domain. We designed four SxIP-iLID constructs to generate a set of constructs with varying MT plus end tracking activity. All constructs contained a N-terminal eGFP to allow detection and tracking (Fig. 2.1A). The first construct, SKIP-iLID, contains a single 18-amino acid SKIP motif from the spectraplakin MT-actin crosslink factor 2 (MACF2). Two constructs contain a pair of tandemly arrayed SxIP motifs, either SKIP-SKIP or SKIP-SRIP, with the two motifs separated by the linker sequence that bridges the two endogenous SxIP motifs in cytoplasmic linker protein-associated protein 2 (CLASP2) (Honnappa et al., 2009). A fourth construct contains a single MACF2 SKIP motif followed by the GCN4 leucine zipper (LZ) homodimerization domain (Fig. 2.1A and Table 2.1)(Honnappa et al., 2009, Steinmetz et al., 2007). The tandem SKIP constructs and the dimerized SKIP construct were designed to enhance binding to EB dimers via avidity, which has previously been shown to enhance the apparent MT plus end tracking activity of SxIP constructs (Honnapppa et al., 2009; Kumar et al., 2012).

We assayed the ability of these constructs to track polymerizing MT plus ends in *Drosophila* S2 cells using time-lapse eGFP imaging. Each of the four SxIP-iLID constructs exhibited MT plus end tracking activity as revealed by distinctive comet-like patterns that moved throughout the cytoplasm (Fig. 2.1C) Monomeric SKIP-iLID comets were dim and difficult to observe in most cells, while the dimeric SKIP-LZ-iLID exhibited robust MT plus ends tracking activity (Fig. 2.1C). Ratiometric analysis of the eGFP comet:cytoplasmic

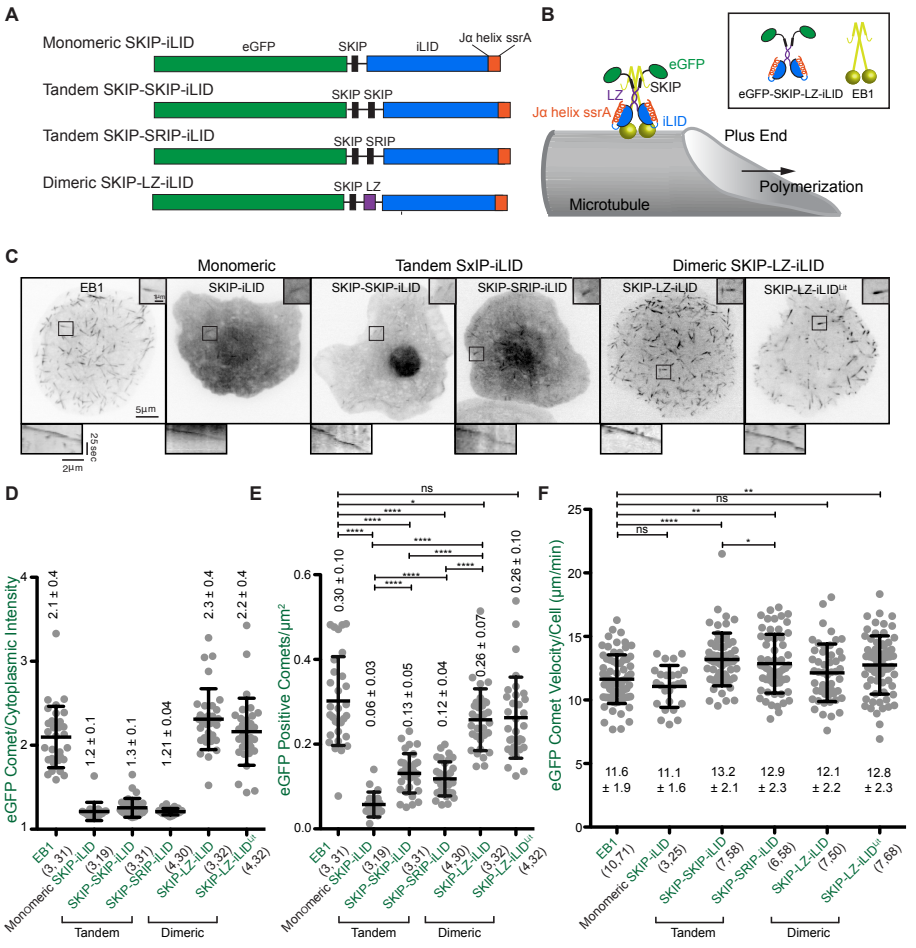

Figure 2.1. SxIP-iLID constructs track MT plus ends and do not dramatically perturb MT comet velocities. (A) Schematic of eGFP-labeled SxIP-iLID constructs. **(B)** Cartoon diagraming eGFP-SKIP-LZ-iLID at a MT plus end. **(C)** Representative images of eGFP-SxIP-iLID constructs in *Drosophila* S2 cells. Scale bar, 5 µm, inset scale bar, 1µm. Comets can be observed in all cells expressing an eGFP-SxIP-iLID construct. Kymographs below each image show a representative eGFP-SxIP-iLID MT plus end comet. Scale bars, 2 µm, 25 seconds. **(D)** The ratio of mean eGFP-SxIP-iLID construct intensity on a MT plus end per area relative to the mean intensity per area in an adjacent cytoplasmic region. The dimeric SKIP-LZ-iLID construct shows the greatest ratio of eGFP comet intensity relative to cytoplasmic background, comparable to that calculated for EB1-GFP. **(E)** The number of GFP positive comets per µm^2. The SKIP-LZ-iLID construct yields the highest density of detectable eGFP positive comets per area, the monomeric SKIP-iLID construct yields the lowest, and the tandem SxIP-iLID constructs both yield intermediate levels. **(F)** SxIP-iLID constructs show some variation in eGFP comet velocities, however, the mean comet velocity of the dimeric SKIP-LZ-iLID construct is not significantly different from the mean comet velocity of an EB1-GFP control. Error bars indicate the SD. Numbers in parenthesis indicate (number of experiments, total number of cells quantified). P-values were determined by two-way unpaired Student's t-test. * $p<0.05$, ** $p<0.005$, **** $p<0.0001$.

Table 1: Sequences of SxIP Motifs, Linkers, and Leucine Zipper for iLID constructs

Construct		Sequence
Monomeric	**SKIP-**iLID	ENIRSAAKP**SKIP**TPQRKSPASGS
Tandem	**SKIP-SRIP-**iLID	ENIRSAAKP**SKIP**RSQGCSREASPSRLSVARS**SRIP**RPSVGS
Tandem	**SKIP-SKIP-**iLID	ENIRSAAKP**SKIP**RSQGCSREASPSRLSVARP**SKIP**RPSVGS
Dimeric	**SKIP-*LZ*-**iLID	ENIRSAAKP**SKIP**TPQRKSPASGSGSGS***RMKQLEDKVEELL SKNYHLENEVARLKKLVGER***GSG

intensities revealed that the levels of monomeric and tandem SxIP-iLID constructs on MT plus ends were only slightly enhanced above their respective cytoplasmic level (~1.2x) whereas the level of the dimeric SKIP-LZ-iLID construct on MT plus ends was 2.3 times higher than cytoplasmic, similar to the ratio measured for EB1-GFP (Fig. 2.1D). Analysis of the observable GFP comet density revealed that the SKIP-LZ-iLID construct yielded the highest level (0.26 ± 0.07 comets per μm^2), just below that of EB1-GFP (0.30 ±0.10 comets per μm^2) (Fig. 2.1E). The monomeric construct showed the lowest number of observable comets (0.06 ± 0.03 comets per μm^2) and the tandem constructs showed an intermediate number (SKIP-SKIP-iLID 0.13 ± 0.05, SKIP-SRIP-iLID 0.12 ± 0.04 comets per μm^2) (Fig. 2.1E). While the monomeric and tandem SxIP-iLID constructs exhibited varying degrees of nuclear localization, the SKIP-LZ-iLID construct showed minimal nuclear localization. As a test tool, we generated a constitutively active, lit mimetic construct, SKIP-LZ-iLID^{Lit} (iLID^{I539E})(Harper et al., 2004, Lungu et al., 2012), that is competent to bind SspB without blue light activation. SKIP-LZ-iLID^{Lit} robustly tracked MT plus ends (Fig. 2.1C)

To determine if SxIP-iLID constructs altered MT plus end polymerization rates, we tracked individual eGFP-SxIP-iLID comets over time. There was no significant difference between the EB1 control and the monomeric SKIP-iLID construct, nor the dimeric SKIP-LZ-iLID WT, however, there was a slight increase in the average comet velocities for the tandem SxIP-iLID constructs (Fig. 2.1F).

To determine if SxIP-iLID construct expression level, or the amount of SxIP-iLID construct at MT plus ends affected comet velocities we analyzed the total cell intensity/cell area and the MT comet/cytoplasmic intensities in each cell and plotted this against the average comet velocity. We also analyzed the GFP comet intensity per area versus the

cytoplasmic intensity per area as well as the density of GFP positive comets versus the average GFP comet/cytoplasmic intensity ratio per cell, and calculated the Pearson's correlation coefficient (Fig. S2.1A-D). We observed that EB1 showed a slightly significant correlation ($p=0.039$) between comet velocity per cell versus the ratio of eGFP comet intensity/cytoplasmic intensity (Fig. S21B). Interestingly, the expression level of EB1 did not correlate with comet velocity (Fig. S21A) and the ratio of eGFP comet intensity/cytoplasmic intensity did not correlate with the number of observed comets per area (Fig. S21D). This observation is in line with previous in vitro reconstitution work that found that the levels of *S. pombe* EB1 (Mal3) at MT plus ends increased with comet speed, as did the length of the Mal3-eGFP comet (Bieling et al., 2007). This indicates that fast growing MT plus ends have more lattice area that is in the GTP hydrolysis transition state / post hydrolysis GDP-Pi state, that EB1 can engage. That this trend was not observed with the iLID constructs suggests that it was detectable only when EB1 was expressed above endogenous levels. The only SxIP-iLID construct that showed a slightly significant correlation between total cell intensity or plus end fluorescence intensity with comet velocity was the tandem SKIP-SRIP-iLID construct (velocity versus total cell intensity/cell area: positive correlation ($p=0.017$) and velocity versus MT comet/cytoplasmic intensity: negative correlation ($p=0.036$)). We cannot explain why this occurred for the SKIP-SRIP iLID construct and not the other iLID constructs analyzed (such as the SKIP-SKIP iLID construct). The opposite correlations may reflect a preferential, low affinity binding of the SKIP-SRIP iLID construct to a specific EB dimer, such as the EB1-EB3 heterodimer, or EB2, that is not preferentially targeted by the other SxIP-iLID constructs. Whether the binding of SKIP-SRIP to EB1-EB3 heterodimers or EB2 homodimers stabilizes these EBs or cross-links them to other EBs to yield enhanced MT

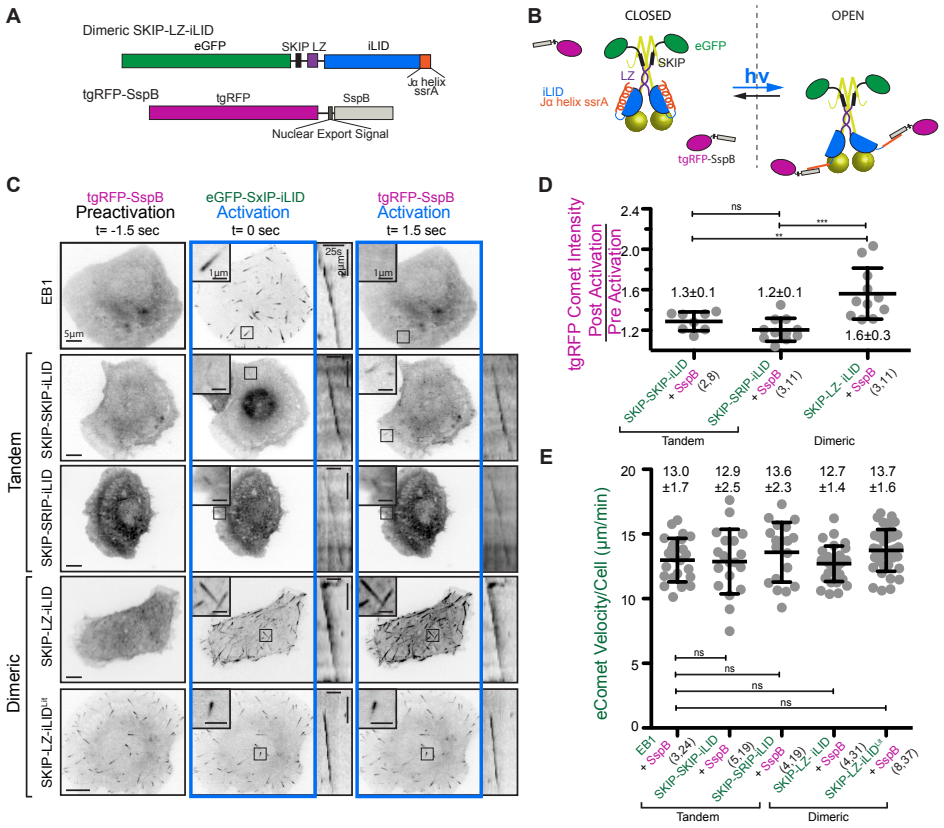

Figure 2.2. Photoactivated SxIP-iLID constructs rapidly recruit tgRFP-SspB to MT plus ends without altering MT comet velocities. **(A)** Diagram of SKIP-LZ-iLID and tgRFP-SspB constructs. **(B)** Cartoon diagraming the binding of tgRFP-SspB to SKIP-LZ-iLID upon blue light activation (hν). SKIP-LZ-iLID localizes to MT plus ends via association with EB dimers. When exposed to blue light the iLID Jα helix releases from the LOV domain. The ssrA motif embedded in the Jα helix becomes accessible to bind SspB and thereby recruits tgRFP-SspB to MT plus ends. **(C)** Representative images of S2 cells co-transfected with either a tandem SxIP-iLID construct or a dimeric SKIP-LZ-iLID construct and a tgRFP-SspB control construct, repeatedly pulsed with blue light (700 msec) every 3 seconds at 488 nm. Representative images are of tgRFP-SspB localization pre and post photoactivation in *Drosophila* S2 cells. The SKIP-LZ-iLID^{Lit} construct is constitutively competent to bind SspB in the absence of blue light. Scale bars at left, 5 μm, inset scale bar, 1 μm. Kymograph scale bars: 2 μm, 25 seconds. **(D)** The post activation/preactivation ratio of mean tgRFP comet intensity demonstrating effective tgRFP-SspB recruitment. tgRFP comet intensity per area on a MT plus end was calculated relative to the mean intensity per area in an adjacent cytoplasmic region. The dimeric SKIP-LZ-iLID construct shows the greatest post-activation enrichment on MT plus end comets. **(E)** SxIP-iLID-based recruitment of tgRFP-SspB to MT plus ends does not significantly alter mean MT plus end comet velocities compared to control cells co-transfected with EB1-GFP and tgRFP-SspB. Error bars indicate SD. Numbers in parenthesis indicate (number of experiments, total number of cells quantified). P-values were determined by two-way unpaired Student's t-test. ** p<0.005, ***p<0.0005.

polymerization rates remains to be determined. There is a statistically significant, positive correlation between eGFP comet intensity per area and cytoplasmic intensity per area for all constructs analyzed (Fig. S2.1C), indicative that eGFP construct expression level relates directly to the amount of eGFP at MT plus ends. None of the iLID constructs yielded a statistically significant correlation between the number of comets per area and the ratio of eGFP comet/cytoplasmic intensity (Fig. S2.1D). However, apparent iLID plus end localization may be limited by the relative amounts of iLID constructs versus endogenous EB levels. Additionally, the dimeric iLID construct may show enhanced MT plus end localization because it effectively has two GFP modules rather than one as found in the monomeric and tandem SxIP-iLID constructs.

This establishes four SxIP-iLID constructs with differential MT plus end tracking activities and highlights the interesting observation that specific, multivalent EB-binding scaffolds can themselves affect (enhance) MT growth rates.

2.2.2 The SxIP-iLID switch recruits tgRFP-SspB upon photactivation

To determine whether the SxIP-iLID constructs could recruit an SspB-tagged protein to polymerizing MT plus ends we observed localization of a tgRFP-SspB construct pre and post photoactivation (Fig. 2.2, A-C). We transfected *Drosophila* S2 cells with a SxIP-iLID construct (either a tandem SxIP-iLID construct or the SKIP-LZ-iLID construct) as well as tgRFP-SspB (Fig. 2.2A). Prior to blue light photoactivation, tgRFP-SspB had a diffuse cytoplasmic signal (Fig. 2.2C). Strikingly, upon blue light photoactivation, tgRFP-SspB rapidly colocalized with the SxIP-iLID constructs at polymerizing MT plus ends (Fig. 2.2C). This demonstrates that blue light can effectively liberate the SsrA sequence from its dark state embedded conformation in the iLID Jα helix, to an open conformation competent to

bind and recruit an SspB-tagged protein to the MT plus end. As observed with the SxIP-iLID modules, more robust tgRFP-SspB MT plus end recruitment was observed with the dimeric SKIP-LZ-iLID construct (Fig. 2.2C and D). In comparison, the constitutively active lit mimetic (SKIP-LZ-iLID^{Lit}) recruited tgRFP-SspB to MT plus ends both pre- and post-blue light exposure, demonstrating the efficacy of ssrA-SspB engagement (Fig. 2.2C). To determine if recruitment of tgRFP-SspB to MT plus ends altered comet velocities we continuously activated SxIP-iLID constructs with pulses of blue light, thereby maintaining SxIP-iLID-tgRFP-SspB interaction and tgRFP-SspB MT plus end localization over time. Using the eGFP signal from the SxIP-iLID constructs, we again acquired time-lapse movies and used MTrackJ to determine comet velocities (Fig. 2.2E). tgRFP-SspB MT plus end recruitment via dimeric SKIP-LZ-iLID yielded comet velocities that were not statistically different from control cells containing tgRFP-SspB and EB1-GFP and no SxIP-iLID construct. Continually activated tandem SxIP-iLID constructs also recruited tgRFP-SspB to MT plus ends, and did not alter comet velocities as compared to the tandem SxIP-iLID construct alone (Fig. 2.2E). Monomeric SKIP-iLID construct plus end tracking activity was too weak to ascertain tgRFP-SspB MT plus end recruitment and was not pursued further. This establishes a two-component blue light-inducible heterodimerization system for recruiting proteins of interest to MT plus ends with temporal resolution.

2.2.3 tgRFP-SspB MT plus end recruitment is rapidly reversible

In order for an optogenetic system to regulate cytoskeletal dynamics with spatial and temporal efficacy, the system must transition to an active or inactive state within seconds. We observed rapid (< 1.5 second) recruitment of tgRFP-SspB to MT plus ends that peaked between 12 and 33 seconds post activation (Figs. 2.2C, 3A and B). The decay of tgRFP-SspB

signal from MT plus ends post activation reflects an apparent dissociation rate. This rate is a convolution of many factors including the nucleotide state of tubulin at growing MT plus ends, the association kinetics of EB to the MT plus end, SxIP-EB binding, inherent kinetics between the iLID lit and dark state conformations in the presence and absence of blue light, and the association kinetics of the ssrA sequence with SspB (Fig. 2.3B (inset)). We defined the apparent off-rate as the rate of loss of tgRFP-SspB fluoresence from MT plus ends post blue light exposure after peak recruitment of tgRFP-SspB. *Drosophila* S2 cells co-transfected with SKIP-LZ-iLID and tgRFP-SspB were exposed to blue light to activate tgRFP-SspB plus end tracking. Time lapse images to monitor tgRFP-SspB localization were initiated at 3 second intervals and blue light exposure was terminated, enabling the iLID system to return to the dark state (Fig. 2.3A and B). Whole cell tgRFP-SspB comet intensities were quantitated over time. tgRFP-SspB MT plus end tracking activity observed in the frame following blue light activation showed an initial increase in signal over a 30 sec timeframe and then decayed with an apparent half life of 25.1 ± 6.7 seconds (Fig. 2.3B). The apparent MT plus end off rate of the system indicates that it can deactivate within a timeframe appropriate for probing many cytoskeletal activities. This apparent decay rate is on par with the reported *in vitro* iLID decay rate (18 ± 2 sec.) and cellular iLID decay rates in systems designed for membrane localization (52.5 ± 2 sec.) and mitochondrial localization (23.2 ± 1.5 sec.) (Hallett et al., 2016). Once tgRFP-SspB dissociated from MTs, it could again be recruited to MT plus ends, demonstrating the system's efficacy for multiple, reiterative recruitment cycles (Fig. 2.3C). However, we did observe decreasing levels of recruitment over time. This may be due to photo damage to tgRFP and the LOV domain's chromophore as well as limits in the ability of the iLID to structurally cycle between lit and dark states.

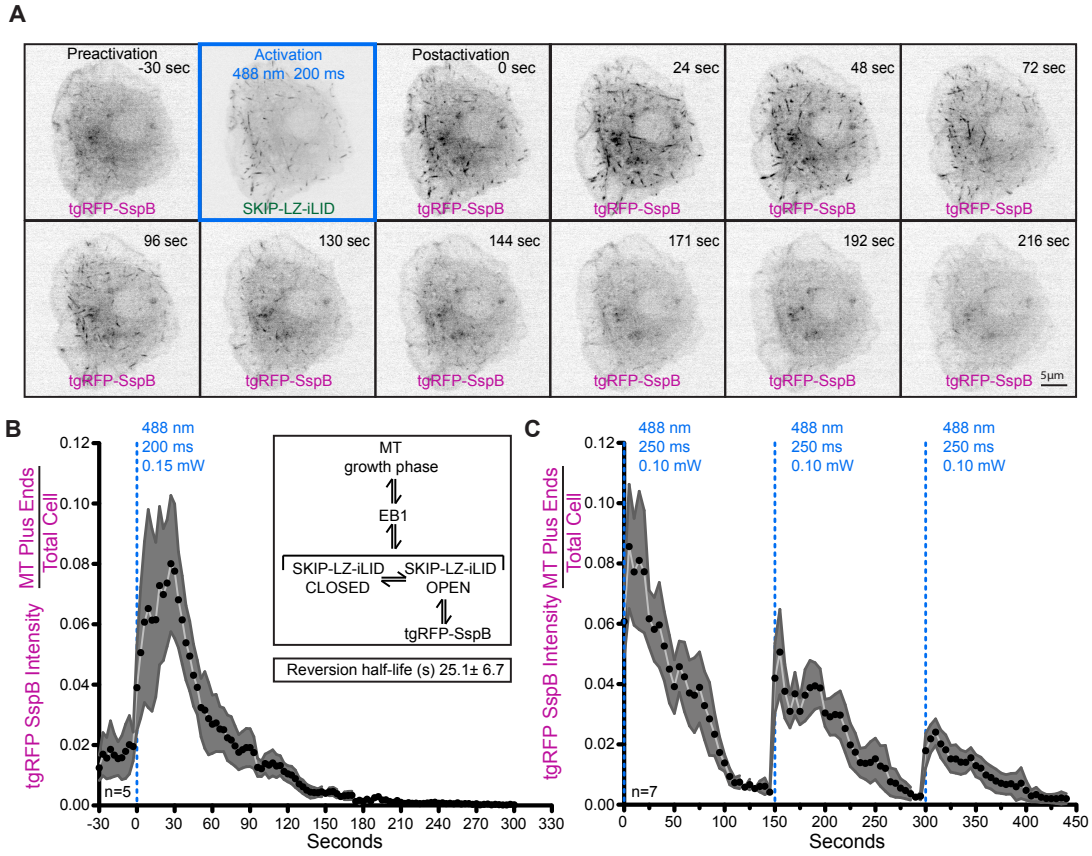

Figure 2.3. Dynamics of blue light-dependent tgRFP-SspB MT plus end recruitment and dissociation. (A) Montage of tgRFP-SspB pre activation and post activation in a *Drosophila* S2 cell co-transfected with eGFP-SKIP-LZ-iLID. Time in seconds is relative to t=0 at which time the cell was activated with a single 200 msec pulse of 0.15 mW 488 nm light. The montage shows blue light-dependent tgRFP-SspB recruitment to MT plus ends as well as subsequent dissociation over time. Scale bar, 5 µm. **(B)** Plot displaying the apparent cellular kinetics of tgRFP-SspB association to, and disassociation from, MT plus ends over time. The system was activated at t=0 with a single pulse of 0.15 mW 488 nm light. n=5 cells. In cells co-transfected with SKIP-LZ-iLID, tgRFP-SspB immediately associates with MT plus ends, reaches maximal recruitment within 30 seconds post activation, and dissociates within 90 seconds. Inset shows the general kinetic steps that enable tgRFP-SspB MT plus end association, the convolution of which yields the apparent kinetics observed. The apparent half-life of tgRFP-SspB on the MT plus end post activation is 25.1 ± 6.7 sec. **(C)** Multiple rounds of activation of cells co-transfected with SKIP-LZ-iLID and tgRFP-SspB show the ability of tgRFP-SspB to be recruited to MT plus ends multiple times. Cells were activated at t=0, t=150, and t=300 seconds with a single pulse of 0.10 mW 488 nm light n=7 cells. For (B) and (C) black points and grey area represent the mean and SEM respectively.

2.2.4 Cross-linking MT plus ends to the F-actin network decreases MT growth rates and increases the area of the cell void of MTs in *Drosophila* S2 cells

Cytoskeletal networks are cross-linked and their dynamic actions integrated and regulated. How cross-linking dictates downstream cell morphological changes is poorly understood. To understand how coupling of the F-actin and MT cytoskeleton networks affects MTs and MT network architecture, we examined how the optogenetic recruitment of an F-actin binding domain to MT plus ends would affect MT dynamics. Spectaplakins are large MT-F-actin cross-linking proteins with N-terminal tandem calponin homology domains (CH-CH) that bind F-actin and a C-terminal MT-binding module that includes a MT-binding GAR domain and an EB-binding SxIP motif that collectively localize spectraplakins to MT plus ends (Fig. 2.4A). We fused the tandem CH-CH domain from the sole *Drosophila* -spectraplakin Shot to tgRFP-SspB (Fig. 2.4A) and co-transfected *Drosophila* S2 cells with CH-CH-tgRFP-SspB and SKIP-LZ-iLID. Pre-activation, the CH-CH-tgRFP-SspB construct demonstrated retrograde flow-like behavior, indicative of coupling to the dynamic F-actin lamellar network (Fig. 2.4A'). We next pulsed cells with blue light, and monitored eGFP and tgRFP signals. CH-CH-tgRFP-SspB was robustly recruited to MT plus ends upon blue light activation (Fig. 2.4B). We tracked eGFP comets to determine how CH-CH-tgRFP-SspB recruitment affected MT plus end comet velocities. Surprisingly, MT plus end comet velocities decreased dramatically from 11.6 ± 1.9 μm/min (tgRFP-SspB control) to 7.3 ± 2.1 μm/min when CH-CH-tgRFP-SspB was recruited to MT plus ends (Fig. 2.4D). To determine the long-term effect of MT-actin cross-linking on MT dynamics we co-transfected cells with the constitutively lit mimetic, SKIP-LZ-iLID^{Lit}, and CH-CH-tgRFP-SspB (Fig. 2.4C), induced expression of the iLID construct, and analyzed cells 24-30 hours post induction. MT comet

cross-linked) (Fig. 2.4B-D). These data suggest that within a short time frame (3 minutes) MT comet velocities are slowed and remain slowed to the same degree as after a 24-30 hour period of constitutive cross-linking. Blue-light induced MT plus end-F-actin cross-linking also resulted in a dramatic exclusion of MT plus ends from the lamellar region (Fig. 2.4B and C (max projections, see arrowheads) and E). When cells expressing CH-CH-tgRFP-SspB and SKIP-LZ-iLID were continuously activated for 3 minutes, the ability of MTs to enter the F-actin-rich lamellar zone of the cell was compromised. Figure 2.4C shows maximum intensity projections of 60 frames (3 minutes of activated cross-linking) illustrating the dramatic change in the distribution of MTs within the cell upon cross-linking. The area of the cell void of MTs increased from 8.1 ± 4.2% to 12.4 ± 5.7% (Fig. 2.4E). This MT void region was further enhanced (18.7 ± 10.3% of the cell's area) when the SKIP-LZ-iLID^{Lit} construct was used with the CH-CH-tgRFP-SspB construct to induce long-term (24-30 hours) cross-linking. To determine if this void area lacked all MTs we fixed and stained SKIP-LZ-iLID^{Lit} expressing cells for tubulin. In cells co-transfected with CH-CH-SspB (but not SspB control cells), peripheral areas devoid of SKIP-LZ-iLID^{Lit} also lacked MTs (Fig. S2.2A). We then fixed and stained SKIP-LZ-iLID^{Lit} expressing cells for actin and observed actin in the lamellar regions of cells, overlapping with the peripheral zone devoid of MTs in cells co-transfected with CH-CH-SspB (Fig. S2.2B and C). These data suggest that the dynamic branched F-actin network in the lamella immediately engaged growing MT plus ends and continuously restricted their entry into the periphery of the cell.

2.2.5 The effects of MT-F-actin cross-linking are F-actin-dependent

To determine if the decrease in MT comet velocity and the increase in MT-void area in cross-linked cells were F-actin-dependent, we treated SKIP-LZ-iLID^{Lit}-transfected cells

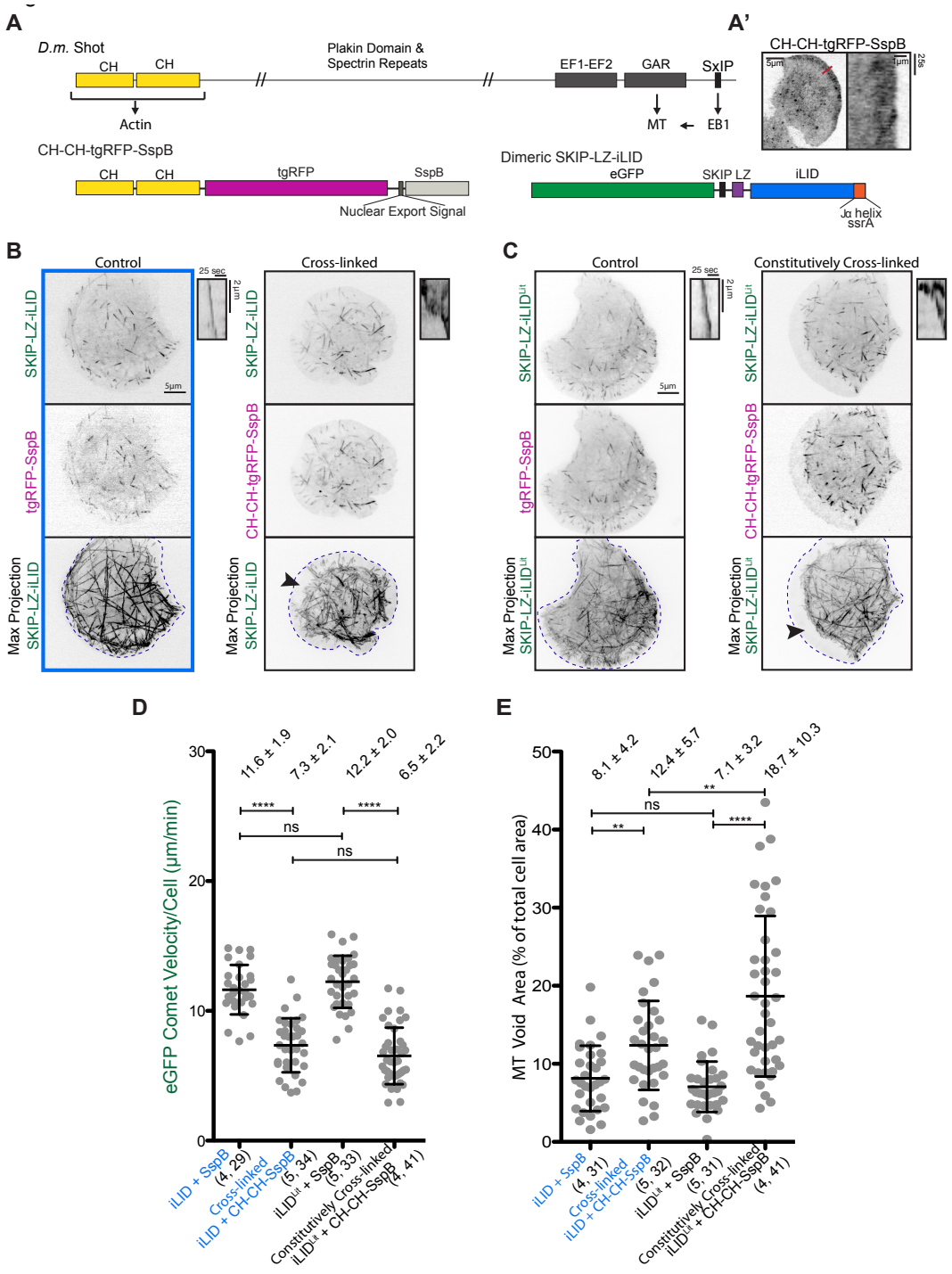
A
D.m. Shot
CH
CH
Actin
Plakin Domain &
Spectrin Repeats
EF1-EF2
GAR
SxIP
MT
EB1
A'
CH-CH-tgRFP-SspB
CH-CH-tgRFP-SspB
tgRFP
SspB
Nuclear Export Signal
Dimeric SKIP-LZ-iLID
eGFP
SKIP LZ
iLID
Jα helix
ssrA
B
Control
Cross-linked
SKIP-LZ-iLID
tgRFP-SspB
CH-CH-tgRFP-SspB
Max Projection
25 sec
2μm
5μm
C
Control
Constitutively Cross-linked
D
eGFP Comet Velocity/Cell (μm/min)
11.6 ± 1.9
7.3 ± 2.1
12.2 ± 2.0
6.5 ± 2.2
****
ns
ns
****
iLID + SspB (4, 29)
Cross-linked iLID + CH-CH-SspB (5, 34)
iLID^Lit + SspB (5, 33)
Constitutively Cross-linked iLID^Lit + CH-CH-SspB (4, 41)
E
MT Void Area (% of total cell area)
8.1 ± 4.2
12.4 ± 5.7
7.1 ± 3.2
18.7 ± 10.3
**
ns
**
****
iLID + SspB (4, 31)
Cross-linked iLID + CH-CH-SspB (5, 32)
iLID^Lit + SspB (5, 31)
Constitutively Cross-linked iLID^Lit + CH-CH-SspB (4, 41)

Figure 2.4. Optogenetically-induced cytoskeletal cross-linking decreases MT comet velocities and increases the MT void area. **(A)** Schematic of the *Drosophila* spectraplakin family member Shot (*D.m.* Shot). Shot contains tandem N-terminal CH domains that bind F-actin, a C-terminal GAR domain that binds MTs, and a SxIP motif that confers MT plus end localization. We functionally parsed the bivalent F-actin- and MT-binding activity of Shot into the two components of our iLID MT plus end tracking system. Shot's tandem CH domains were fused to tgRFP-SspB. The SKIP-LZ-iLID construct tracks MT plus ends using a SxIP motif from the mammalian spectraplakin MACF2. (A') Image of CH-CH-tgRFP-SspB in a transfected *Drosophila* S2 cell (left). Scale bar, 10 μm. The kymograph at right represents a time-lapse of the red line scan at left, and shows retrograde movement of the CH-CH-tgRFP-SspB construct in the lamellar region. Kymograph scale bars: 1 μm, 25 seconds. **(B)** Representative images of S2 cells co-transfected with eGFP-SKIP-LZ-iLID and either a tgRFP-SspB control, or the F-actin-binding CH-CH-tgRFP-SspB construct, and repeatedly pulsed with blue light (250 msec every 3 seconds at 488 nm). Top and middle panels show single images from the GFP and RFP channels. Scale bar, 5 μm. Kymographs at right show representative eGFP-SKIP-LZ-iLID plus end comets. Kymograph bars, 2 μm, 25 sec. Max projections of 60 frames (total 3 min) are shown below, revealing the area of the cell traversed by eGFP-SKIP-LZ-iLID-containing MT plus ends. Areas void of MT plus ends can be seen in the cross-linked cell (arrowhead). Blue boxes indicate blue light recruitment of tgRFP-SspB constructs. **(C)** Representative images of S2 cells co-transfected with eGFP-SKIP-LZ-iLID^{Lit} and either a tgRFP-SspB control, or the F-actin-binding CH-CH-tgRFP-SspB construct. Top and middle panels show single images from the GFP and RFP channels. Scale bar, 5 μm. Kymographs at right show representative eGFP-SKIP-LZ-iLID^{Lit} plus end comets. Kymograph bars, 2 μm, 25 seconds. Max projections of 60 frames (total 3 minutes) are shown below, revealing the area of the cell traversed by eGFP-SKIP-LZ-iLID^{Lit}-containing MT plus ends. Areas void of MT plus ends can be seen in the constitutively cross-linked cell. **(D)** eGFP comet velocity/cell (μm/min) for control cells (iLID +SspB and iLID^{Lit}+SspB), light-activated cross-linked cells (iLID + CH-CH-SspB) and constitutively cross-linked cells (iLID^{Lit} + CH-CH-SspB). Cells with blue light-activated cross-linking and with constitutively cross-linked MT and F-actin networks show decreased eGFP comet velocities compared to control cells. Numbers in parenthesis indicate: (number of experiments, total number of cells quantified). Line represents the mean, error bars indicate SD. P-values were determined by two-way unpaired Student's *t* test. **** $p<0.0001$. **(E)** MT void area as a percentage of the total cell area for control and cross-linked cells. Max projection images of 60 frames (spanning 3 minutes) were used to determine the area of the cell void of MTs (representative image used for quantification are shown in B and C. Blue light-activated cross-linked and constitutively cross-linked cells show an increase in the area of the cell void of MTs. Numbers in parenthesis indicate: (number of experiments, total number of cells quantified). Line represents the mean, error bars indicate SD. P-values were determined by two-tailed nonparametric Mann–Whitney *U* test. *$p<0.05$, **$p<0.005$, **** $p<0.0001$.

with latrunculin A (LatA) to inhibit F-actin assembly. Titrating LatA significantly reduced the ability of the CH-CH-tgRFP-SspB construct to retard MT growth rates (Fig. 2.5A and B). In cells in which CH-CH-tgRFP-SspB was constitutively recruited to MT plus ends, the mean MT growth velocity was partially restored to WT levels with 2 nM LatA (8.9 ± 2.7 μm/min) while 2 μM LatA resulted in a mean MT growth velocity that exceeded that observed in the control tgRFP-SspB transfected cells (13.9 ± 3.9 μm/min vs. 12.2 ± 1.9 μm/min) (Fig. 2.5B). This result could potentially be due to liberating MTs from endogenous MT-F-actin cross-linking activity. The ability of the CH-CH-tgRFP-SspB construct to exclude MTs from the peripheral zone was also F-actin-dependent as titrating LatA promoted the ability of MTs to fully occupy the peripheral zone of the cell (Fig. 2.5A, max projection). When the MT-void area was quantified in cells in which CH-CH-tgRFP-SspB was constitutively recruited to MT plus ends, 2 nM LatA treatment lead to a slight decrease in the MT-void area compared to DMSO control-treated cells (13.4 ± 5.8 % vs. 17.4 ± 7.3 %) while 2 μM LatA treatment dramatically decreased the MT-void area to 4.1 ± 3.0 %, significantly less than that of SspB control transfected cells treated with DMSO (7.3 ± 3.2 %), suggesting again that endogenous cross-linkers promote MT exclusion from the lamellar zone (Fig. 5C). In support, the MT-void region in SspB control transfected cells was further reduced when treated with 2 μM LatA (4.4 ± 2.9 %, not significantly different from the CH-CH-tgRFP-SspB transfected cells).

2.2.6 MT-F-actin cross-linking decreases comet velocities and increases the MT void area in a MT plus end-dependent manner

To determine if the decrease in MT comet velocity and increase in the MT-void area were dependent on MT plus end engagement we co-transfected cells with a CH-CH- tgRFP

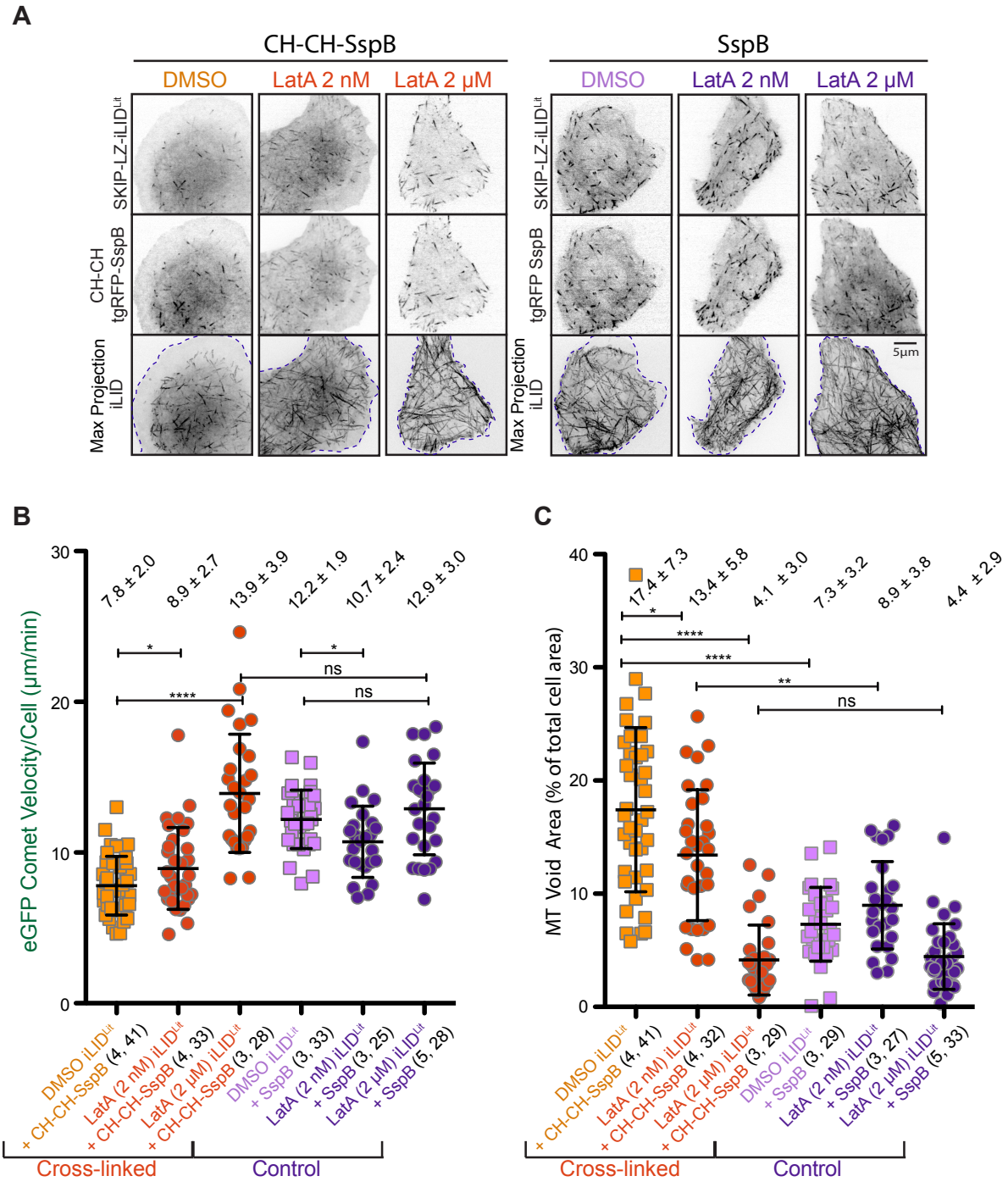
A
CH-CH-SspB
SspB
DMSO
LatA 2 nM
LatA 2 µM
DMSO
LatA 2 nM
LatA 2 µM
SKIP-LZ-iLID^Lit
CH-CH tgRFP-SspB
Max Projection iLID
SKIP-LZ-iLID^Lit
tgRFP SspB
Max Projection iLID
5µm
B
eGFP Comet Velocity/Cell (µm/min)
7.8 ± 2.0
8.9 ± 2.7
13.9 ± 3.9
12.2 ± 1.9
10.7 ± 2.4
12.9 ± 3.0
*
****
*
ns
ns
DMSO iLID^Lit
+ CH-CH-SspB (4, 41)
LatA (2 nM) iLID^Lit
+ CH-CH-SspB (4, 33)
LatA (2 µM) iLID^Lit
+ CH-CH-SspB (3, 28)
DMSO iLID^Lit
+ SspB (3, 33)
LatA (2 nM) iLID^Lit
+ SspB (3, 25)
LatA (2 µM) iLID^Lit
+ SspB (5, 28)
Cross-linked
Control
C
MT Void Area (% of total cell area)
17.4 ± 7.3
13.4 ± 5.8
4.1 ± 3.0
7.3 ± 3.2
8.9 ± 3.8
4.4 ± 2.9
*
****
****
**
ns
DMSO iLID^Lit
+ CH-CH-SspB (4, 41)
LatA (2 nM) iLID^Lit
+ CH-CH-SspB (4, 32)
LatA (2 µM) iLID^Lit
+ CH-CH-SspB (3, 29)
DMSO iLID^Lit
+ SspB (3, 29)
LatA (2 nM) iLID^Lit
+ SspB (3, 27)
LatA (2 µM) iLID^Lit
+ SspB (5, 33)
Cross-linked
Control

Figure 2.5. Optogenetically induced cross-linking decreases MT comet velocities and increases the area void of MT plus ends in an F-actin dependent manner. (A) Representative images of eGFP-SKIP-LZ-iLID^{Lit} co-expressed with CH-CH-tgRFP-SspB or tgRFP-SspB in S2 cells treated with DMSO as a control, or Latrunculin A (LatA; 2 nM or 2 μM) for one hour prior to imaging. Top and middle panels show GFP and RFP channels respectively. Bottom panel: max projections of the GFP channel (60 frames collected over 3 min) show that in constitutively cross-linked cells, MT comets are excluded from the peripheral region in DMSO control treated cells, but when the actin network is depolymerized via treatment with LatA, MT comets traverse all the way to the cell edge. Scale bar: 5 μm. **(B)** eGFP comet velocity/cell (μm/min) for control cells (SKIP-LZ-iLID^{Lit} + SspB) and constitutively cross-linked cells (SKIP-LZ-iLID^{Lit} + CH-CH-SspB) treated with DMSO or LatA (2 nM or 2 μM). Constitutively cross-linked cells treated with LatA show an increase in comet velocities compared to DMSO treated cells. Numbers in parenthesis indicate: (number of experiments, total number of cells quantified). Central lines represent the mean, error bars indicate SD. P-values were determined by two-way unpaired Student's *t* test. * $p<0.05$, **** $p<0.0001$. **(C)** MT void area as a percentage of the total cell area for constitutively cross-linked cells and control cells treated with DMSO, 2 nM LatA, or 2 μM LatA. Max projection images of 60 frames (collected over 3 minutes) were used to determine the area of the cell void of growing MT plus ends (representative image used for quantification shown in A). MT void area decreased in constitutively cross-linked cells with the addition of LatA as compared to control DMSO treatment. Numbers in parenthesis indicate: (number of experiments, total number of cells quantified). Central lines represent the mean, error bars indicate SD. P-values were determined using a two-tailed nonparametric Mann–Whitney *U* test. * $p<0.05$, ** $p<0.005$, ***$p<0.0005$, **** $p<0.0001$.

construct lacking the SspB domain and either SKIP-LZ-iLID or SKIP-LZ-iLID^{Lit} (Fig. 2.6A). In contrast to the dramatically decreased comet velocities observed when CH-CH-tgRFP-SspB was recruited to MT plus ends (7.3 ± 2.1 μm/min in SKIP-LZ-iLID-expressing cells and 6.5 ± 2.2 μm/min in SKIP-LZ-iLID^{Lit} expressing cells), expressing CH-CH-tgRFP yielded MT comet velocities of 9.5 ± 2.2 μm/min and 9.8 ± 1.4 μm/min in SKIP-LZ-iLID and SKIP-LZ-iLID^{Lit} expressing cells, respectively (Fig. 2.6B). This indicates that recruiting the F-actin-binding CH-CH domain to MT plus ends effectively retards MT comet velocities. Expressing the CH-CH-tgRFP construct that lacked iLID binding capabilities did yield slightly reduced MT comet velocities (9.5 ± 2.2 μm/min tgRFP-CH-CH vs. 11.6 ± 1.9 μm/min tgRFP-SspB control) which may be the result of CH-CH-dependent effects on the stability and/or density of the F-actin network, which in turn could affect MT comet velocity. Although CH-CH-tgRFP expression partially reduced MT comet velocities, MTs were still able to enter the lamellar region (Fig. 2.6A, max projection) which contrasts with the MT exclusion observed when CH-CH-tgRFP-SspB was recruited to MT plus ends. In cells expressing CH-CH-tgRFP and SKIP-LZ-iLID or SKIP-LZ-iLID^{Lit}, the MT-void area was not significantly different than in control cells (Fig. 2.6C). These data show that cross-linking of the F-actin and MT networks leads to decreased MT comet velocities and an increase in the area of the cell void of MTs in an F-actin and MT plus end-dependent manner. Cross-linking rapidly stalls MTs and prevents entry into the peripheral region of the cell.

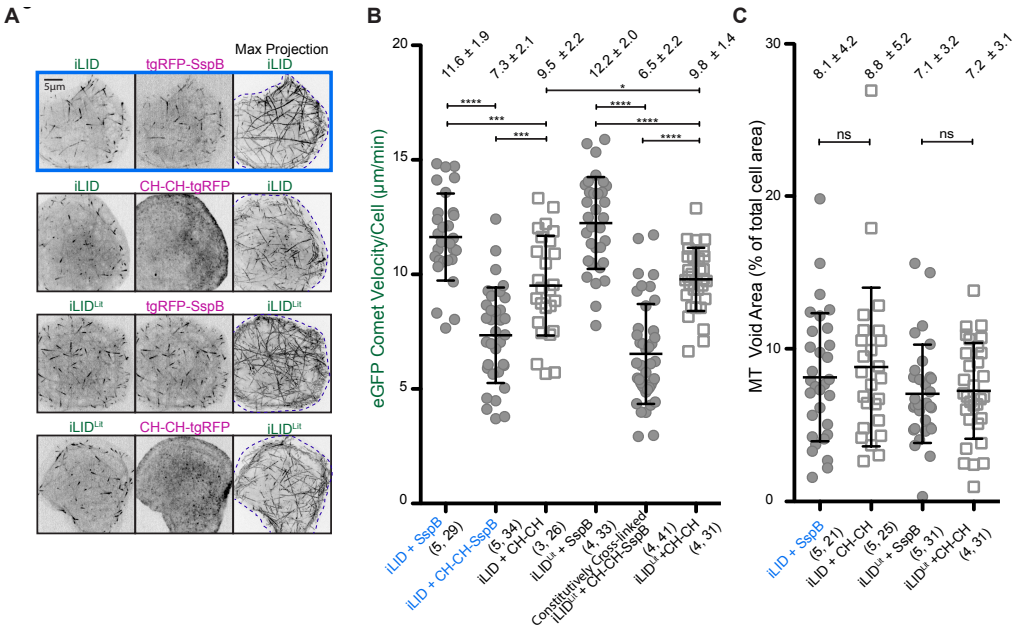

Figure 2.6. CH-CH MT plus end recruitment is required to decrease MT comet velocities and generate a peripheral zone where MTs are excluded. (A) Representative still images of SKIP-LZ-iLID or SKIP-LZ-iLID^{Lit} co-expressed with CH-CH-tgRFP or tgRFP-SspB in cells, showing GFP and RFP channels. Panels at right: max projections of 60 frames (collected over 3 minutes) showing the area traversed by MT plus ends. Scale bar: 5 μm. **(B)** eGFP comet velocity/cell (μm/min) for cross-linked control cells (SKIP-LZ-iLID + SspB activated with blue light and SKIP-LZ-iLID^{Lit} + SspB) and cells transfected with a CH-CH-tgRFP construct that binds F-actin, but lacks the SspB domain that mediates cross-linking to MT plus ends (SKIP-LZ-iLID + CH-CH and SKIP-LZ-iLID^{Lit} + CH-CH). Cells in which the CH-CH construct engages the actin network but cannot engage MT plus ends yields MT comet velocities that are near to control, non-cross-linked velocities. Numbers in parenthesis indicate: (number of experiments, total number of cells quantified). Central lines represent the mean, error bars indicate SD. P-values were determined by two-way unpaired Student's *t* test. * p<0.05, ***p<0.0005, **** p<0.0001. **(C)** Area void of MT plus ends as a percentage of the total cell area for control cells (SKIP-LZ-iLID + SspB activated with blue light and SKIP-LZ-iLID^{Lit} + SspB) and cells in which the CH-CH construct engages the actin network, but is not cross-linked to MT plus ends (SKIP-LZ-iLID + CH-CH and SKIP-LZ-iLID^{Lit} + CH-CH). Max projection images of 60 frames (collected over 3 minutes) were used to determine the area of the cell void of MT plus ends (representative image used for quantification shown in A). The MT void area does not change significantly if MT plus ends do not engage the CH-CH construct. Numbers in parenthesis indicate (number of experiments, total number of cells quantified). Central lines represent the mean, error bars indicate SD. P-values were determined using a two-tailed nonparametric Mann–Whitney *U* test.

2.2.7 MT-F-actin cross-linking decreases comet velocities in all regions of the cell and alters MT behavior

We next examined the effect of cross-linking on MT behavior in different regions of the cell, comparing MT plus end comets from constitutively cross-linked cells (co-transfected with SKIP-LZ-iLID^{Lit} + CH-CH-SspB) with those of control cells (co-transfected with SKIP-LZ-iLID^{Lit} + CH-CH) (Fig. 2.7). We delineated three cellular regions: peripheral zone, boarder, and center, and scored MT plus end comet behavior within or across these regions categorically (Fig.7A). Comet velocities in all regions of the cell were significantly decreased except for comets that traveled from the boarder to the peripheral zone as this group was poorly represented in control cells (Fig.7 A and B). The reduction in average velocity varied across categories, was greatest for comets within the boarder whose trajectories were not parallel to the periphery (Δ = -3.3 μm/min), and was the least for comets within the peripheral zone (Δ = -1.7 μm/min).

We next calculated the percentage of MT plus end comets in each category (Fig. 2.7B, number above plots). Cross-linked cells displayed a significant decrease in the percentage of comets traveling from the cell center into the boarder region (9.7% versus 19.0% in non cross-linked cells) and peripheral zone (4.2% versus 13.4% in non cross-linked cells) (Fig. 2.7B). Cross-linked cells also had an increase in the percentage of MT plus end comets that approached the peripheral zone and were swept along its boundary (12.7 % of comets in cross-linked cells, versus 4.3% in non cross-linked cells) (Fig. 2.7B). These data show that cytoskeletal cross-linking limits MT entry into the F-actin-rich peripheral zone and promotes MT plus end sweeping parallel to the zone's edge, thus driving MT exclusion from the region (Fig. 2.8).

Figure 7

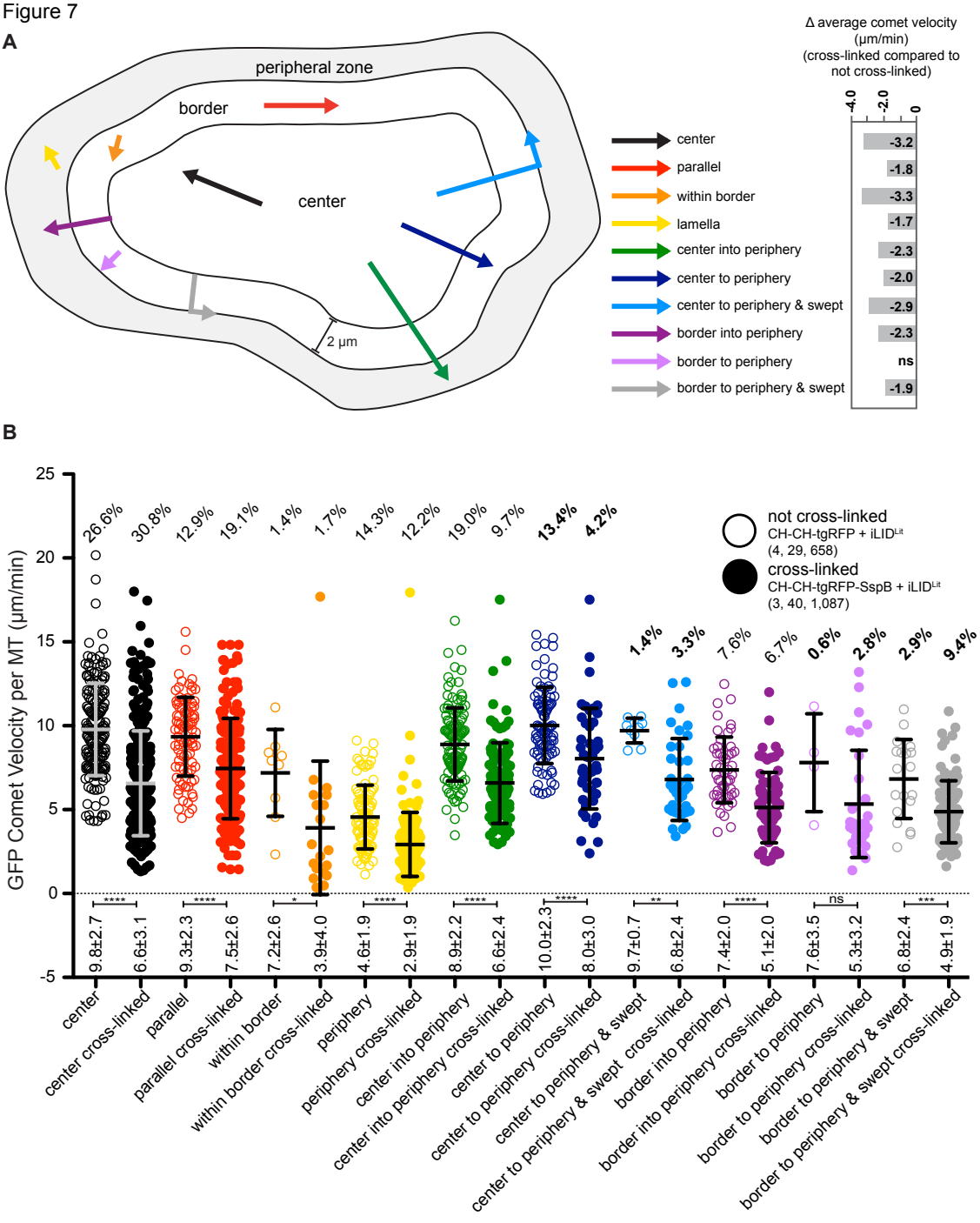
A
peripheral zone
border
center
2 µm
Δ average comet velocity (µm/min) (cross-linked compared to not cross-linked)
-4.0
-2.0
0
center
parallel
within border
lamella
center into periphery
center to periphery
center to periphery & swept
border into periphery
border to periphery
border to periphery & swept
-3.2
-1.8
-3.3
-1.7
-2.3
-2.0
-2.9
-2.3
ns
-1.9
B
GFP Comet Velocity per MT (µm/min)
not cross-linked
CH-CH-tgRFP + iLIDLit
(4, 29, 658)
cross-linked
CH-CH-tgRFP-SspB + iLIDLit
(3, 40, 1,087)
26.6%
30.8%
12.9%
19.1%
1.4%
1.7%
14.3%
12.2%
19.0%
9.7%
13.4%
4.2%
1.4%
3.3%
7.6%
6.7%
0.6%
2.8%
2.9%
9.4%
9.8±2.7
6.6±3.1
9.3±2.3
7.5±2.6
7.2±2.6
3.9±4.0
4.6±1.9
2.9±1.9
8.9±2.2
6.6±2.4
10.0±2.3
8.0±3.0
9.7±0.7
6.8±2.4
7.4±2.0
5.1±2.0
7.6±3.5
5.3±3.2
6.8±2.4
4.9±1.9
center
center cross-linked
parallel
parallel cross-linked
within border
within border cross-linked
periphery
periphery cross-linked
center into periphery
center into periphery cross-linked
center to periphery
center to periphery cross-linked
center to periphery & swept
center to periphery & swept cross-linked
border into periphery
border into periphery cross-linked
border to periphery
border to periphery cross-linked
border to periphery & swept
border to periphery & swept cross-linked

Figure 2.7. Cross-linking decreases MT comet velocities throughout the cell, limits MT entry into the peripheral zone, and increases in the percent of comets that are swept along the peripheral zone boundary. (A) Schematic of MT comet trajectories categorized in *Drosophila* S2 cells (left) and change in average comet velocity in cross-linked compared to non cross-linked cells (right, based on mean velocities presented in B). **(B)** GFP comet velocities from control cells (co-transfected with SKIP-LZ-iLID^{Lit} + CH-CH, shown as open circles) and constitutively cross-linked cells (co-transfected with SKIP-LZ-iLID ^{Lit} + CH-CH-SspB, shown as filled circles), grouped based on comet trajectory as delineated in A. Multiple individual eGFP-labeled comet velocities were determined and compiled across multiple cells. Numbers in parenthesis indicate: (number of independent experiments, total number of cells analyzed, total number of tracks annotated). Comet track histories were used to categorize each comet, using the trajectory rubric established in A. Mean comet velocities are reported below the dotted line and the relative percentage of comets in each category are shown at the top of the plot (bold percentages indicates greater than a 2-fold difference between cross-linked and non cross-linked cells). eGFP comet velocities were significantly decreased in constitutively cross-linked cells compared to control cells across all regions of the cell and categories analyzed, except for comets that appeared in the border and entered the peripheral zone due to limited representation in control cells. There were differences in the percentage of MTs which had certain trajectories in constitutively cross-linked cells compared to control cells. There was a decrease in the percentage of MTs that went from the cell center into the peripheral zone (control: 19.0%, constitutively cross-linked: 9.7%) and an increase in the percentage of MTs swept along the peripheral zone boundary (control: 4.3%, constitutively cross-linked: 12.7%). Line represents the mean, error bars indicate SD. P-values were determined by two-way unpaired Student's *t* test. * $p<0.05$, ** $p<0.005$, ***$p<0.0005$, **** $p<0.0001$.

We next inquired if MT comet behavior over the course of these trajectories was different between constitutively cross-linked and control cells. We first investigated if comets that travel from the center or boarder region into the peripheral zone show changes in velocity over time, or have altered lifetimes. We plotted the instantaneous velocity of comets that travelled from the center (Fig. S2.3) or boarder (Fig. S2.4) into the peripheral zone. In control cells, comets that originated in the cell center decelerated as they approached and entered the peripheral zone (Fig. S2.3A). In contrast, comets in cross-linked cells began to decelerate closer to the peripheral zone (Fig. S2.3B). The average instantaneous velocities of individual comets after peripheral zone entry is significantly decreased relative to their velocity prior to entry (Fig. S2.3C) and the magnitude of change was similar for control and cross-linked cells (control: $\Delta\langle velocity\rangle = -3.9 \pm 3.5$ μm/min, cross-linked: $\Delta\langle velocity\rangle = -4.2 \pm 3.7$ μm/min) (Fig. S2.3C and D). Comets traveling from the boarder region into the peripheral zone in non cross-linked cells began to decelerate prior to peripheral zone entry and continued to decelerate once in the peripheral zone (Fig. S2.4A). Comets in cross-linked cells exhibited more variation in velocities upon peripheral zone entry, but yielded a net change in average velocity that was on par with control cells (control: $\Delta\langle velocity\rangle = -4.6 \pm 4.2$ μm/min, cross-linked: $\Delta\langle velocity\rangle = -3.9 \pm 4.4$ μm/min) (Fig. S2.4C and D). Interestingly, comets in cross-linked cells that travelled into the peripheral zone had a longer lifetime in the peripheral zone than comets in non cross-linked cells (Fig. S2.3A and B and Fig. S2.4A and B). We next asked if MT comets that were swept from the peripheral zone behaved differently in control versus cross-linked cells. When we plotted the instantaneous comet velocities over time relative to the time each comet encountered the peripheral zone edge, we found that comets in cross-linked cells exhibited a longer lifetime (Fig. S2.5).

Collectively, this data shows that MT plus end - F-actin cross-linking differentially slows MT comet velocity throughout the cell, alters the distribution of comet trajectories in the cell, actively excludes MT comets from the peripheral zone, and extends comet lifetime in the peripheral zone by redirecting comet trajectory parallel to the zone's edge, or potentially by treadmilling on F-actin retrograde flow within the zone.

2.3 Discussion

Advances in cellular optogenetics have allowed for spatial and temporal control of many biological processes, enabling researchers to test the role of specific proteins or protein domains during different phases of the cell cycle and in different cellular locations. Here, we generated a novel optogenetic tool, SxIP-iLID, which can recruit proteins of interest to MT plus ends. Four SxIP-iLID constructs were generated which offer a range of MT plus end tracking activities that can be selectively utilized to match the physiological requirements of a specific cytoskeletal processes. In addition, the dimeric SKIP-LZ-iLID construct would enable avidity-based recruitment of multimeric SspB-tagged constructs. The SxIP- iLID system also serves as a generalizable platform that can incorporate recently sequence, and enhanced detection of the dimeric construct, which has two GFP domains. While our current work illustrates the temporal use of SxIP-iLID, future work will probe the efficacy of spatial activation in a region of interest, probing the role of cytoskeletal regulators across space and time at cellular and organismal levels. As a proof of principal we used the SxIP-iLID system to examine the temporal effects of cross-linking the F-actin and MT networks using a minimalist spectraplakin analog. While it is known that spectraplakins play critical roles in cytoskeletal cross-linking, how cross-linking activity affects the terminal CH, actin binding domains from the *Drosophila* protein Shot to SspB, generating a light inducible

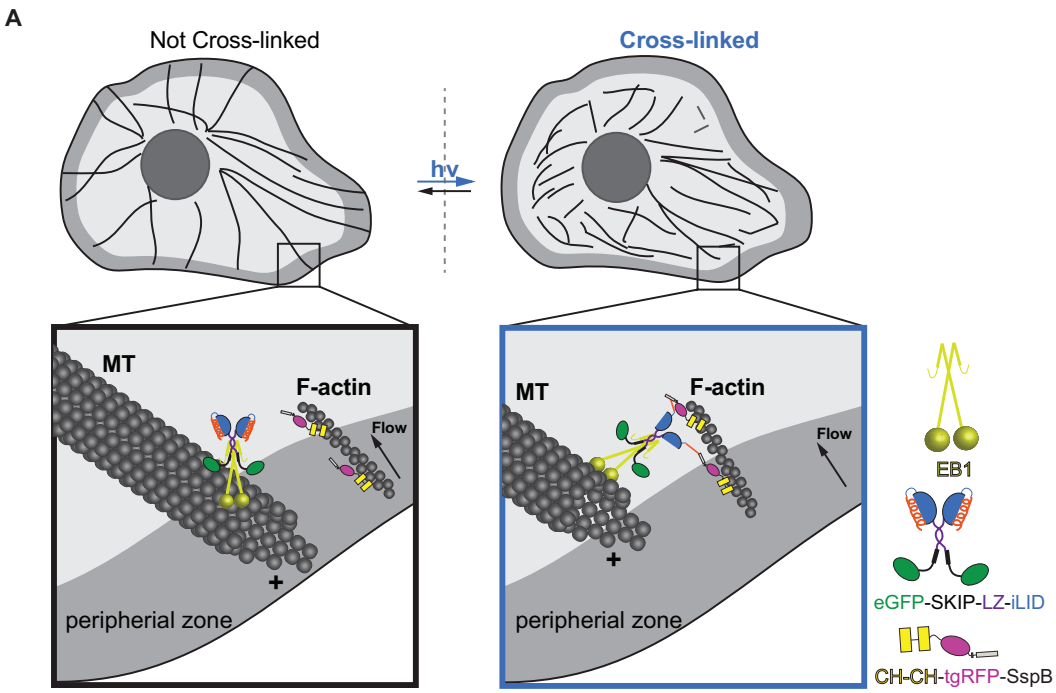

Figure 2.8. Schematic of MT exclusion upon optogenetically induced cross-linking in *Drosophila* S2 cells. EB1 (yellow) tracks and recruits eGFP-SKIP-LZ-iLID to the growing MT plus end. CH-CH-tgRFP-SspB engages actin filaments. Upon blue light activation, the iLID module engages CH-CH-tgRFP-SspB, effectively cross-linking the MT and F-actin networks. In the F-actin-rich peripheral zone, the F-actin density and/or retrograde flow drives the exclusion of the cross-linked MT plus ends from the region and promotes MT comet "sweeping" along the peripheral zone boundary.

morphology and dynamics of the MT network is poorly understood. We fused the N-

cross-linking system when used with the SKIP-LZ-iLID construct. Light-induced MT-F-actin cross-linking rapidly decreased MT comet velocities and increased the cellular area void of MTs (Fig. 8). Whether the decreased MT comet velocity is due to diminished MT polymerization rates or MT sliding remains to be determined. MT comets in constitutively cross-linked cells were also swept parallel to the peripheral zone's edge with greater frequency than in non cross-linked cells. Comets that did enter the peripheral zone in cross-linked cells had a slower velocity and an extended lifetime as compared to comets in non cross-linked cells. Our results suggest that cross-linking in cells may

mechanically stall/slow MT growth and/or entry into the F-actin rich lamella/peripheral zone. This may reflect the role of MT-F-actin cross-linkers in focal adhesion turnover during cell migration.

2.4 Materials and methods

2.4.1 Molecular biology

The iLID micro domain (Guntas et al., 2015) was amplified and sub-cloned using the Gateway TopoD pEntr system (Invitrogen) into an ampicillin-selectable backbone containing a methallothionein promoter and a N-terminal GFP (pMTeGFP). The minimal MT plus end tracking motif from MACF2 (Slep et al., 2005; Honnappa et al., 2009) followed by a two-stranded leucine zipper (LZ) coiled-coil sequence corresponding to GCN4-p1 (Steinmetz et al., 2007) was PCR amplified with primers containing restriction enzyme sites, and cloned into the pMTeGFP-iLID backbone. The remaining SxIP-iLID constructs were generated via site directed mutagenesis to the pMTeGFP-LZ-SKIP-iLID parent vector. The constitutively lit mutant (I539E of the iLID domain (Harper et al., 2004): SKIP-LZ-iLID^{Lit}) was generated using KOD Xtreme site directed mutagenesis following the manufacture's protocol (Novagen).

tgRFPt-NES-SspB nano (referred to as tgRFP-SspB in this paper) was PCR amplified from a pLL7.0 vector and sub-cloned using the Gateway TopoD pEntr system (Invitrogen) into a final ampicillin-selectable actin promoter backbone (pAW). DNA encoding the tandem CH domains from *Drosophila* Shot was PCR amplified and inserted into the pAW-tgRFPt-NES-SspB nano construct using restriction enzymes. The EB1-GFP expression construct, under control of the EB1 promoter, was constructed as described in Currie et al., 2011.

2.4.2 Cell culture and transfection

Drosophila S2 cells were cultured using the standard protocol described in Rogers and Rogers, 2008. In short, S2 cells (*Drosophila* Genomics Resource Center, Bloomington, IN) were grown in Sf900II SFM (Gibco) supplemented with 1x antibiotic-antimycotic (Invitrogen). To express the desired constructs, 2.5 x 10^5 cells were plated in 12 well dishes and transfected with 1.5 μg of DNA using FuGENE HD (Promega) following the manufacturer's protocol. Expression of pMT constructs was induced using 50 μM of $CuSO_4$ 24 hours post transfection and 24-30 hours prior to imaging.

2.4.3 Live-cell imaging

S2 cells were seeded onto 0.5 mg/ml conconavlin A (ConA) (MP Biomedicals, LLC) treated covererslips attached by UV-curable adhesive (Norland Products) to drilled 35-mm tissue culture dishes in 1 ml of Schneider's *Drosophila* media (Gibco) supplemented with 1x antibiotic-antimycotic (Invitrogen) and 10% fetal bovine serum (Gibco) and allowed to spread for 2 hours prior to imaging. Imaging dishes were prepared by attaching glass coverslips to drilled 35 mm tissue culture dishes using UV curable glue (Norland Products). Time-lapse imaging was performed on a VT-HAWK confocal system (VisiTech) using an inverted microscope (Nikon Ti) equipped with a 100x/1.45 N.A. objective lens driven by VoxCell software (VisiTech). Images were captured with a Flash 4.0 camera (Hamamatsu). To assess comet velocities in cells exclusively transfected with either EB1-GFP or an eGFP-SxIP-iLID construct, time lapse images were acquired every 2 seconds using 488 nm excitation at 40% laser power (0.15 mW entering the back of the objective) for 700 ms. To assess comet velocities in cells co-transfected with an eGFP-SxIP-iLID construct and a tgRFP-SspB construct, cells were

imaged every 3 seconds using alternating 561 nm and 488 nm excitation (40% 488 nm laser power for 700 ms). To determine the apparent off rate of the system, images were acquired every 3 seconds using 561 nm excitation for 10 frames, a single pulse of 488 nm light at 40% laser power for 200 ms was then applied to induce recruitment of the tgRFP-SspB construct to MT plus ends, then excitation at 561 nm resumed and frames were captured every 3 seconds over the course of 3 minutes to record the re-localization of the SspB-tgRFP construct to the cytoplasm. To analyze tgRFP-SspB behavior over multiple rounds of activation, single pulses of 488 nm light at 30% laser power (0.10 mW entering the back of the objective) for 250 ms were applied to induce recruitment of the tgRFP-SspB construct to MT plus ends at t=0, t=150 and t=300 sec. After each 488 nm pulse, frames were captured every 5 seconds for 2.5 minutes using 561 nm excitation. Images were processed using Fiji (Schindelin et al., 2012).

2.4.4 Fixed cell analysis

S2 cells were seeded onto 0.5 mg/ml conconavlin A (ConA) (MP Biomedicals, LLC)-treated covererslips attached by UV-curable adhesive (Norland Products) to drilled 35-mm tissue culture dishes in 1 ml of Schneider's *Drosophila* media (Gibco) supplemented with 1x antibiotic-antimycotic (Invitrogen) and 10% fetal bovine serum (Gibco) and allowed to spread for 2 hours prior to fixation with either ice cold MeOH (Thermo Fisher Scientific) or 4% paraformaldehyde (Ted Pella, Inc.). In brief, for MeOH fixation, cells were rinsed 1x with PBS, 1x with ice cold MeOH, then fresh MeOH was added and cells were placed at -20°C for 8 min. The fixed cells were rinsed 3x with PBST (PBS + 0.5% TritonX100 (Thermo Fisher Scientific)) and blocked overnight with PBST+1% BSA (Thermo Fisher Scientific). Primary antibodies were added at 1:100 for

mouse monoclonal anti–α-tubulin (DM1α, T6199; Sigma-Aldrich) and mouse monoclonal anti-actin clone C4 (which yields sparse, punctate-like labeling of the F-actin network; MAB1501, EMD Millipore) for 1 hour or overnight. Cells were rinsed 3x with PBST and anti-mouse Cy5 secondary antibody (Jackson ImmunoResearch Laboratories, Inc.) was added at a 1:500 dilution for 40 minutes. Cells were rinsed 1x with PBST, 1x with PBS, 1x with PBS+DAPI (Molecular Probes, D1306; Invitrogen) and 1x with PBS. For paraformaldehyde fixation, cells were quickly fixed with PHEM Fix (4% paraformaldehyde (Ted Pella, Inc.) in PHEM (5 mM HEPES, 60 mM PIPES pH 7.0, 10 mM EGTA, and 2 mM $MgCl_2$)) for 20 seconds, quickly permeabilized with PHEM-T (PHEM + 0.2% Triton) for 30 seconds and fixed with PHEM Fix for 20 minutes. Cells were then rinsed 3x with PHEM-T and blocked overnight in PHEM-T + 1% BSA (Thermo Fisher Scientific). Alexa Fluor 647 conjugated phalloidin (Molecular Probes, A22287; Invitrogen) was added to the cells for 20 minutes then the cells were rinsed 1x PHEM-T, 1x PHEM, 1x PBS+DAPI (Molecular Probes, D1306; Invitrogen) and 1x PBS. All cells were imaged at room temperature with a Nikon Apo DIC 100X oil/-1.40-NA objective on an Eclipse Ti-E microscope (Nikon), driven by NIS Elements software (Nikon). Images were acquired with a CoolSNAP HQ cooled charge-coupled device camera (Roper Technologies). 9 Z-steps were acquired at 0.3 μm intervals. Images shown in Figure S2 are a max projection of 3 steps. The central frame included in the maxprojection was the dominant frame in which the peripheral region was in focus. The six frames not included in the max projection did not include data for the peripheral region.

2.4.5 Comet velocity, intensity analysis, and kinetic rate analysis

Comet velocities were determined using the MTrackJ plugin in Fiji (Meijering et al., 2012, Schindelin et al., 2012). Twelve MT plus ends were hand tracked per cell for 10 or more consecutive frames. These tracks were then averaged to give the average comet velocity per cell. For binning MTs based on their trajectories, 20-30 MT comets were analyzed per cell. Cellular regions were delineated as follows: the peripheral zone was demarcated by enhanced tgRFP-CH-CH or tgRFP-CH-CH-SspB construct localization around the cell periphery; the border was delineated by a 2-μm wide zone just interior to the peripheral zone; the center was defined by the interior cellular region, not including the peripheral or border zones. The peripheral and border zones went completely around each cell analyzed, and thus included more area than the region devoid of MTs in cross-linked cells, but enabled comparative analyses of comet behavior in select regions in cross-linked versus non-cross-linked cells. Comet trajectories were annotated and average and instantaneous comet velocities were determined using the MTrackJ plugin in Fiji. Fiji was used to determine the total cell fluorescence intensity/area. The cell of interest was selected using the freeform selection tool and an area next to the cell was selected for background intensity measurement. The integrated density and area of these selections was measured. The total cell intensity was then calculated as: [Integrated density – (Area of selected cell * Mean fluorescence of background readings per area)]. Total cell intensity was then divided by the cell area and reported as total cell intensity/area of the selected cell**.** To determine the comet/cytoplasmic intensity ratio for the eGFP constructs (Fig. 2.1D) and the recruitment of tgRFP-SspB to MT plus ends (Fig. 2.2D) 10 comets were analyzed per cell. Using the freeform selection tool the region of the comet was

outlined and the integrated density and the area of each comet was determined. As the cytoplasmic intensity varies throughout the cell, the region surrounding each comet was selected to determine the respective mean cytoplasmic intensity per area by selecting a rectangle encompassing the entire comet. The integrated density and the area of this rectangle were determined. To determine the integrated density of the cytoplasmic region, the integrated density of the comet was subtracted from the integrated density of the rectangle. To determine the area of the cytoplasmic region, the area of the comet was subtracted from the area of the rectangle. The integrated density per area for both the comet and the cytoplasmic region were then determined and corrected for non-cellular background noise. The ratio of the integrated density per area of the comet versus the cytoplasm was then calculated and reported as comet/cytoplasm intensity. Therefore, a value of 1 would represent a cell in which the comet and the cytoplasm have the same mean intensity per area. To determine the fold-increase of tgRFP-SspB on comets upon activation: the comet/cytoplasm intensity was determined for the first frame in the series (delineated as the pre activation value) as well as for the frame in which the cell contained the greatest mean comet intensity (delineated as the post activation value). The ratio of these was then reported in Fig. 2D. To determine the tgRFP-SspB intensity on MT plus ends for the plots of apparent cellular kinetics for single and multiple rounds of activation (Fig. 3B and C), a threshold was applied to encompass the tgRFP-SspB signal at MT plus ends using the first frame post activation that had the peak level of tgRFP-SspB MT plus end recruitment. This threshold was applied to all frames pre and post activation and a mask corresponding to the thresholded area was generated for each frame. Each mask was applied to its respective image to measure the area and raw

integrated intensity of detected MT plus ends. The raw integrated intensity and area was also determined for the whole cell as well as a small off-cell area. The fluorescence density off-cell was used to correct for background fluorescence at MT plus ends and in the whole cell. The total intensity for MT plus ends as well as the whole cell was calculated for each frame and the ratio reported over time. The apparent reversion half-life was determined by fitting points 21-111 (t=30-300 seconds) which correspond to the peak activation through the last data point. The curve fit was generated using Prism (GraphPad) using one-phase decay with least squares fit. Post-activation, particularly post 120 seconds, there are few pixels above the threshold; thus the ratio approaches zero over time.

2.4.6 Statistical analyses

eGFP comet velocity data were analyzed using a two-way unpaired Student's *t* test (GraphPad Prism). MT void area data were analyzed using a two-tailed nonparametric Mann–Whitney *U* test (GraphPad Prism). * $p<0.05$, ** $p<0.005$, ***$p<0.0005$, **** $p<0.0001$.

2.5 Supplemental Information

Supplemental Figure1

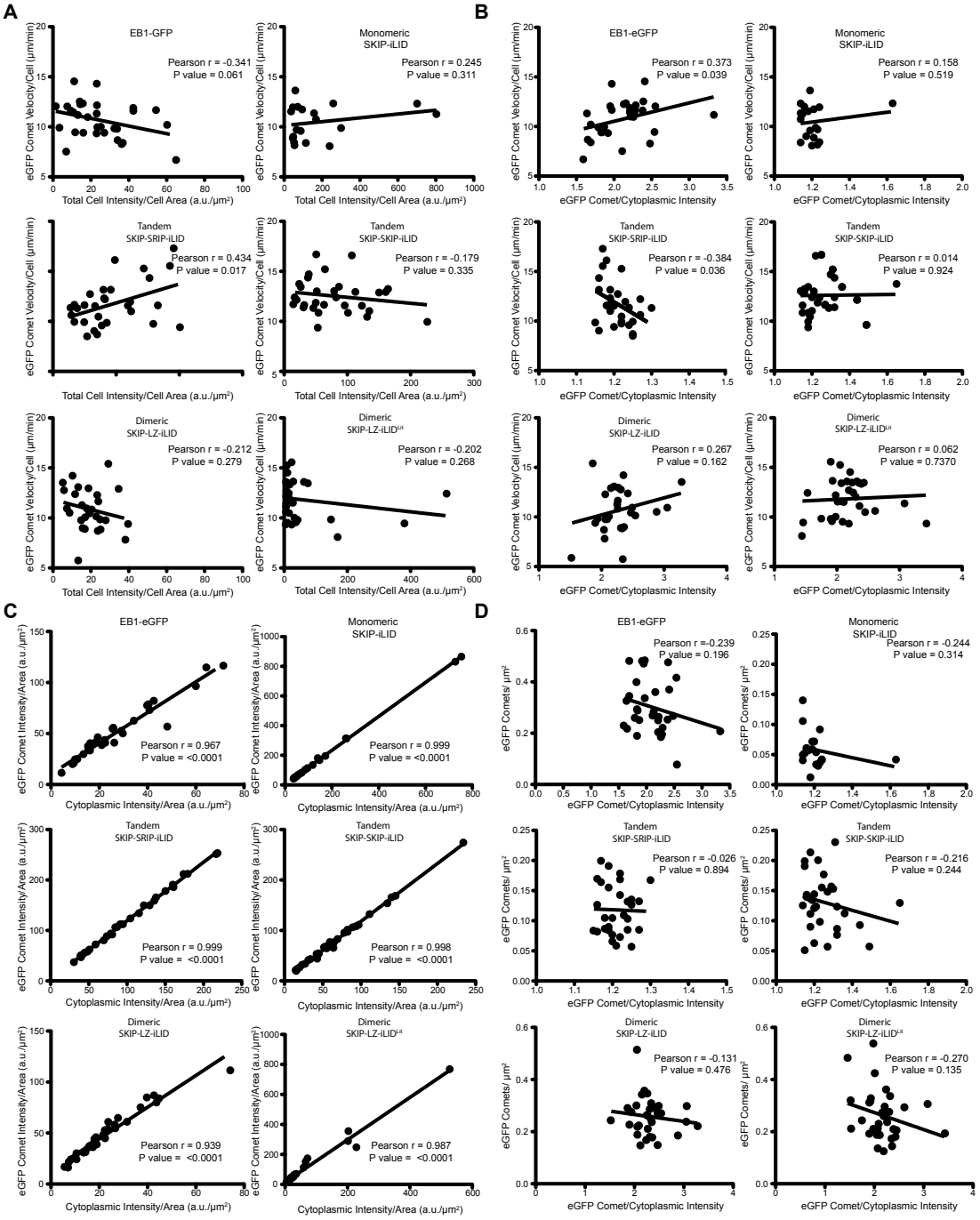

Supplemental Figure 2.1. The amount of eGFP-SxIP-iLID in the cell or on the MT plus end does not strongly correlate with comet velocity. **(A)** The total cell intensity/area (a.u./μm^2) was determined for cells transfected with eGFP-SxIP-iLID constructs or EB1-GFP and plotted against the average eGFP comet velocity for each cell. To assess the strength of the correlation, a Pearson's correlation coefficient was determined. Using this statistical analysis, no correlations we detected except for the SKIP-SRIP-iLID construct which yielded a p-value of less than 0.05, but greater than 0.01. **(B)** The eGFP comet/cytoplasmic intensity plotted against the average eGFP comet velocity for each cell. To assess the strength of the correlation, a Pearson's correlation coefficient was determined. Using this statistical analysis, we found that EB1 shows a slightly significant correlation between plus end fluorescence intensity with comet velocity ($p=0.039$). No correlations were detected except for the SKIP-SRIP-iLID construct which yielded a p-value of less than 0.05, but greater than 0.01. **(C)** The cytoplasmic intensity/area (a.u./μm^2) plotted against the average eGFP comet intensity/area (a.u./μm^2) for each cell. To assess the strength of the correlation, a Pearson's correlation coefficient was determined. Using this statistical analysis, a positive correlation was determined for each of the constructs, showing that with higher levels of expression more of the construct localizes to the MT plus end. **(D)** The eGFP comet/cytoplasmic intensity plotted against the comet density (number of eGFP comets/μm^2) for each cell. To assess the strength of the correlation, a Pearson's correlation coefficient was determined. Using this statistical analysis, no correlations were detected.

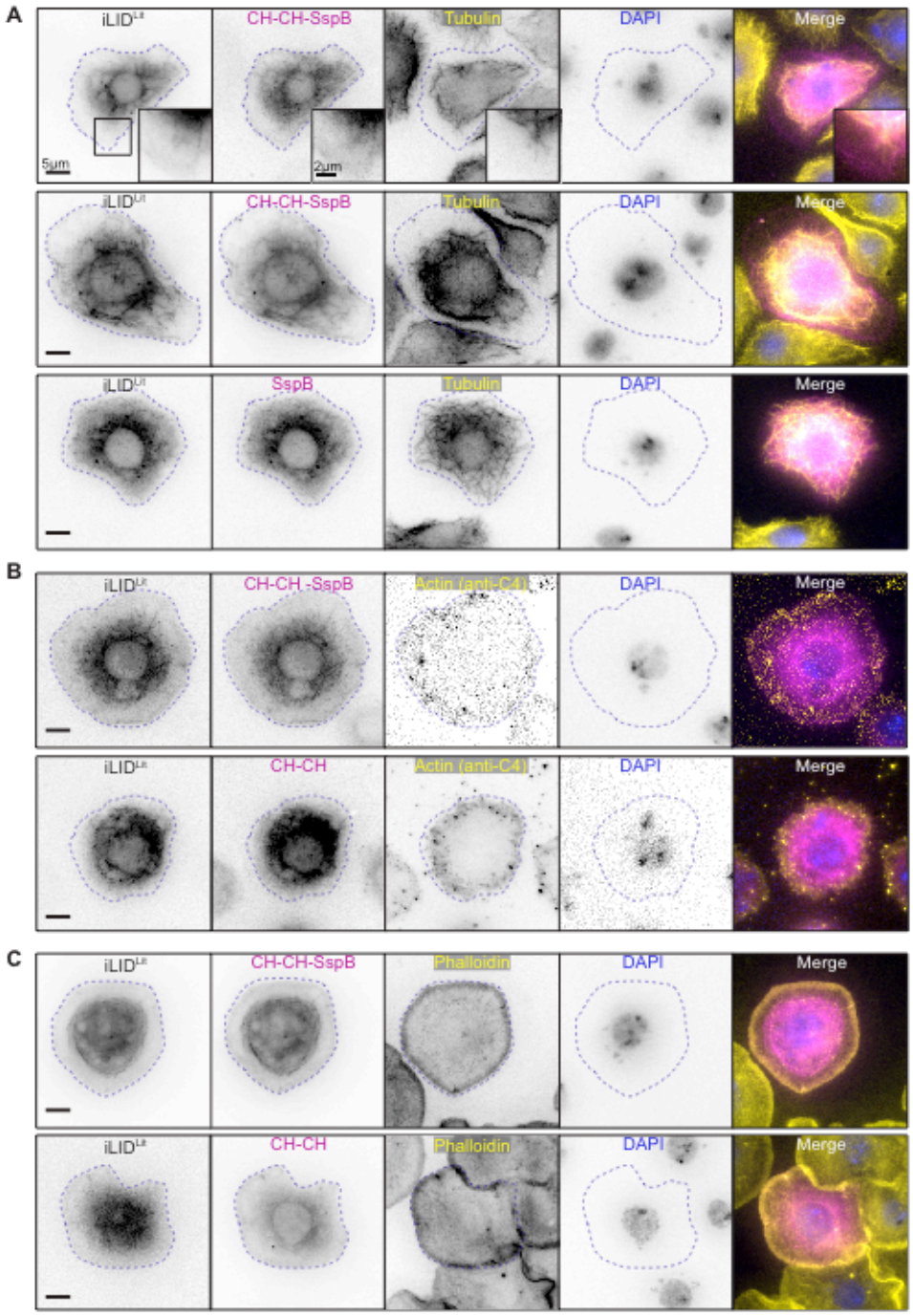

Supplemental Figure 2.2. The peripheral MT exclusion zone created upon cross-linking lacks MTs and contains actin. (A) In constitutively cross-linked cells (co-transfected with SKIP-LZ-iLID^{Lit} and CH-CH-SspB) fixed and stained for α-tubulin (DM1α), MTs are not present in the peripheral zone that lacks SKIP-LZ-iLID^{Lit} localization. In control cells (co-transfected with SKIP-LZ-iLID^{Lit} and SspB) MTs and the SKIP-LZ-iLID^{Lit} construct marking MT plus ends extend to the edge of the lamella. **(B and C)** In constitutively cross-linked cells, fixed and stained for actin using either the actin antibody C4 (B) which labels F-actin in a punctate fashion or phalloidin (C), an actin-rich lamella is evident in the large peripheral MT exclusion zone.

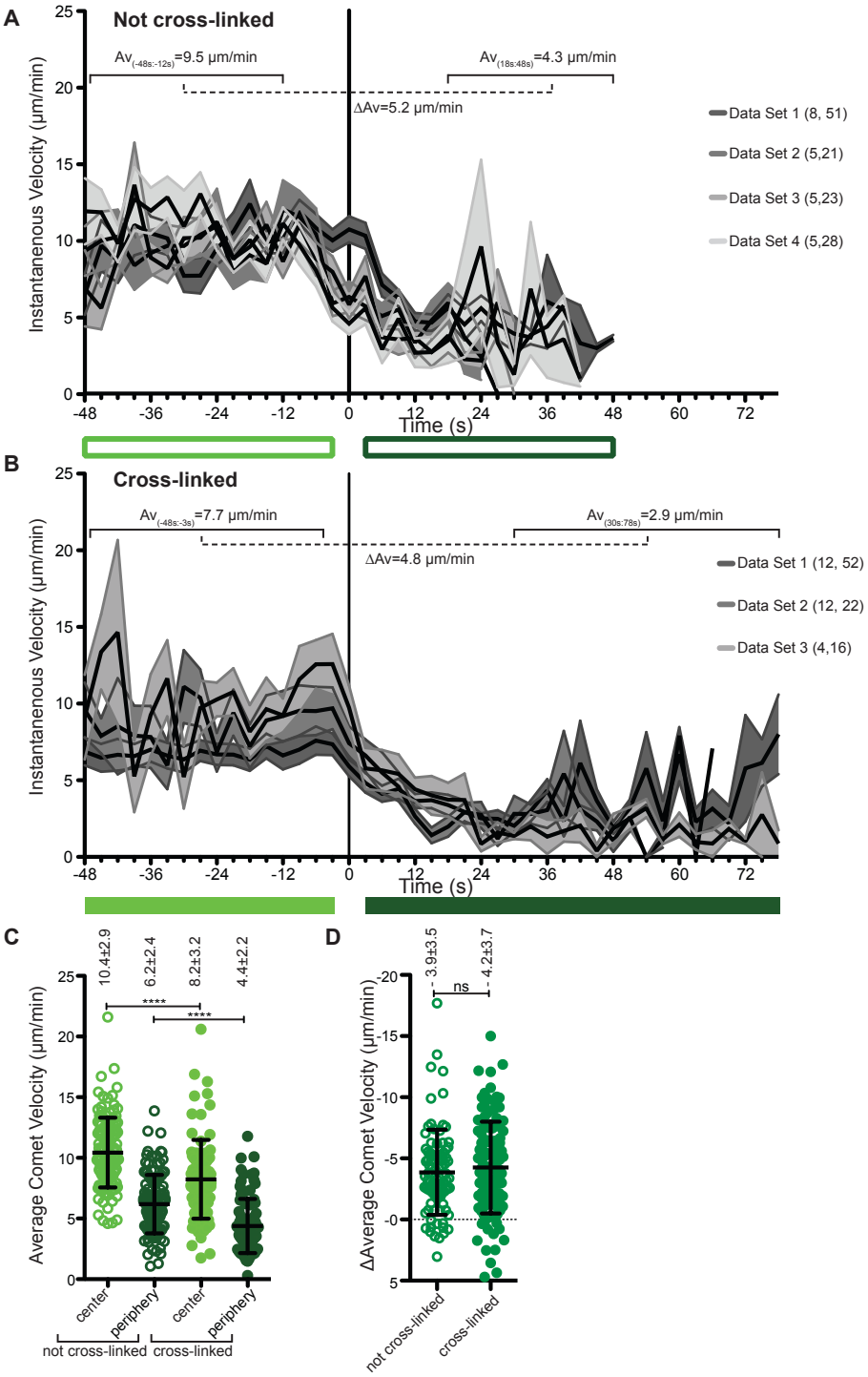
A
Not cross-linked
Av(-48s:-12s)=9.5 µm/min
Av(18s:48s)=4.3 µm/min
ΔAv=5.2 µm/min
Instantaneous Velocity (µm/min)
Time (s)
Data Set 1 (8, 51)
Data Set 2 (5,21)
Data Set 3 (5,23)
Data Set 4 (5,28)
B
Cross-linked
Av(-48s:-3s)=7.7 µm/min
Av(30s:78s)=2.9 µm/min
ΔAv=4.8 µm/min
Instantaneous Velocity (µm/min)
Time (s)
Data Set 1 (12, 52)
Data Set 2 (12, 22)
Data Set 3 (4,16)
C
Average Comet Velocity (µm/min)
10.4±2.9
6.2±2.4
8.2±3.2
4.4±2.2
****
****
center
periphery
center
periphery
not cross-linked
cross-linked
D
ΔAverage Comet Velocity (µm/min)
-3.9±3.5
-4.2±3.7
ns
not cross-linked
cross-linked

Supplemental Figure 2.3. MT comets traveling from the center of the cell into the peripheral zone decelerate as they enter the peripheral zone. (A) Instantaneous velocity (μm/min) over time plotted for populations of MT comets that traveled from the center of the cell into the peripheral zone in non cross-linked cells (co-transfected with SKIP-LZ-iLID^{Lit} + CH-CH). The timeline for each comet factored into the population track was set to zero at the point that comet first entered the peripheral zone (t=0, black vertical line). MT comet velocity begins to decelerate around -12 seconds and continues to decelerate until +12 seconds. The average instantaneous comet velocity for the periods -48 to -12 seconds and +18 to +48 seconds is indicated above the plot, along with the change in average instantaneous velocity between these periods. Numbers in parenthesis indicate (number of cells, number of tracks analyzed). The green boxes below the x-axis denote the data used in plot (C). **(B)** Instantaneous velocity (μm/min) over time plotted for populations of MT comets that traveled from the center of the cell into the peripheral zone in cross-linked cells (co-transfected with SKIP-LZ-iLID^{Lit} + CH-CH-SspB). The timeline for each comet factored into the population track was set to zero at the point that comet first entered the peripheral zone (t=0, black vertical line). MT comet velocity begins to decelerate at -3 seconds and continues to decelerate until +24 seconds. The average instantaneous comet velocity for the periods -48 to -3 seconds and +30 to +78 seconds is indicated above the plot, along with the change in average instantaneous velocity between these periods. MT comet lifetime in the peripheral zone of cross-linked cells is dramatically extended relative to comet lifetime in non cross-linked cells. Numbers in parenthesis indicate (number of cells, number of tracks analyzed). The green boxes below the x-axis denote the data used in plot (C)**.** Plots in both (A) and (B) display the mean (central line) and SEM (flanking grey area) for each data set. **(C)** The average comet velocity (μm/min) before and after a MT comet entered the peripheral zone in non cross-linked and constitutively cross-linked cells (corresponding to the periods demarcated by green boxes below the plots in (A) and (B)). The average comet velocity significantly decreases after entry into the peripheral zone in both cross-linked and non cross-linked cells. Mean and SD is reported at the top of the plot, **** $p<0.0001$. **(D)** The change in average comet velocity (μm/min) from (C). The change in comet velocity is not significantly different between non cross-linked and cross-linked cells. Mean and SD is reported at the top of the plot.

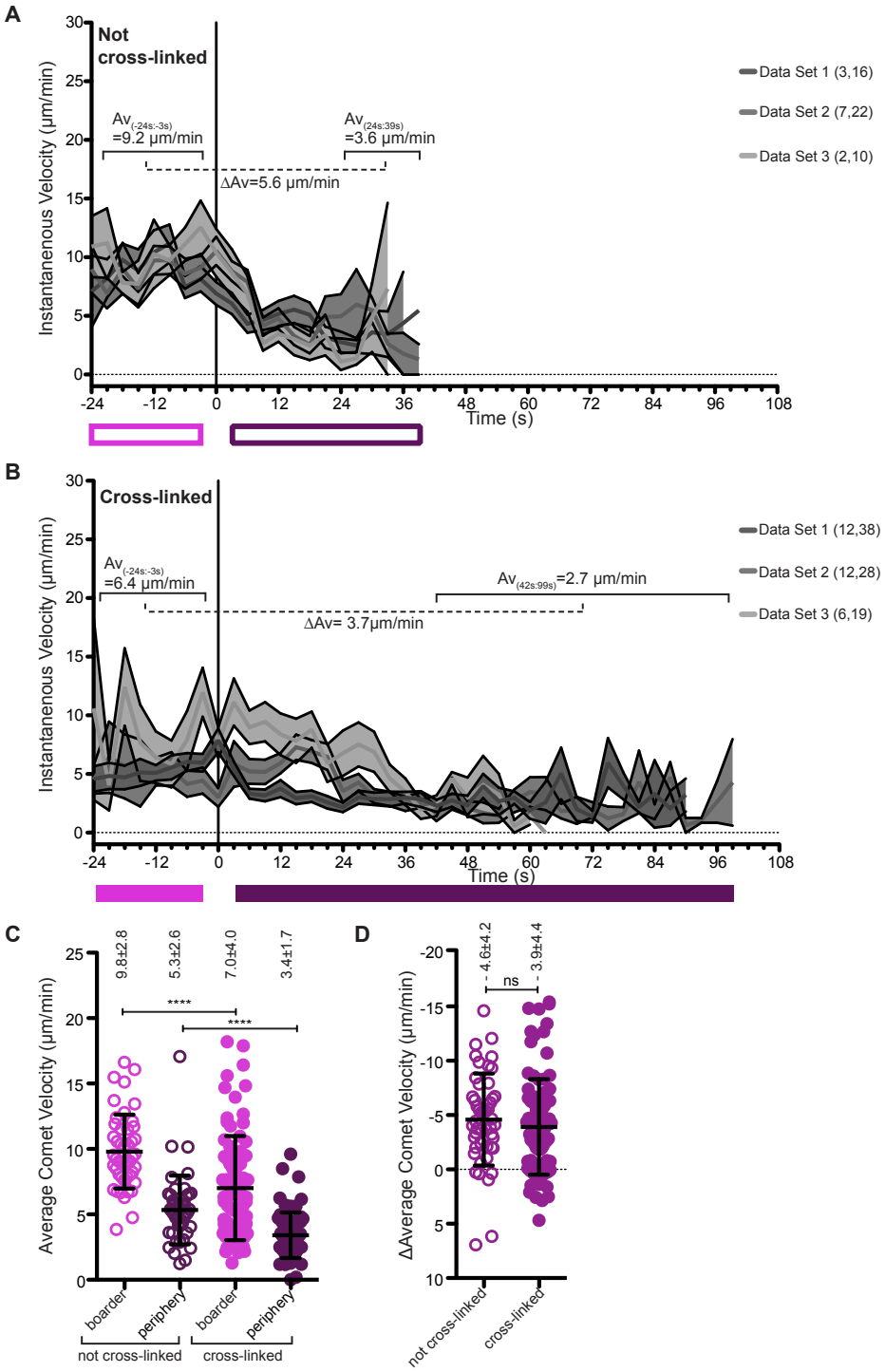
A
Not cross-linked
Instantaneous Velocity (µm/min)
Av(-24s:-3s) =9.2 µm/min
Av(24s:39s) =3.6 µm/min
ΔAv=5.6 µm/min
Data Set 1 (3,16)
Data Set 2 (7,22)
Data Set 3 (2,10)
Time (s)
B
Cross-linked
Instantaneous Velocity (µm/min)
Av(-24s:-3s) =6.4 µm/min
Av(42s:99s)=2.7 µm/min
ΔAv= 3.7µm/min
Data Set 1 (12,38)
Data Set 2 (12,28)
Data Set 3 (6,19)
Time (s)
C
Average Comet Velocity (µm/min)
9.8±2.8
5.3±2.6
7.0±4.0
3.4±1.7
****
****
boarder
periphery
boarder
periphery
not cross-linked
cross-linked
D
ΔAverage Comet Velocity (µm/min)
- 4.6±4.2
ns
- 3.9±4.4
not cross-linked
cross-linked

Supplemental Figure 2.4. MT comets traveling from the boarder of the cell into the peripheral zone decelerate as they enter the peripheral zone. (A) Instantaneous velocity (μm/min) over time plotted for populations of MT comets that traveled from the boarder of the cell into the peripheral zone in non cross-linked cells (co-transfected with SKIP-LZ-iLID^{Lit} + CH-CH). The timeline for each comet factored into the population track was set to zero at the point that comet first entered the peripheral zone (t=0, black vertical line). MTs begin deceleration around -3 seconds and continue to decelerate until +24 seconds. The average instantaneous comet velocity for the periods -24 to -3 seconds and +24 to +39 seconds is indicated above the plot, along with the change in average instantaneous velocity between these periods. Numbers in parenthesis indicate (number of cells, number of tracks analyzed). The purple boxes below the x-axis denote the data used in plot (C). **(B)** Instantaneous velocity (μm/min) over time plotted for populations of MT comets that traveled from the boarder of the cell into the peripheral zone in cross-linked cells (co-transfected with SKIP-LZ-iLID^{Lit} + CH-CH-SspB). The timeline for each comet factored into the population track was set to zero at the point that comet first entered the peripheral zone (t=0, black vertical line). Deceleration occurs over a longer time period (~42 seconds) within the peripheral zone than in non cross-linked cells (~24 seconds). The average instantaneous comet velocity for the periods -24 to -3 seconds and +42 to +99 seconds is indicated above the plot, along with the change in average instantaneous velocity between these periods. Numbers in parenthesis indicate (number of cells, number of tracks analyzed). The purple boxes below the x-axis denote the data used in plot (C)**.** Plots in both (A) and (B) display the mean (central line) and SEM (flanking grey area) for each data set. **(C)** The average comet velocity (μm/min) before and after the MT comet entered the peripheral zone in non cross-linked and constitutively cross-linked cells (corresponding to the periods demarcated by purple boxes below the plots in (A) and (B)). The average comet velocity significantly decreases after entering the peripheral zone in both cross-linked and non cross-linked cells. Mean and SD is reported at the top of the plot, **** $p<0.0001$ **(D)** The change in average comet velocity (μm/min) from (C). The change in average comet velocity is not significantly different between non cross-linked and cross-linked cells. Mean and SD is reported at the top of the plot.

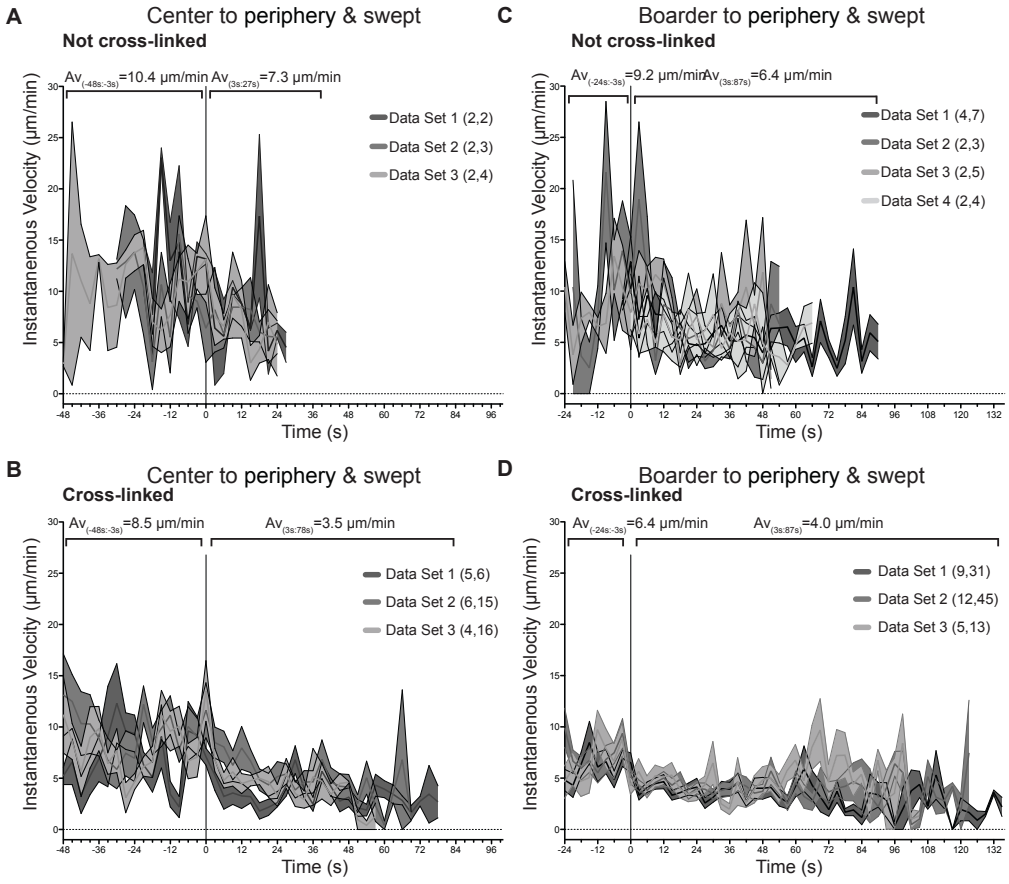

Supplemental Figure 2.5. MTs that are swept away from entering the peripheral zone have a longer lifetime in constitutively cross-linked cells. (A) Instantaneous velocity (µm/min) over time plotted for all MT comets that traveled from the center of the cell to the edge of the peripheral zone and were then swept parallel to the edge of the zone in non cross-linked cells (co-transfected with SKIP-LZ-iLID^{Lit} + CH-CH). **(B)** Instantaneous velocity (µm/min) over time plotted for all MT comets that traveled from the center of the cell to the edge of the peripheral zone and were then swept parallel to the edge of the zone in cross-linked cells (co-transfected with SKIP-LZ-iLID^{Lit} + CH-CH-SspB). Longer MT comet lifetimes in the swept phase can be observed in cross-linked cells. **(C)** Instantaneous velocity (µm/min) over time plotted for all MT comets that traveled from the boarder of the cell to the peripheral zone edge and were then swept parallel to the edge of the zone in non cross-linked cells (co-transfected with SKIP-LZ-iLID^{Lit} + CH-CH). **(D)** Instantaneous velocity (µm) over time plotted for all MT comets that traveled from the boarder of the cell to the peripheral zone edge and were then swept parallel to the edge in cross-linked cells (co-transfected with SKIP-LZ-iLID^{Lit} + CH-CH-SspB). Longer MT lifetimes in the swept phase can be observed in cross-linked cells. The timeline for each comet embedded in a population track was set to zero at the point that comet first encountered the edge of the peripheral zone (t=0, black vertical line). Numbers in parenthesis indicate (number of cells, number of tracks analyzed). All plots display the mean (central line) and SEM (flanking grey area) for each data set.

2.6 Acknowledgments

We thank Seth Zimmerman for the pLL7.0 tgRFPt-NES-SspB vector. We thank the Peifer lab for anti-actin clone C4 and Alex-Fluor 647 phallodin. We thank Derek Applewhite and Thomas Lane for insightful discussions, and Mark Peifer and Alakananda Das for comments regarding this manuscript.

This work was supported by the National Institutes of Health grant RO1GM094415 and March of Dimes grant FY11-434 to K.C. Slep and National Institutes of Health grant DA036877 to B. Kulhman, R.C. Adikes was supported by National Institutes of Health grant F31-GM116476 for this work.

REFERENCES

Applewhite, D.A., K.D. Grode, M.C. Duncan, and S.L. Rogers. 2013. The actin-microtubule cross-linking activity of Drosophila Short stop is regulated by intramolecular inhibition. Mol Biol Cell, 24, 2885-93. doi: 10.1091/mbc.E12-11-0798

Applewhite, D.A., K.D. Grode, D. Keller, A.D. Zadeh, K.C. Slep, and S.L. Rogers. 2010. The spectraplakin Short stop is an actin-microtubule cross-linker that contributes to organization of the microtubule network. Mol Biol Cell, 21, 1714-24. doi: 10.1091/mbc.E10-01-0011

Bieling, P., L. Laan, H. Schek, E.L. Munteanu, L. Sandblad, M. Dogterom, D. Brunner, and T. Surrey. 2007. Reconstitution of a microtubule plus-end tracking system in vitro. Nature, 450, 1100-5. doi: 10.1038/nature06386

Currie, J.D., S. Stewman, G. Schimizzi, K.C. Slep, A. Ma, and S.L. Rogers. 2011. The microtubule lattice and plus-end association of Drosophila Mini spindles is spatially regulated to fine-tune microtubule dynamics. Mol Biol Cell, 22, 4343-61. doi: 10.1091/mbc.E11-06-0520

Duan, L., D. Che, K. Zhang, Q. Ong, S. Guo, and B. Cui. 2015. Optogenetic control of molecular motors and organelle distributions in cells. Chem Biol, 22, 671-82. doi: 10.1016/j.chembiol.2015.04.014

Goryunov, D., C.Z. He, C.S. Lin, C.L. Leung, and R.K. Liem. 2010. Nervous-tissue-specific elimination of microtubule-actin crosslinking factor 1a results in multiple developmental defects in the mouse brain. Mol Cell Neurosci, 44, 1-14. doi: 10.1016/j.mcn.2010.01.010

Gregory, S.L., and N.H. Brown. 1998. kakapo, a gene required for adhesion between and within cell layers in Drosophila, encodes a large cytoskeletal linker protein related to plectin and dystrophin. J Cell Biol, 143, 1271-82.

Guesdon, A., F. Bazile, R.M. Buey, R. Mohan, S. Monier, R.R. García, M. Angevin, C. Heichette, R. Wieneke, R. Tampé, et al. 2016. EB1 interacts with outwardly curved and straight regions of the microtubule lattice. Nat Cell Biol, 18:1102–1108. doi: 10.1038/ncb3412

Guntas, G., R.A. Hallett, S.P. Zimmerman, T. Williams, H. Yumerefendi, J.E. Bear, and B. Kuhlman. 2015. Engineering an improved light-induced dimer (iLID) for controlling the localization and activity of signaling proteins. Proc Natl Acad Sci U S A, 112, 112-7. doi: 10.1073/pnas.1417910112

Guo, L., L. Degenstein, J. Dowling, Q.C. Yu, R. Wollmann, B. Perman, B. and E. Fuchs. 1995. Gene targeting of BPAG1: abnormalities in mechanical strength and cell migration in stratified epithelia and neurologic degeneration. Cell, 81, 233-43.

Hallett, R.A., S.P. Zimmerman, H. Yumerefendi, J.E. Bear, and B. Kuhlman. 2016. Correlating in Vitro and in Vivo Activities of Light-Inducible Dimers: A Cellular Optogenetics Guide. ACS Synth Biol, 5, 53-64. doi: 10.1021/acssynbio.5b00119

Harper, S.M., J.M. Christie, and K.H. Gardner. 2004. Disruption of the LOV-Jalpha helix interaction activates phototropin kinase activity. Biochemistry, 43, 16184-92. doi: 10.1021/bi048092i

Honnappa, S., S.M. Gouveia, A. Weisbrich, F.F. Damberger, N.S. Bhavesh, H. Jawhari, I. Grigoriev, F.J. Van Rijssel, R.M. Buey, A. Lawera, I. Jelesarov, F.K. Winkler, K. Wuthrich, A. Akhmanova, and M.O. Steinmetz. 2009. An EB1-binding motif acts as a microtubule tip localization signal. Cell, 138, 366-76. doi: 10.1016/j.cell.2009.04.065

Honnappa, S., C.M. John, D. Kostrewa, F.K. Winkler, and M.O. Steinmetz. 2005. Structural insights into the EB1-APC interaction. EMBO J, 24, 261-269. doi: 10.1038/sj.emboj.7600529

Jiang, K., G. Toedt, S. Montenegro Gouveia, N.E. Davey, S. Hua, B. van der Vaart, I. Grigoriev, J. Larsen, L.B. Pedersen, K. Bezstarosti, M. Lince-Faria, J. Demmers, M.O. Steinmetz, T.J. Gibson, and A. Akhmanova. 2012. A Proteome-wide screen for mammalian SxIP motif-containing microtubule plus-end tracking proteins. Curr Biol, 22, 1800-7. doi: 10.1016/j.cub.2012.07.047

Kapur, M., W. Wang, M.T. Maloney, I. Millan, V.F. Lundin, T.A. Tran, and Y. Yang. 2012. Calcium tips the balance: a microtubule plus end to lattice binding switch operates in the carboxyl terminus of BPAG1n4. EMBO Rep, 13, 1021-9. doi: 10.1038/embor.2012.140

Kendrick, R.E., J.L. Peters, L.H. Kerckhoffs, A. Van Tuinen, and M. Koornneef. 1994. Photomorphogenic mutants of tomato. Biochem Soc Symp, 60, 249-56.

Kumar, P., M.S. Chimenti, H. Pemble, A. Schönichen, O. Thompson, M.P. Jacobson, and T. Wittmann. 2012. Multisite phosphorylation disrupts arginine-glutamate salt bridge networks required for binding of cytoplasmic linker-associated protein 2 (CLASP) to end-binding protein 1 (EB1). J Biol Chem, 287, 17050-64. doi: 10.1074/jbc.M111.316661

Kunda, P., and B. Baum. 2009. The actin cytoskeleton in spindle assembly and positioning. Trends Cell Biol, 19, 174-9. doi: 10.1016/j.tcb.2009.01.006

Lane, T.R., E. Fuchs, and K.C. Slep. 2017. Structure of the ACF7 EF-Hand GAR module and delineation of microtubule binding determinants. Structure, 25, 1130-8. doi: 10.1016/j.str.2017.05.006

Lee, S., K.L. Harris, P.M. Whitington, and P.A. Kolodziej. 2000. short stop is allelic to kakapo, and encodes rod-like cytoskeletal-associated proteins required for axon extension. J Neurosci, 20, 1096-108.

Lee, T. and L. Luo.1999. Mosaic analysis with a repressible cell marker for studies of gene function in neuronal morphogenesis. Neuron, 22, 451-61.

Lungu, O.I., R.A. Hallett, E.J. Choi, M.J. Aiken, K.M. Hahn, and B. Kuhlman. 2012. Designing photoswitchable peptides using the AsLOV2 domain. Chem Biol, 19, 507-17. doi: 10.1016/j.chembiol.2012.02.006

Maurer, S. P., Bieling, P., Cope, J., Hoenger, A. & Surrey, T. 2011. GTPγS microtubules mimic the growing microtubule end structure recognized by end-binding proteins (EBs). Proc. Natl Acad. Sci. USA 108, 3988–3993. doi: 10.1073/pnas.1014758108

Maurer, S. P., Fourniol, F. J., Bohner, G., Moores, C. A. & Surrey, T. 2012. EBs recognize a nucleotide-dependent structural cap at growing microtubule ends. Cell 149, 371–382. doi: 10.1016/j.cell.2012.02.049

Meijering, E., O. Dzyubachyk, and I. Smal . 2012. Methods for Cell and Particle Tracking. *In Methods in Enzymology. P.M. Conn, editor.* Elsevier, Ch. 9, 183-200.

Prokop, A., J. Uhler, J. Roote, and M. Bate. 1998. The kakapo mutation affects terminal arborization and central dendritic sprouting of Drosophila motorneurons. J Cell Biol, 143, 1283-94.

Rao, M.V., P.H. Chu, K.M. Hahn, and R. Zaidel-Bar. 2013. An optogenetic tool for the activation of endogenous diaphanous-related formins induces thickening of stress fibers without an increase in contractility. Cytoskeleton (Hoboken), 70, 394-407. doi: 10.1002/cm.21115

Rivera, V.M., T. Clackson, S. Natesan, R. Pollock, J.F. Amara, T. Keenan, S.R. Magari, T. Phillips, N.L. Courage, F., Cerasoli Jr., D.A. Holt, and M. Gilman. 1996. A humanized system for pharmacologic control of gene expression. Nat Med, 2, 1028-32.

Rogers, S.L., and G.C. Rogers. 2008. Culture of Drosophila S2 cells and their use for RNAi-mediated loss-of-function studies and immunofluorescence microscopy. Nat Protoc, 3, 606-11. doi: 10.1038/nprot.2008.18

Roper, K., and N.H. Brown. 2003. Maintaining epithelial integrity: a function for gigantic spectraplakin isoforms in adherens junctions. J Cell Biol, 162, 1305-15. doi: 10.1083/jcb.200307089

Sanchez-Soriano, N., M. Travis, F. Dajas-Bailador, C. Goncalves-Pimentel, A.J. Whitmarsh, and A. Prokop. 2009. Mouse ACF7 and drosophila short stop modulate

filopodia formation and microtubule organisation during neuronal growth. J Cell Sci, 122, 2534-42. doi: 10.1242/jcs.046268

Schindelin, J., I. Arganda-Carreras, E. Frise, V. Kaynig, M. Longair, T. Pietzsch, S. Preibisch, C. Rueden, S. Saalfeld, B. Schmid, J.Y. Tinevez, D.J. White, V. Hartenstein, K. Eliceiri, P. Tomancak, and A. Cardona. 2012. Fiji: an open-source platform for biological-image analysis. Nat Methods, 9, 676-82. doi: 10.1038/nmeth.2019

Slep, K.C., S.L. Rogers, S.L. Elliott, H. Ohkura, P.A. Kolodziej, and R.D. Vale. 2005. Structural determinants for EB1-mediated recruitment of APC and spectraplakins to the microtubule plus end. J Cell Biol, 168, 587-98. doi: 10.1083/jcb.200410114

Steinmetz, M.O., I. Jelesarov, W.M. Matousek, S. Honnappa, W. Jahnke, J.H. Missimer, S. Frank, A.T. Alexandrescu, and R.A. Kammerer. 2007. Molecular basis of coiled-coil formation. Proc Natl Acad Sci U S A, 104, 7062-7. doi: 10.1073/pnas.0700321104

Strickland, D., Y. Lin, E. Wagner, C.M. Hope, J. Zayner, C. Antoniou, T.R. Sosnick, E.L. Weiss, and M. Glotzer. 2012. TULIPs: tunable, light-controlled interacting protein tags for cell biology. Nat Methods, 9, 379-84. doi: 10.1038/nmeth.1904

Strumpf, D., and T Volk. 1998. Kakapo, a novel cytoskeletal-associated protein is essential for the restricted localization of the neuregulin-like factor, vein, at the muscle-tendon junction site. J Cell Biol, 143, 1259-70.

Takacs, Z., F. Jankovics, P. Vilmos, P. Lenart, K. Roper, and M. Erdelyi. 2017. The spectraplakin Short stop is an essential microtubule regulator involved in epithelial closure in Drosophila. J Cell Sci, 130, 712-724. doi: 10.1242/jcs.193003

Tortosa, E., C. Montenegro-Venegas, M. Benoist, S. Hartel, C. Gonzalez-Billault, J.A. Esteban, and J. Avila. 2011. Microtubule-associated protein 1B (MAP1B) is required for dendritic spine development and synaptic maturation. J Biol Chem, 286, 40638-48. doi: 10.1074/jbc.M111.271320

van Bergeijk, P., M. Adrian, C.C. Hoogenraad, and L.C. Kapitein. 2015. Optogenetic control of organelle transport and positioning. Nature, 518, 111-4. doi: 10.1038/nature14128

van Haren J., A. Ettinger, H. Wang, K. Hahn, and T. Wittmann. 2017. Local control of intracellular microtubule dynamics by End Binding protein 1 (EB1) Photo-Dissociation. *bioRxiv*. doi.org/10.1101/099598 (Preprint posted on January 10, 2017)

Wang H., and K.M. Hahn. 2016. LOVTRAP: A versatile method to control protein function with light. *Curr Protoc Cell Biol*, 73, 21 10 1-21 10 14. doi: 10.1002/cpcb.12

Walsh, E.P., and N.H. Brown. 1998. A screen to identify Drosophila genes required for integrin-mediated adhesion. Genetics, 150, 791-805.

Weitzman, M., and K.M. Hahn. 2014. Optogenetic approaches to cell migration and beyond. Curr Opin Cell Biol, 30, 112-20. doi: 10.1016/j.ceb.2014.08.004

Wu, X., A. Kodama, and E. Fuchs. 2008. ACF7 regulates cytoskeletal-focal adhesion dynamics and migration and has ATPase activity. Cell, 135, 137-48. doi: 10.1016/j.cell.2008.07.045

Wu, X., Q.T. Shen, D.S. Oristian, C.P. Lu, Q. Zheng, H.W. Wang, and E. Fuchs. 2011. Skin stem cells orchestrate directional migration by regulating microtubule-ACF7 connections through GSK3beta. Cell, 144, 341-52. doi: 10.1016/j.cell.2010.12.033

Zanic, M., Stear, J. H., Hyman, A. A. & Howard, J. 2009 EB1 recognizes the nucleotide state of tubulin in the microtubule lattice. PloS ONE 4, e7585. doi: 10.1371/journal.pone.0007585

Zimmerman, S.P., R.A. Hallett, A.M. Bourke, J.E. Bear, M.J. Kennedy, and B. Kuhlman. 2016. Tuning the Binding Affinities and Reversion Kinetics of a Light Inducible Dimer Allows Control of Transmembrane Protein Localization. Biochemistry, 55, 5264-71. doi: 10.1021/acs.biochem.6b00529

CHAPTER 3: STRUCTURE AND FUNCTIONAL ROLE OF THE C-TERMINAL DOMAIN OF THE *DROSOPHILA* XMAP215 PROTEIN FAMILY MEMBER MINISPINDLE

3.1 Introduction

Microtubules (MTs) are cytoskeletal polymers that change their cellular distribution during the cell cycle and development. MTs are responsible for multiple cytoplasmic activities, such as enabling intracellular transport, stabilizing the cell's shape, and forming the mitotic spindle to separate chromosomes during mitosis. MTs are composed of α β-tubulin heterodimers that assemble to create a hollow tube like structure. The α β-tubulin heterodimers provide the polymer with polarity: with α-tubulin exposed at the MT minus end and β-tubulin exposed MT plus end (Walker et al., 1988, Cassimeris et al., 1988; Desai and Mitchison, 1997; Howard and Hyman, 2003). MTs are inherently dynamic due to MT polymerization-dependent hydrolysis of the GTP molecule bound to the α β-tubulins exchangeable GTP site (Mitchison and Kirshner, 1984, Desai and Mitchison, 1997). This dynamic instability enables MTs to transition between phases of polymerization, depolymerization and pause (Mitchison and Kirshner, 1984). MT-associated proteins (MAPs) spatially and temporally localize to MTs to modulate MT dynamics through molecular and structural changes to the MT to facilitate cytoskeletal network restructuring. Members of a subgroup of MAPs that specifically localize to the polymerizing MT plus end are referred to as +TIPs. +TIPs play a pivotal role in the regulation of the dynamic behavior of MT plus ends (Schuyler and Pellman, 2001;

Akhmanova and Hoogenraad, 2005; Akhmanova and Steinmetz, 2008). Five major +TIP protein families include end-binding 1 (EB1), cytoskeletal linker protein 170 (CLIP 170), CLIP-170-associated protein (CLASP), *Xenopus* microtubule-associated protein 215 (XMAP 215) and Sentin/SLAIN1/2 (Gard and Kirschner, 1987; Vasquez et al., 1994; Komarova et al., 2002; Minori-Kiysoue et al., 2005; Slep et al., 2005; Slep and Vale, 2007, Li et al., 2011; van der Vaart et al., 2011).

The XMAP215 family of proteins accelerates MT assembly and promotes MT polymerization by directly binding tubulin heterodimers under high tubulin concentrations (Charrasse et al., 1998; Al-Bassam et al., 2006; Slep and Vale, 2007; Brouhard et al., 2008; Slep, 2009; Widlund et al., 2011). XMAP215 family members promote polymerization and drive bipolar spindle assembly using an N-terminal array of tumor over expressed gene (TOG) domains that bind to tubulin heterodimers. TOG domains contain tandem Huntington, elongation factor 2, phosphate A2, and TOR PI-3 kinase (HEAT) repeats with highly conserved intra-HEAT loops essential for interacting with tubulin (Al-Bassam et al., 2006; Slep and Vale, 2007; Ayaz et al., 2012). Studies of XMAP215 family members in multiple species (*S. pombe*, *C. elegans*, *Xenopus* egg extracts, *Drosophila* and HeLa cells) have shown that they play an essential role during interphase and mitosis, as their depletion leads to decreased MT growth rates and short spindles or defects in spindle architecture (Gard and Kirschner, 1987; Vasquez et al, 1994; Matthews et al., 1998; Cullen et al., 1999; Tournebize et al., 2000; Kosco et al., 2001; Gergley et al., 2003, Brittle and Ohkura et al., 2005; Kawamura and Wasteneys, 2008; Kronja et al., 2009; Cassimeris et al., 2009; Zanic et al., 2013). Members of the XMAP215 family contain a varying number of N-terminal TOG domains and the details

of the structure and function of these domains has been well characterized (Al-Bassam et al., 2007; Slep and Vale, 2007; Ayaz et al., 2012; Fox et al, 2014; Howard et al., 2015; Byrnes and Slep, 2017). However, the structure and functional role of the C-terminal region (CTD) remains poorly understood.

Previous research has elucidated that the CTD domain of XMAP215 family members has multiple binding partners. These include TACC family proteins, Sentin/SLAIN, clathrin, CLASP, gammaTuRC and in *S. Pombe* Ndc80. The interaction of Msps with these binding partners has been shown to be required for proper localization of the protein, proper interphase MT dynamics and network architecture as well as proper spindle formation and dynamics (Lee et al., 2001; Bellanger and Gönczy, 2003; Le Bot et al., 2003; Srayko et al., 2003; Gergely et al., 2003; Li et al., 2011; van der Vaart et al., 2011; Hood et al., 2013; Trogden and Rogers 2015; Miller et al., 2016). While some details have been uncovered about the role and mechanisms of this region, how of XMAP215 family members interact with their binding partners remains poorly understood. We hypothesize that structural elements within the conserved CTD of the XMAP215 family of proteins are responsible for regulating MT dynamics by properly localizing the full-length molecule to MT plus ends during mitosis and interphase.

Here we investigate the role of the CTD of the XMAP215 family member, minispindles (Msps), during interphase and mitosis. We show that the CTD and in particular TOG6 is necessary and sufficient to localize Msps to MT plus ends during interphase and mitosis. TOG6 is required but not sufficient to rescue MT polymerization, spindle architecture and bipolar spindle length. Key conserved residues within TOG6 are required to localize the full-length molecule to MT plus ends during interphase and

mitosis. Here we propose that these residues interact with the plus end protein Sentin. These data show that Msps is recruited to MT plus ends via an interaction between Msps TOG6 domain and the first 36 amino acids of Sentin. This recruitment mechanism is required to properly position Msps at the MT plus end and promote MTpolymerization.

3.2 Results

3.2.1 The CTD of Msps is necessary but not sufficient to rescue MT growth velocities

To establish the cellular role of the CTD of Msps we created *Drosophila* cell expression constructs lacking the CTD or containing just the CTD and preformedMT polymerization rescue experiments in *Drosophila* S2 cells (Fig. 3.1A). Cells were depleted of endogenous Msps using *msps* dsRNA and co-transfected with EB1-tRFP to determine MT polymerization rates. As expected, we found that the construct lacking the CTD failed to localize to MT plus ends and did not fully rescue MT growth velocities (Fig. 3.1B and C). These data match previously reported results from Fox et.al., 2014 and Byrnes and Slep, 2017. The CTD alone was able to localize the MT plus ends, observed as small puncta (Fig. 3.1C), but failed to rescue MT growth velocities (Fig. 3.1B). These data show that the CTD is necessary and sufficient to localize Msps to MT plus ends and is necessary but not sufficient to rescue MT growth velocities.

3.2.2 Forced localization of the N-terminal TOG domains does not rescues MT growth velocities

We next asked if the CTD of XMAP215 family members simply acts to target the full-length molecule to MT plus ends, sites of MT nucleation, or both. To answer this question we removed the CTD of Msps and replaced it with domains to target the N-terminal TOG domains to MT plus ends or the centrosome or both. We created four

forced localization constructs, two to primarily target centrosomes and two to target to MT plus ends. To generate centrosome targeting we utilized the PACT domain from the

Drosophila centrosome pericentrin-like-protein, which affords robust localization to the centrosome (Martinez-Campos et al., 2004). We utilized the TACC domain from the Drosophila TACC homologue DTACC. This domain has been shown to recruit TACC proteins to centrosomes and it can recruit XMAP215 homologues to the centrosome (Lee et al., 2001; Bellanger and Gönczy, 2003; Le Bot et al., 2003; Srayko et al., 2003; Gergely et al., 2003). Furthermore, recent data has shown that TACC proteins, including DTACC can track MTs plus ends themselves and the TACC domain alone can plus end track (Adikes et al., unpublished). Therefore, fusion of the N-terminal TOG domains to the TACC domain could lead to both centrosome and plus end targeting. To target Msps exclusively to MT plus ends we used the 18 residue motif with a central SKIP motif from the microtubule actin cross-linking factor 2 (MACF2). This 18 residue motif has been well studied and has shown to plus end track in many systems by interacting with EB proteins. Although this 18-residue motif confers plus end binding, plus end affinity can be increased via dimerization which increases avidity for EB proteins. Thus, to confer dimerization we used the Leucine Zipper (LZ) from GCN4 (Honnappa et al., 2009, Steinmetz et al., 2007). We next asked if these fusion constructs could rescue MT growth velocities. Msps depleted cells were co-transfected with a fusion construct of interest and EB1-tRFP. MT growth velocities were determined from tracking EB1 comets in the cells over time. We observed that for all fusion constructs there was an increase in plus end localization as compared to Msps TOG 1-5 (Fig. 3.2B). We determined that all the fusion

constructs were able to rescue MT growth velocities above that of Msps TOG 1-5 alone (0.6-2 μm/min above Msps TOG 1-5), however, none of these constructs were able to fully rescue MT growth velocities (Fig. 3.2C). Furthermore, only the constructs that

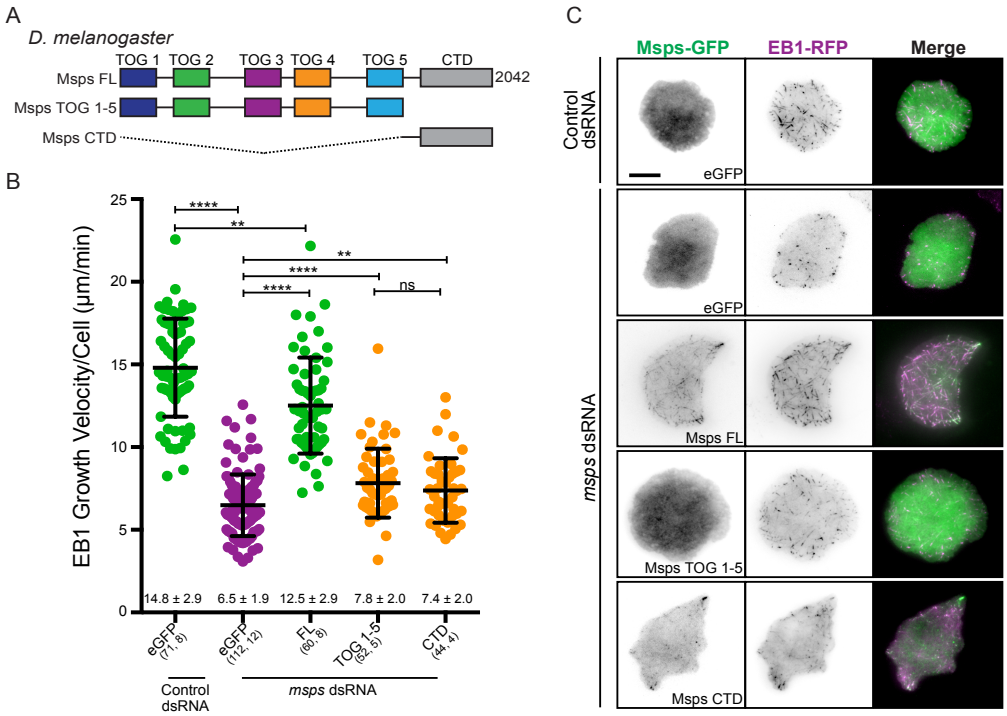

Figure 3.1. The C-terminal region of Msps is necessary but not sufficient to rescue MT growth velocities. (A) Schematic of Msps domain architecture. (B) EB1 growth velocities from Msps N-terminal TOG domain deletion experiments in *Drosophila* S2 cells. Depletion of Msps leads to decreased MT growth velocities, which are rescued with FL Msps. Msps TOG 1-5 or the CTD alone fail to fully rescue MT growth velocities. Numbers below plots indicate the mean ± standard deviation. Numbers in parentheses indicate number of cells analyzed, number of experiments. * $p<0.05$, ** $p<0.005$, ***$p<0.0005$, **** $p<0.000$. (C) Localization of Msps N-terminal TOG domain deletion experiments. Msps FL localizes to MT plus ends and has a comet-like appearance, Msps TOG 1-5 fails to localize to MT plus ends and the CTD can localizes to MT plus ends.

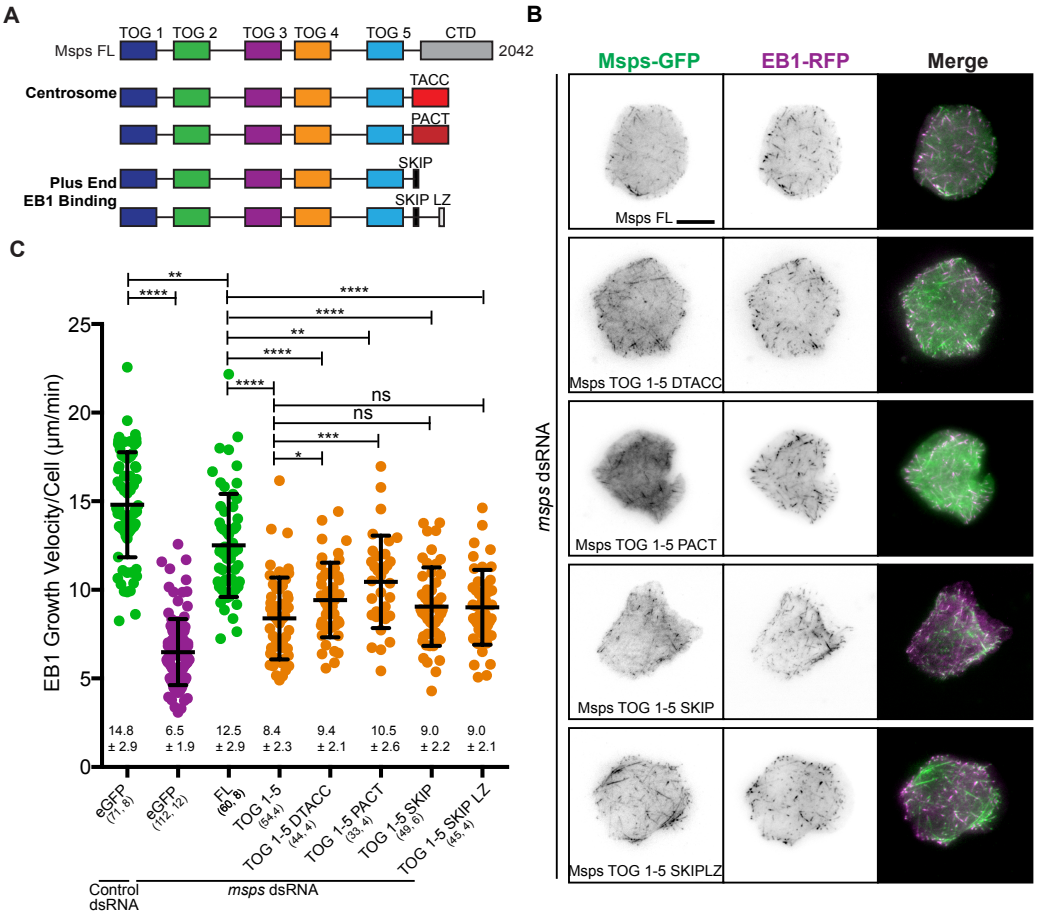

Figure 3.2. Forced localization of the N-terminal TOGs domains does not rescues MT growth velocities. (A) Schematic of Msps fusion constructs for forced localization experiments. (B) Localization of Msps TOG 1-5 fusion constructs, all fusion construct are able to rescue MT plus end localization. (C) EB1 growth velocities of Msps TOG 1-5 fusion constructs. Msps TOG 1-5 partially rescues MT growth velocities. Fusion of a centrosome targeting domain, either the TACC domain or PACT, increases MT growth velocities above the average velocity of TOG 1-5 while fusion to a SKIP motif fails to rescue MT growth velocities about that of TOG 1-5. Numbers below plots indicate the mean ± standard deviation. Numbers in parentheses indicate number of cells analyzed, number of experiments. * $p<0.05$, ** $p<0.005$, ***$p<0.0005$, **** $p<0.000$.
Note the controls shown here are the same as in Figure 3.1.

contained a centrosome-targeting (PACT)/ centrosome and plus end targeting (DTACC) domain were able to significantly increase MT growth velocities above that of Msps TOG 1-5, however the average growth velocity of these constructs was significantly lower than Msps FL. These data suggest that the CTD severs more than just a simple plus end localize module and hints at the potential importance of having a centrosome targeting domain present during interphase.

3.2.3 The Msps CTD has a conserved central region, predicted to have 12 alpha helices

To understand what role the CTD plays in promoting MT polymerization we analyzed the conservation, secondary structure and the oligomeric state of the CTD of Msps. When we aligned the CTD sequences from six species, and preformedsecondary structure predictions we found that the CTD contains highly conserved regions. Secondary structure predications showed a high percentage of alpha helical content. These analyses uncovered a region within the CTD (residues 1596-1852) that is highly conserved and predicted to have 12 helices (Fig. 3.3A). Since TOG domains contain 12 alpha helices, which form 6 heat repeats these data suggest that the central region of the CTD could contain a 6th TOG domain. The presence of a 6th TOG domain has previously been suggested by NMR data from the work by the Royle and Bayliss labs. (Hood et al., 2013; Burgess et al., 2015).

To experimentally determine the secondary structural content and oligomeric state of the CTD domain 2 recombinant CTD domains were expressed and purified (Fig. S3.1A). Circular dichroism (CD) experiments on the CTD (1596-2042) (black line) and the predicted TOG6 (1596-1852) (purple line) confirmed these constructs are alpha helical (Fig. 3B) and cooperatively unfold (Fig. 3.3C). Size exclusion chromatography

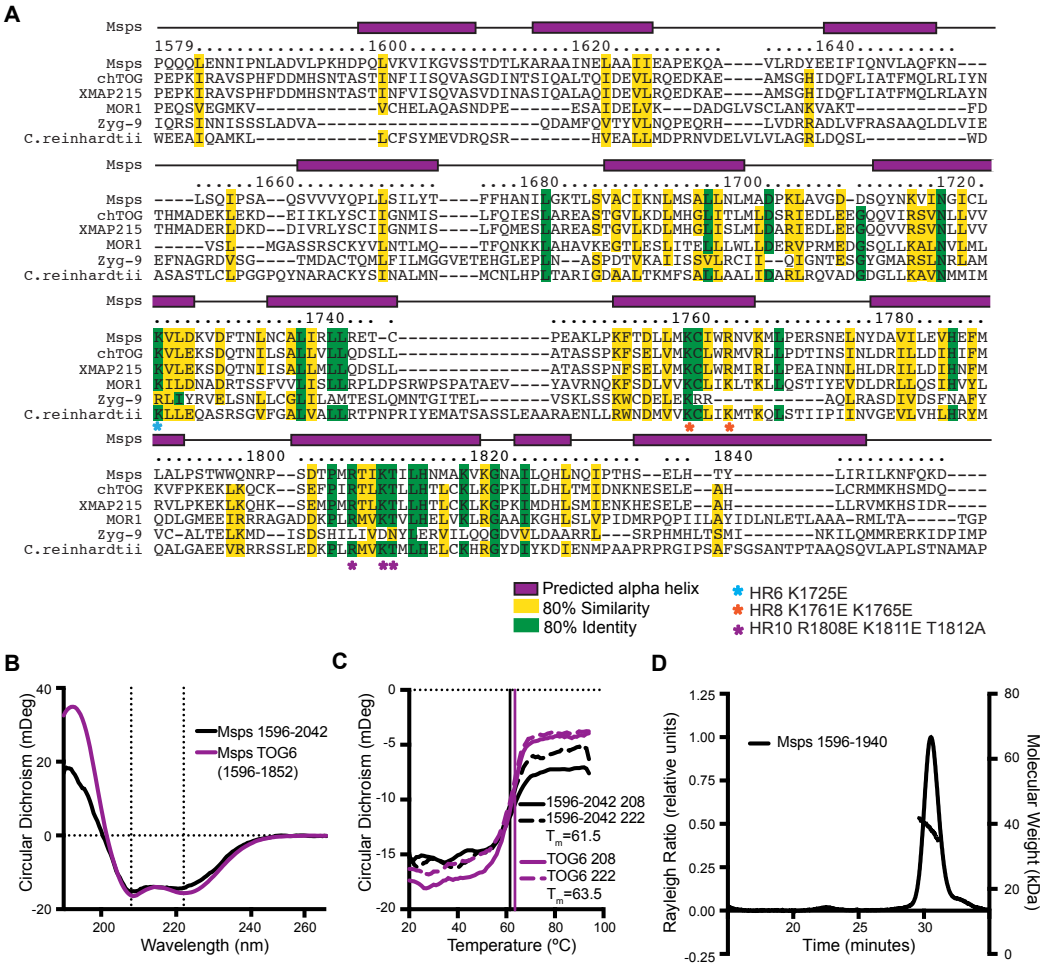

Figure 3.3. The Msps CTD has a conserved central region, predicted to have 12 alpha helices. (A) Multiple species alignment of the TOG6 region of the Msps CTD of *D. melanogaster* Msps, *H.sapiens* ch-TOG, *X. Laevis* XMAP215, *Arabadopsis* MOR1, *C.elegans* Zyg-9, *C. reinhardtii*. Purple boxes about the alignment indicate predicated secondary structure resides highlighted in green are 80% identical and those in yellow are 80% similar. Residues annotated with *'s indicate resides mutated in Fig. 5 and Fig. 7. (B-C) Circular dichroism spectra of Msps 1596-2042 (black line) and Msps TOG 6 (1596-1852) (purple lines) at 20°C (B) and thermal melt curves monitored using 208nm (solid line) and 222nm light (dotted line). (D) Size exclusion chromatography coupled with multi-angle light scattering of Msps 1596-1940.

coupled with multi-angle light scattering (SEC-MALS) showed that the CTD (1596-1940) of Msps is monomeric (Fig. 3.3D).

3.2.4 Deletion of TOG6 fails to localize Msps to MT plus ends and rescue MT growth velocities

We next asked what role the predicted CTD 6th TOG domain could play in the context of the FL molecule. To address this question we created a GFP-tagged construct lacking this region of the CTD, Msps Δ TOG6. Msps-depleted cells were co-transfected with Msps Δ TOG6 and EB1-tRFP. Msps Δ TOG6 failed to localize to MT plus ends, occasionally it could be observed along the length of the MT on a subset of MTs within a cell, this is also occasionally observed with Msps TOG 1-5 (Fig. 3.4A). Msps Δ TOG6 failed to fully rescue MT dynamics (Fig. 3.4A and B). Interestingly, Msps Δ TOG6 growth velocities are increased above Msps TOG 1-5 growth velocities suggesting that regions within in the CTD, outside of TOG6, could minimally aid in promoting MT polymerization (Fig. 3.4B). To determine if the TOG6 domain alone could engage MT plus ends and rescue MT growth velocities we co-transfected a GFP-tagged TOG6 with EB1-tRFP. TOG6 was able to localize to MT plus ends in a punctate fashion (Fig. 4A). However, TOG6 alone failed to rescue MT growth velocities and was not significantly different than MT growth velocities in Msps-depleted cells. Therefore, TOG6 is necessary and sufficient for MT plus end localization, however TOG6 is necessary but not sufficient to rescue MT growth velocities.

3.2.5 Conserved residues within the predicted CTD TOG domain are required to localize Msps to MT plus ends and rescue MT growth velocities

To further investigate the role of the predicted CTD TOG domain we asked if there were specific residues within this domain that could confer plus end localization

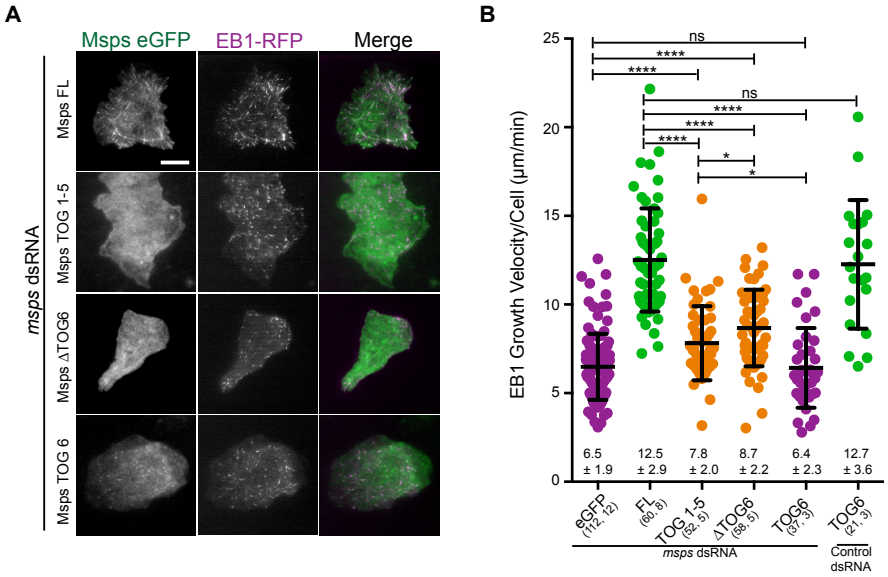

Figure 3.4. Depletion of the proposed TOG6 fails to localize Msps to MT plus ends and rescue MT growth velocities. (A) Localization of Msps Δ TOG6 in *Drosophila* S2 cells. Msps Δ TOG6 fails to localize to MT plus ends. (B) EB1 growth velocities from Msps TOG 6 deletion experiments. Msps Δ TOG6 fails to fully rescue MT growth velocities. Numbers below plots indicate the mean ± standard deviation. Numbers in parentheses indicate number of cells analyzed, number of experiments. * $p<0.05$, ** $p<0.005$, ***$p<0.0005$, **** $p<0.000$.

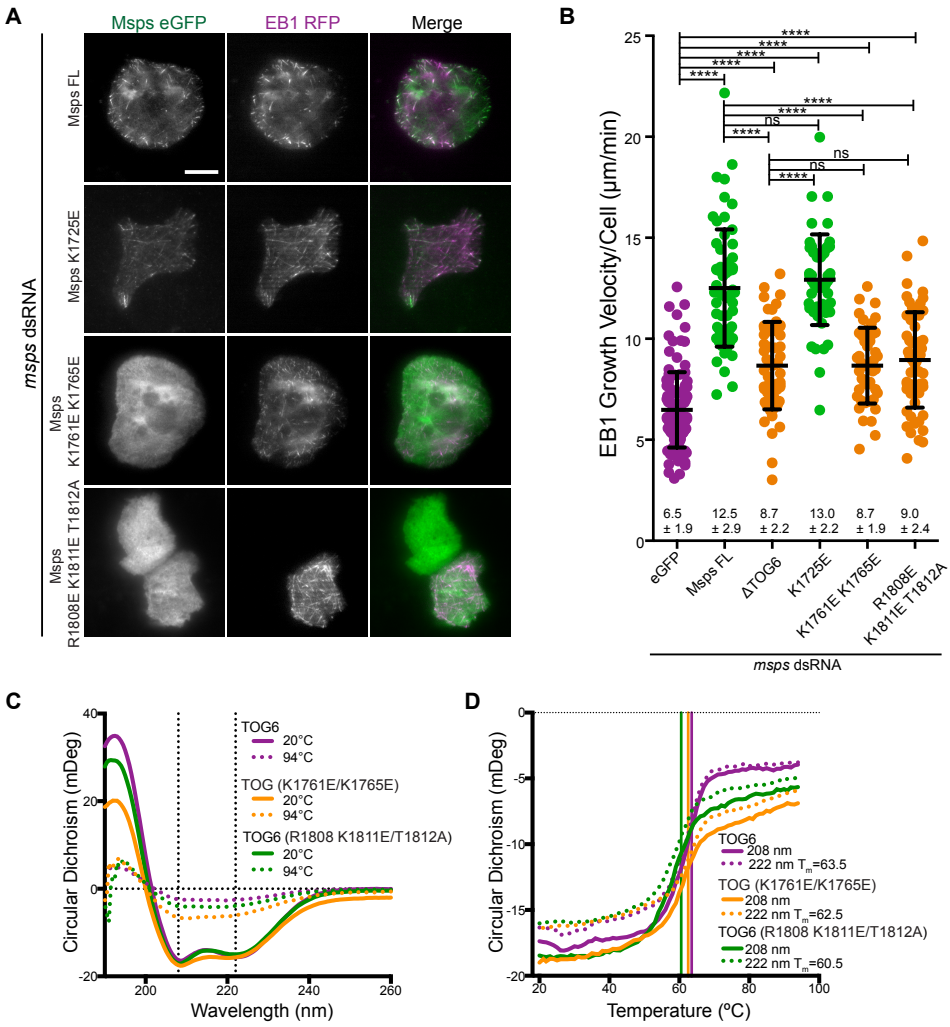

Figure 3.5. Conserved residues within the predicted TOG domain are required to localize Msps to MT plus ends and rescue MT growth velocities. (A) Localization of Msps mutant constructs. Msps localizes to plus ends with mutation K1725E. Mutation of K1761E/K1765E and R1808E/K1811E/T1812A prevent Msps plus end localization. (B) EB1 growth velocities of Msps point mutations within the TOG6. Msps K1725E does not alter MT growth velocities mutation of K1761E/K1765E and R1808E/K1811E/T1812A both decrease MT growth velocities are not significantly different than Msps Δ TOG6. Numbers below plots indicate the mean ± standard deviation. Numbers in parentheses indicate number of cells analyzed, number of experiments. * p<0.05, ** p<0.005, ***p<0.0005, **** p<0.000. (C-D) Circular dichroism spectra of Msps TOG 6 (1596-1852) (purple line) Msps TOG 6 K1761E/K1765E (yellow) and Msps TOG6 R1808E/K1811E/T1812A at 20°C (solid line) and 94°C (dotted line) (C) and thermal melt curves monitored using 208nm (solid line) and 222nm light (dotted line) (D).

and therefore be required to rescue MT growth velocities. Based on the multiple sequence alignment and structural predictions of TOG6 we identified three sets of residues to investigate (Fig. 3.3A annotated with *). Set one contains a single charged residue at position 1725, set two contains two residues K1761 and K1765, and set three contains three residues R1808, K1811, and T1812. All of the residues were predicted to be surface exposed and are highly conserved (Fig. 3.3A annotated with *). Four of the five residues are charged and one could potentially be phosphorylated. To determine the role of these sets of residues we reversed the charge of the charged residues (K/R to E), and changed the T to A at position 1812 (Fig. 3.3A annotated with *). We found that charge reversal at position 1725 did not change the localization of Msps or alter MT growth rates (Fig. 3.5A and B). Mutation of K1761E/K1765E or R1808E/K1811E/T1812A decreased the plus end localization of Msps and failed to fully rescue MT growth rates. The MT growth velocities of K1761E/K1765E and R1808E/K1811E/T1812A were not significantly different than Msps Δ TOG6 (Fig. 3.5A and B). To ensure that these residues did not alter the stability of the domain recombinant protein was purified for the native CTD TOG6 domain and TOG6 mutants (Fig. S3.1B). Circular dichroism (CD) analyses showed that mutating these residues does not change the α-helical character or stability of the domain (Fig. 3.5C and D). These data show that key conserved residues within TOG6, in particular 1761/1765 and 1808/1811/ 1812 are required to localize Msps to MT plus ends and rescue MT polymerization rates.

3.2.6 TOG6 is required to properly localize Msps during mitosis, establish the bipolar spindle and regulate spindle length

In addition to playing a key role in promoting MT polymerization during interphase, Msps is required to generate a proper bipolar spindle during mitosis. Previous

data show that Msps depletion from *Drosophila* S2 cells leads to a decreased percentage of bipolar spindles and an increased percentage of cells with improper mitotic structures (Cullen et al., 1999, Byrnes and Slep, 2017). The bipolar spindles that do form in the absence of Msps are shorter in pole-to-pole distance (Goshima et al., 2005). To investigate if TOG6 is required to generate a bipolar mitotic spindle, we assessed mitotic structure formation in control and *msps* dsRNA treated cells. Mitotic structures were classified into five categories, bipolar, bipolar/monastral, misaligned, monopolar and multipolar (Fig. 3.6A). Control dsRNA treated cells were 70.3% bipolar or bipolar/monastral and 29.7% abnormal (misaligned, monoploar or multipolar). Msps depletion lead to a decrease in the percentage of bipolar or bipolar/monastral structures (42.3%) and an increase in abnormal structures (61.6%). Transfection of Msps FL into Msps-depleted cells rescued the percentage of bipolar and bipolar/monastral structures to 64.7%. Msps TOG 1-5 or Msps Δ TOG6 were both unable to rescue the percentage of bipolar and bipolar/monastral structures to the same degree as Msps FL. For Msps TOG 1-5 transfected cells 48.4% were bipolar or bipolar/monastral and Msps Δ TOG6 transfected 48.9% bipolar or bipolar/monastral.

In cells that formed a proper bipolar spindle we measured the pole-to-pole distance. Preliminary data show that TOG6 could be required to generate spindles of the proper length as cells transfected with Msps Δ TOG6 seem to have slightly shorter spindles, however many more spindles need to be measured in order to make any conclusions (Fig. 3.6B).

Since TOG6 is required to rescue the mitotic phenotypes we asked if TOG6 was required for proper localization of Msps during mitosis. Msps has been shown to localize

to centrosomes, MTs, MT plus ends at the kinetochore and shows an enriched localization on kinetochore fiber MTs (Buster et al., 2007). Msps does not appear to bind directly to the kinetochore and thus the enrichment observed at the kinetochore is due to binding MT plus ends (Fig. S3.2). GFP tagged Msps FL, Msps TOG 1-5 or Msps Δ TOG6 were transfected into wild-type *Drosophila* S2 cells (i.e. containing endogenous Msps) and the localization was observed during mitosis in cells that generated bipolar spindles (Fig. 3.6C). Msps FL localizes to the centrosome, MT plus ends at the kinetochore and appears enriched along the length of the kinetochore fibers. Msps TOG 1-5 localizes to MTs throughout the spindle, the centrosome, and on the DNA during mitosis (Fig. 3.6C). Msps Δ TOG6 recapitulates the localization pattern of Msps TOG 1-5 with a more variable DNA localization observed (Fig. 3.6C). These data show that TOG6 is required during mitosis to properly localize Msps to the bipolar spindle to ensure bipolar spindle formation, and potentially regulate spindle size.

3.2.7 Conserved residues within the predicted CTD TOG domain are required to localize Msps during mitosis

To determine if the resides which are required to localize Msps to MT plus ends in interphase cells are also required for localization during mitosis (Fig. 3.7). GFP tagged Msps FL K1725E, Msps FL K1761E/K1765E and Msps FL R1808E/K1811E/T1812A were transfected into *Drosophila* S2 cells and the localization was observed during mitosis. As observed for cells in interphase, charge reversal at position 1725 did not alter Msps localization during mitosis (Fig. 3.7A). However, Msps FL K1761E/K1765E and R18008E/K1811E/T1812A showed decrease localization to MT plus ends at the kinetochore and R1808E/K1811E/T1812A seems to have less enrichment on kinetochore fibers (Fig. 3.7A).

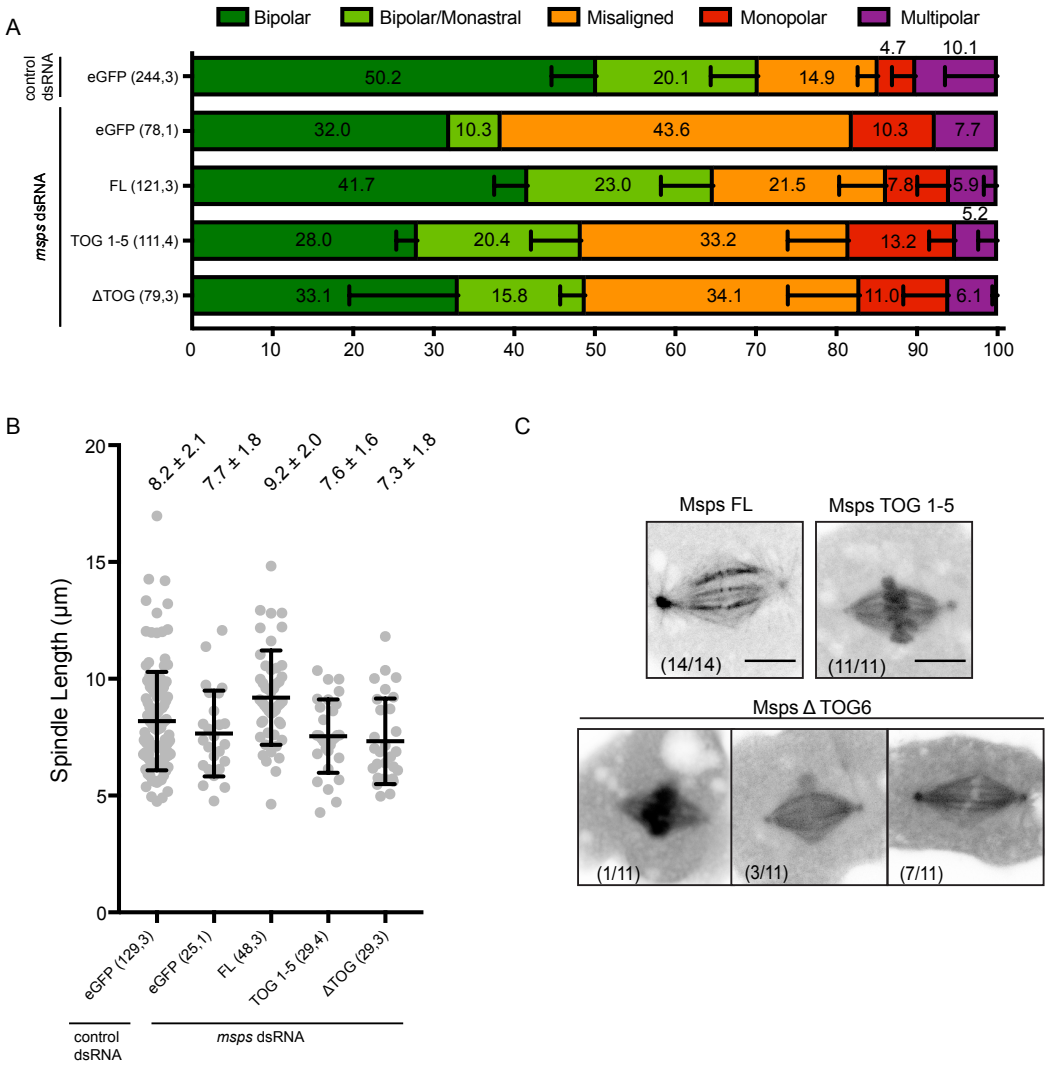

Figure 3.6. TOG6 is required to properly localize Msps during mitosis, establish the bipolar spindle and regulate spindle length. (A) Quantification of mitotic phenotypes for Msps depletion and rescue experiments. Depleting Msps leads to a decrease in the number of bipolar and bipolar/monastral compared to control cells and an increase in the number of misaligned and monoploar phenotypes. Transfection of FL Msps rescues mitotic phenotypic defect. Deleting the CTD or Msps TOG6 result in a dramatic decrease in the ability of these constructs to rescue mitotic spindle phenotypes. (B) Msps mitotic spindle pole-to-pole distance in Msps-depleted cells and cells transfected with Msps FL, Msps TOG 1-5 and Msps Δ TOG6. (C) Localization of GFP tagged Msps constructs during mitosis; FL Msps localizes to the centrosome, MT plus ends in the spindle and at the kinetochore, and is enriched on kinetochore fibers. Depletion of the CTD of Msps or TOG6 leads to miss-localization of Msps during mitosis.

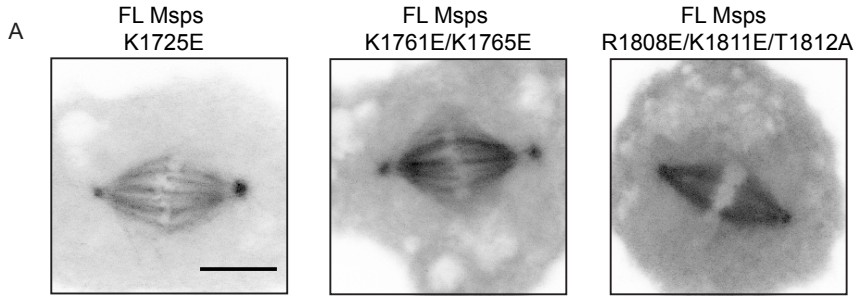

Figure 3.7. Conserved residues within the predicted CTD TOG domain are required to localize Msps during mitosis. FL Msps K1725E properly localizes to bipolar mitotic spindles. Msps FL K1761E/K1765E and Msps FL R1808E/K1811E/T1812A do not properly localize to bipolar mitotic spindles.

3.2.8 Conserved residues within TOG6 are required to robustly interact with Sentin in a knocksideways assay

XMAP215 family members. Previous data showed that Sentin, an EB1 cargo protein, contributes to XMAP215 MT plus end accumulation. Data from Li et al. suggest that the N-terminus of Sentin (residues 1-590) interact with the CTD of Msps. We hypothesized that TOG6 could interact with the N-terminus of Sentin (Li et al., 2011). To further test if these regions in fact interact we turned to a knocksideways assay. In this assay one protein of interest is targeted the mitochondrial membrane via fusion to TOM20R. The other protein will either remain in the cytoplasm if the two proteins do not interact or be 'knocked sideways' and co-localize with the TOM20R-fusion protein on the mitochondria. To establish if Sentin binds to TOG6 we used this assay. An N-terminal piece of Sentin was fused to RFP-TOM20, Mito-RFP-Sentin 1-237. This construct was co transfected with Msps TOG6 GFP. Co-localization of Msps TOG6 on the mitochondria with the Mito-RFP-Sentin 1-237 was observed, localization which was not observed when TOG6 was transfected alone (Fig. 3.8A). This mito-RFP-Sentin 1-237 construct was used to probe the effect of mutations within the TOG6 domain on the

Msps:Sentin interaction. Mito-RFP-Sentin 1-237 was co-transfected with GFP tagged Msps FL, Msps K1725E, Msps K1761E/K1765E or Msps R1808E/K1811E/T1812A (representative images Fig. 8B). Cells were then scored for the level of co-localization between the Mito-Sentin and Msps (Fig. 3.8C). Based on the knocksideways assay, Msps FL co-localizes with Mito-RFP-Sentin 1-237 strongly (100% of cells). Msps K1725E shows a decreased tendency to co-localize with Mito-RFP-Sentin 1-237 with 40% of cells having cytoplasmic, localization of Msps K1725E. Msps FL K1761E/K1765E co-localizes with Sentin 1-237 very weakly 87% of cells are cytoplasmic Msps FL R1808E/K1811E/T1812A shows a decreased tendency to co-localize with Mito-RFP-Sentin 1-237 with 30% cytoplasmic (Fig. 3.8C). These data indicate that Msps residues 1725, 1808/1811/1812 are moderately required for proper interaction between Msps and Sentin 1-237 while residues 1761/1765 are essential for a robust interaction between Msps and Sentin.

To further investigate the interaction between Msps and Sentin. GFP tagged Msps constructs containing single point mutations of 1761, 1765, 1808, 1811 and 1812 were generated in FL Msps. Individually, Msps FL K1761E and Msps FL K1765E both weekly co-localize with Sentin 1-237. These data indicate that the Msps residues 1761 and 1765 are both important for robust interaction between Msps and Sentin 1-237 (Fig. S3.3). Interestingly, Msps R1808E and Msps K1811E both very weakly co-localize with Sentin 1-237 while Msps T1812A co-localizes with Sentin 1-237 more strongly than Msps R1808E and Msps K1811E (Fig. S3.3).

3.2.9 Sentin 1-36 is the minimal region of Sentin that interacts with Msps TOG6 in a knocksideways assay

To determine the specific region of Sentin that interacts with Msps TOG6, further

knocksideways assays were conducted. Smaller truncated constructs of the N-terminus of Sentin were generated based on conservation across 8 insect species and tested for their ability to knock Msps TOG6 sideways (Fig. 9A). Mito-RFP-Sentin 49-237, and Sentin 37-237 were not able to knock showed no co-localization with Msps TOG6 sideways to the mitochondria. However, Sentin 1-159, Sentin 1-49, and Sentin 1-36 strongly co-localized Msps TOG6 to the mitochondria. Therefore, the very N-terminal region of Sentin is responsible for interacting with Msps TOG6. The shortest Sentin construct that co-localized with Msps TOG6 is Sentin 1-36. Constructs that were shorter than Sentin 1-36 (Sentin 1-19, Sentin 20-36, Sentin 1-14, and Sentin 15-36) did not co-localize with Msps TOG6 (Fig. 9A and Fig. S5).

Taken together these data show that Sentin 1-36 is the smallest construct of Sentin that can robustly knocksideways TOG6 and Msps residues 1761 and 1765 within TOG6 are necessary to robustly knocksideways with Sentin 1-237. Therefore, these data suggest that Msps residues 1761 and 1765 play a key role in engaging the N-terminal region of Sentin within the first 36 residues as schematized in Fig. 9B.

3.2.10 The CTD of Msps binds taxol stabilized MTs and promotes tubulin assembly into higher order structures in vitro

Msps has many MT binding surfaces along its length, both the N-terminal TOG domains as well as MT lattice binding regions found in the linker regions between the TOG domains (Currie et al, 2011). We wanted to investigate if the CTD could bind MTs. Furthermore, there is evidence from Trogden and Rogers that there is one MT lattice-binding region at the beginning of the CTD (Trogden and Rogers, 2015). To test the ability of Msps to bind MTs we preformeda MT co-sedimentation assay with the largest CTD constructs that we could purify that encompasses Msps resides 1596-2042, which

spans the beginning of TOG6 through the end of the protein. Msps 1596-2042 bound and co- sedimented with taxol stabilized MTs (Fig. 3.10A). To determine the apparent binding affinity of Msps 1596-2042 to taxol stabilized MTs by varying the tubulin concentration (2.5 μ M, 5 μ M, 10 μ M, and 15 μ m). We calculated the fraction of Msps 1596-2042 that bound and then fit a curve to the data and found the Kapp = 2.1 μ M (Fig. 3.10B). Since this region potentially contains a TOG domain we hypothesized that the CTD could potentiate tubulin–tubulin interactions and promote the assembly of MTs. To test this hypothesis we used a light scattering assay (Fig. 3.10C). Tubulin alone polymerized at 37°C after 500 seconds of lag time. When Msps 1596-2042 was incubated with tubulin the lag time was dramatically reduced (Fig. 3.10C). This suggests that the CTD domain of Msps could play an important role in promoting MT nucleation, or recognizing a specific structure of the polymerizing MT. In order to show how the CTD compares to other TOG domains of Msps, which have been well characterized in their ability to bind either free tubulin or MTs, we plotted the Msps CTD light scattering along side data of the five N-terminal TOG domains of Msps (the data from the N-terminal TOG domains are from Amy Byrnes and these data were published in Byrnes and Slep, 2017). It is interesting to note that the light scattering profile of the CTD is similar to TOG4 and TOG 5 – which have been suggested to play are role in promoting MT nucleation and TOG 5 has features that recognize the MT lattice (Byrnes and Slep, 2017). These data show that Msps 1596-2042 contains a region or regions that bind to taxol stabilized MT and could promote MT nucleation and polymerization.

3.3 Discussion

Subcellular and cell-cycle dependent regulation of MT dynamics is essential for

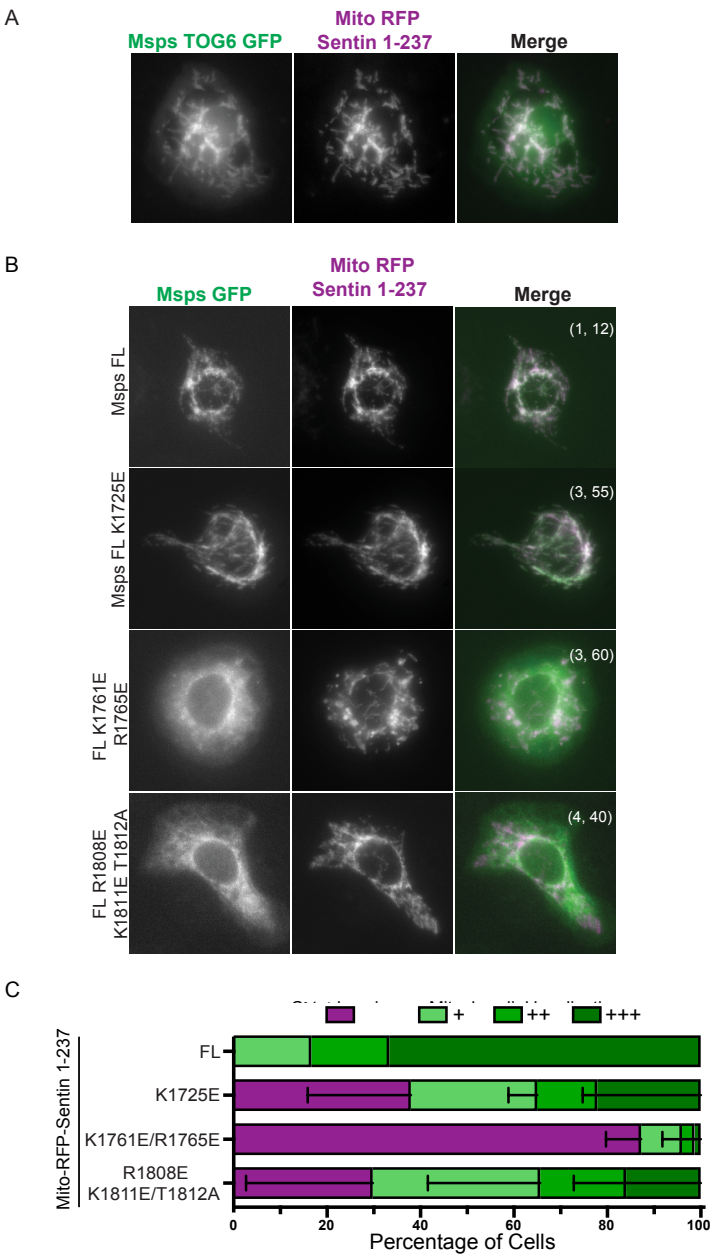

Figure 3.8. Conserved residues within TOG6 are required to robustly interact with Sentin in a knocksideways assay. (A) Msps TOG 6 knocksideways with Mito-RFP-Sentin 1-237. (B) Knocksideways assay with FL Msps mutations within TOG 6 with Mito-RFP-Sentin 1-237. Msps FL K1725E is knocked sideways. Msps FL K1761E/R1765E and Msps FL K1808E/K1811E/T1812A do not knocksideways with Mito-RFP-Sentin 1-237. Numbers in parenthesis indicate (number of experiments, number of cells analyzed). (C) Percentage of cells in the knocksideways assay that do not knocksideways, and thus show a cytoplasmic distribution (purple), and that do knocksideways (green). Level of localization of a given construct to the mitochondria is designated by weak (+, light green) to strong (+++, dark green).

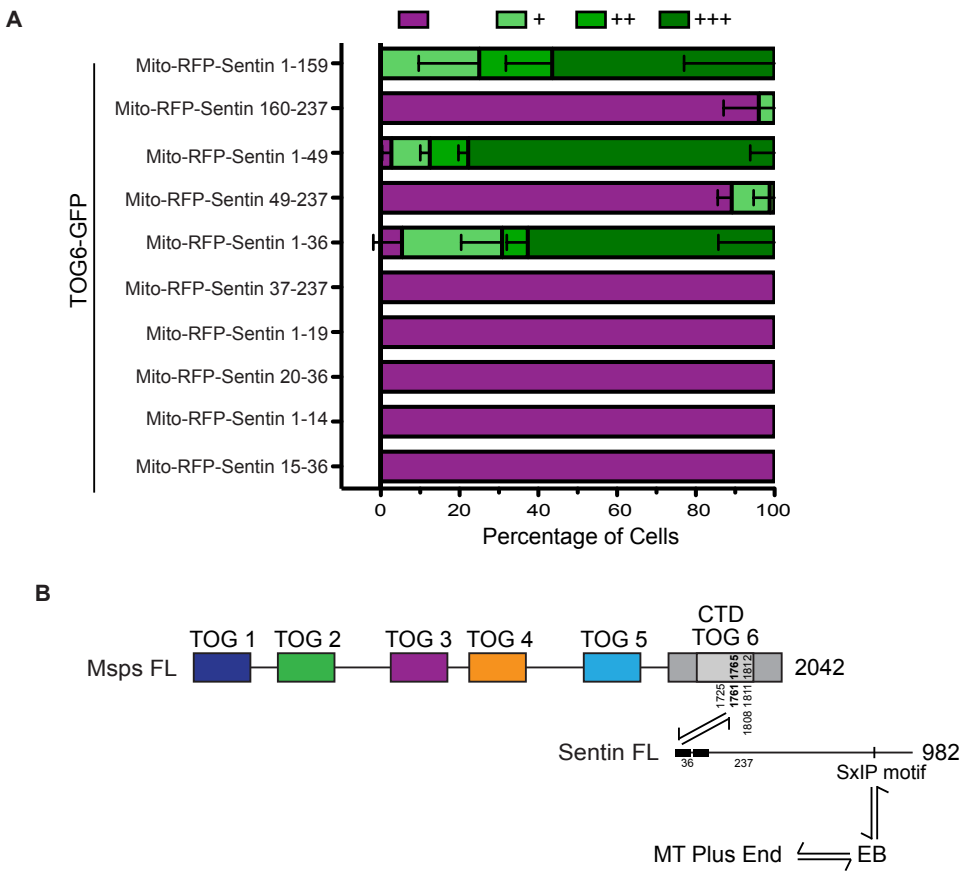

Figure 3.9. Sentin 1-36 is the minimal region of Sentin that interacts with Msps in a knocksideways assay. (A) Mito-RFP-Sentin truncation constructs co-transfected with Msps TOG6 were analyzed. The percentage of cells in the knocksideways assay that do not knocksideways, and thus show a cytoplasmic distribution (purple), and that do knocksideways (green). Level of localization of a given construct to the mitochondria is designated by weak (+, light green) to strong (+++, dark green). (C) Schematic to Msps:Sentin interaction proposed in this work.

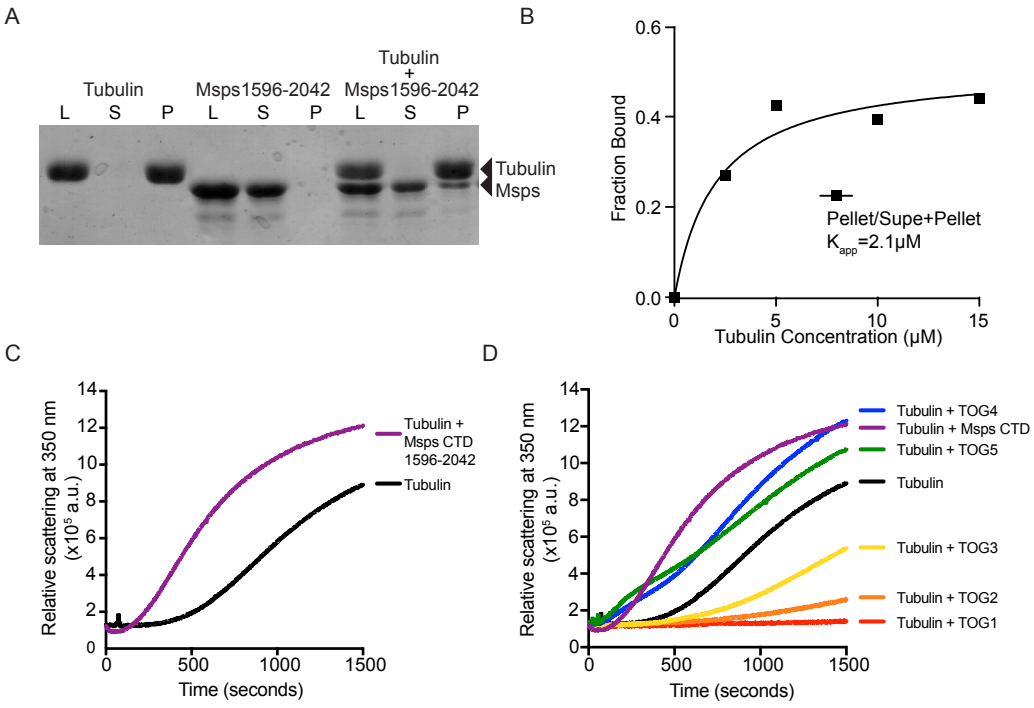

Figure 3.10. The CTD of Msps binds taxol stabilized MTs and promotes tubulin assembly into higher order structures in vitro. (A) Msps 1596-2042 co-sediments with taxol stabilized MTs. (B) Msps 1596-2042 bind to taxol stabilized MTs with an apparent affinity of 2.1 μM. (C) The CTD of Msps 1596-2042 promotes MT nucleation and polymerization in a light scattering assay. (D) TOG domains differentially promote MT nucleation and polymerization. TOGs 1, 2 and 3 sequester tubulin and lead to increased lag time, while TOGs 4, 5 and the CTD decrease lag time. (Data for TOGs 1-5 from Amy Byrnes – published in Byrnes and Slep, 2017).

cellular processes. Mechanisms encoded within MAPs allow for altered microtubule interactions in different places at different times. In the case of XMAP215 and CLASP family of proteins the respective, unique CTDs appear to be responsible for this regulation. The CTD plays an essential role in targeting and positing the Msps N-terminal TOG array at the MT plus and/or along the MT lattice so as to effect MT dynamics. While much work has been done to establish the structural and functional role of TOG arrays across the XMAP215, CLASP and Crescerin families of proteins, less is understood about the regions outside of the TOG array, such as the CTDs of the CLASP and XMAP215 family.

Here we focus on expanding our understanding the role of the XMAP215 family CTD. While previous studies showed that the C-terminal region is necessary to localize the FL molecule as well as to rescue MT growth velocities (Currie et al., 2011, Fox et al., 2014, Byrnes and Slep 2017) the specific role of the CTD remains unclear. We hypothesized that this region simply acts to target the N-terminal TOG domains to the plus end where they could potentate robust MT polymerization. However, our data using forced localization constructs to target the N-terminal TOG domains to the MT plus end, centrosomes, or both suggest that indeed the C-terminal domain provides additional mechanisms to regulate MT dynamics (Fig. 3.1C). The ability of the CTD to regulate MT polymerization could be through a variety of different mechanism which could include 1) more precise spatial positioning of the N-terminal TOG domains at the MT plus end allowing for the proper positioning of each TOG domain within the array 2) interactions with other proteins at the plus end which were abrogated with the fusion constructs 3) interactions with the MT lattice itself. These mechanisms could act to stabilize the MT plus end and/or promote polymerization.

Data from Byrnes and Slep show that domain swapping as well as permutation of the linker length between TOG domains fails to fully rescue MT polymerization dynamics (Byrnes and Slep, 2017, Byrnes et al., under revision). These data argue that precise nm spatial resolution of the position of the TOG domains is required; therefore the CTD could also be essential to regulate the precise position at the MT plus end.

The CTD has been shown to interact with a number of MAPs. To date the CTD has been shown to interact with CLASP, clathrin, Sentin/SLAIN, and TACC. These interactions haven been shown to play an essential role in regulating MT dynamics during interphase and mitosis. During mitosis these interactions ensure the proper density of MTs and spindle size is achieved through regulation of MT nucleation capacity at centrosomes, kinetochore fiber stability and kinetochore positioning (Lee et al., 2001; Bellanger and Gönczy, 2003; Le Bot et al., 2003; Srayko et al., 2003; Gergely et al., 2003; Li et al., 2011; van der Vaart et al., 2011; Hood et al., 2013; Mortuza et al., 2014; Trogden and Rogers 2015; Miller et al., 2016). Therefore, constructs lacking the CTD would fail to interact with these proteins and potentially others yet to be discovered and lead to aberrant MT regulation. While some of the binding interfaces have been mapped to the CTD, the specific regions, and domains of the CTD of XMAP215 that engage this multitude of biding partners are poorly understood (Li, et al, 2011; van der Vaart et al., 2011; Hood et al., 2013; Mortuza et al., 2014; Trogden and Rogers 2015). Furthermore, the structure of most of the CTD of the XMAP215 family is not known at high resolution. We hypothesized that there are key conserved domains within CTD of the XMAP215 family that could bind various binding partners. Through multiple sequence alignments and secondary structure predictions we identified three regions that appeared to be conserved and contain alpha helical content. The first region in the N-terminal

region of the CTD could contain 2-3 alpha helices, the central region appears to contain 12 alpha helices, and the most C-terminal region could contain 4 alpha helices. The central region potentially having 12 alpha helices stood out to us, as this composition was suggestion of a potential 6th TOG domain. Furthermore, recent work from the Royle and Bayliss lab showed that this region is indeed a TOG domain using nuclear magnetic resonance (Hood et al., 2013; Burgess et al., 2015, personal communication R. Bayliss). Our investigation of this domain elucidated that this domain, TOG6, is required to localize Msps to MT plus ends, rescue MT growth velocities, and prevent aberrant mitotic structure formation.

During interphase Sentin depletion dramatically decreases the amount of Msps on MT plus ends (Li et al., 2011; personal observation). Therefore, we hypothesized that Sentin could interact with the CTD TOG domain and recruit Msps to MT plus ends. Using a knocksideways assay we show that Msps TOG6 interacts with the N-terminus of Sentin. Furthermore, we show that residues 1761 and 1765 as well as residues 1808, 1811 and 1812 within TOG6 are required to localize Msps to MT plus ends, rescue MT dynamics. We show that residues 1761 and 1765 are required for interactions with Sentin, and residues 1808, 1811 and 1812 may be required to interact with Sentin using a knocksideways assay. Our data suggest a key interaction between Msps TOG6 and Sentin, which is required to properly regulate MT dynamics. We are currently working to understand if this interaction could play a role in regulating bipolar spindle formation. Mutation of 1761 and 1765 fails to properly localize Msps during mitosis and thus we hypothesize that this interaction is important for regulating proper bipolar spindle formation. Further experiments need to be conducted to determine if these residues and the Msps TOG6: Sentin interaction is required for proper spindle formation. Additionally, key experiments to biochemically show the direct

interaction between Msps TOG6 and Sentin and characterize this interaction are currently underway. Further in vivo experiments will further test the cellar importance of the Msps TOG6 interaction. Sentin-depleted S2 cells will be assayed for their ability to rescue MT growth velocities with various Sentin truncation constructs.

Although our data point to the potential role of the TOG6:Sentin interaction being required for mitotic spindle regulation and the data from other groups highlight the importance of the interaction of the XMAP215 CTD with TACC and clathrin during mitosis, it is interesting to note that recent data from the Biggins lab showed that Stu2, the yeast XMAP215 homologue, can directly interact with Ndc80 during mitosis and regulate MT dynamics in a tension-dependent fashion (Miller et al., 2015). The structure of the CTD of Stu2 is quite different from the proposed structural elements of the CTD of other XMAP215 family members. Stu2 contains a coiled-coil and dimerizes the specific binding partners and binding mechanisms would therefore differ compared to other members of the XMAP215 family (Wang et al., 1997; Haase et al., 2018). Furthermore, our data show that depolymerization of MTs during mitosis leads to loss of Msps localization at the kinetochore, establishing that Msps enrichment at the kinetochore is dependent on dynamic MTs. Further studies need to be done in order to understand the specific recruitment and enrichment of Msps at MT plus ends within the kinetochore.

While much focus has been directed toward the interaction of the CTD with other MAPs the CTD of Msps could interact with the MT lattice itself. Surprisingly, not only did we find that the CTD (residues 1596-2042) co-sediments with taxol stabilized MTs, but this region of the CTD appears to promote MT nucleation and polymerization to approximately the same degree as Msps TOG4 or Msps TOG5 (Fig.3.10, Byrnes and Slep, 2017). Key next

experiments will establish if TOG6 is responsible for this MT binding and promotion of polymerization or if this requires a region outside of TOG6 (residues 1853-2042).

Taken together these data point to two mechanisms that can be used by the CTD of Msps to recruit Msps to MT plus ends and regulate MT dynamics 1) through interaction with the EB1 binding +TIP Sentin and 2) through direct MT binding.

3.4 Methods and Materials

3.4.1 Molecular Biology

3.4.1.1 Bacterial expression constructs

Msps CTD domain fragments was generated using restriction enzyme cloning and were cloned into the pET-28bp vector, a bacterial expression vector with a PreScission protease-cleavable poly-histidine (poly-his) tag and Kanamycin (KAN) selection cassette. Msps 1596-1852 mutants were generated using Quikchange PCR with KOD extreme and specifically designed primers, which can introduce site-specific point mutations (K1725E; K1761E K1765E; R1808E K1811E T1812A).

3.4.1.2 *Drosophila* S2 expression constructs

Expression constructs for full-length EB1:EB1-tRFP and Msps-GFP were described previously (Rogers et al., 2002; Currie et al., 2011; Grode and Rogers, 2015; Trogden and Rogers, 2015, Fox et al., 2014). GFP tagged Msps CTD (1411-2016), and Msps TOG6 were generated using standard Gateway cloning into the pMT GFP Gateway destination vector.

Msps fusion constructs were generated through modification of pIZ/pMT Msps TOG 1-5 (1-1406) GFP construct from Fox et al., 2014. Msps TOG 1-5 DTACC was cloned by introduction an Nhe1 restriction enzyme site following the end of the 5th TOG, DTACC 9721308 (which includes the full TACC domain and the Aurora A phosphorylation site) was

amplified from FL DTACC and cloned into Msps TOG 1-5. Msps TOG 1-5 SKIP and Msps SKIP 1-5 SKIP LZ were generated using Quikchange PCR with KOD extreme to insert the desired base pairs to generate the desired sequence. Msps TOG 1-5 PACT was generated using a previously modified Gateway vector, which contained the PACT domain after the Gateway cassette (Rusan Lab). An LR reaction was preformedusing pENTR Msps 1-5 into the pMTGWPACTGFP vector.

3.4.1.3 Generation of Msps TOG6 FL point mutations

Msps K1725E, Msps K1761E/K1765E and Msps K1808E/K1811E/T1812A mutations were generated in pIZ/pMT Msps FL eGFP using Quickchange PCR with KOD extreme and specifically designed primers to introduce site-specific point mutations (K1761E K1765E; K1761E; K1765E; R1808E K1811E T1812A; R1808E; K1811E; T1812A).

3.4.1.4 Cloning of Sentin Constructs

An original Mito-RFP-Sentin 1-397 was generated via Gateway cloning by cloning Sentin 1-397 into the pENTR backbone and then preforming an LR reaction to shuttle Sentin constructs were generated using Quickchange PCR with KOD extreme and specifically designed primers to remove base pairs to make smaller Mito-RFP-Sentin constructs (Mito Sentin 1-237, Mito Sentin 1-159, Mito Sentin 160-237, Mito Sentin 1-49, Mito Sentin 49-237, Mito Sentin 1-36, Mito Sentin 37-237, Mito Sentin 1-19, Mito Sentin 20-36, Mito Sentin 1-14, and Mito Sentin 15-36).

3.4.2 *Drosophila* S2 cell culture and dsRNA generation

3.4.2.1 *Drosophila* S2 cell culture

Drosophila melanogaster S2 cells were cultured as described previously (Rogers and Rogers, 2008). In brief, cells were maintained in a SF900 media containing 1X anti-anti

at 40-90% confluence. For knock down experiments, ¼ million cells were seeded into a well of a 12 well plate on Day 0. For five days the cells were treated with 4 µL of Msps 3'UTR dsRNA of 800 base pairs and 4 µL of Msps 5'UTR dsRNA of 375 base pairs or 4 µL of scrambled control dsRNA. dsRNA was generated using a previously published (Slep and Byrnes, 2017) and described below. On Day 3, cells were transfected with the desired DNA. The 100 µl transfection reaction contained 750 ng of desired Msps-eGFP construct and 500 ng of EB1-tRFP, 3 µL of the transfection reagent, Fugene HD, and the rest of sterile water. On Day 4 the expression of the transfected DNA in cells was induced with copper sulfate at a final concentration of 200 µM. On Day 5 the cells were seeded on Concanavalin A (Con A) coated plates for 2 hours for either live-cell imaging or immunofluorescence experiments.

3.4.2.2 Double stranded RNA production

Double stranded RNA (dsRNA) was produced in order to eliminate endogenous Msps from *Drosophila* S2 cells. The knock down design utilized a 3' UTR dsRNA (Msps 3' 800) and a 5' UTR dsRNA (Msps 5' 375) introduced to *Drosophila* S2 cells in tandem. Scrambled dsRNA was generated and introduced into *Drosophila* S2 cells as a control. The original Msps and scrambled DNA, from which the dsRNA was created, were amplified from pUC19 vectors containing the desired DNA and PCR purified. The purified DNA was used to generate dsRNA via a reaction performed with 50ng DNA, RNA nucleotides (25mM rATP, rCTP, rGTP, rUTP), T7 RNA polymerase (1mg/mL), Ribolock, pyrophosphates and IVT 5X Buffer (200mM Tris-HCL (pH 7.9), 30mM $MgCl_2$, 10mM spermidine, 50mM NaCl). The reaction mixture was kept at 37°C to allow for dsRNA production. Reactions were then treated with RNAase free DNase for 1 hour at 37°C and then stored at -20°C.

3.4.3 Cell Fixation and Immunohistochemistry and Fixed Cell Imaging

3.4.3.1 Knocksideways assay

Dropsophila melanogaster S2 cells were seeded onto 0.5 mg/mL Con-A glass-bottom dishes 2 hours before fixation in Schneider's medium supplemented with 10% fetal bovine serum and 1x antibiotic/antimycotic (Invitrogen). For MeOH fixation, cells were rinsed with 1x PBS, 1x with ice cold MeOH, then fresh MeOH was added and cells were placed at -20°C for 8 min. The fixed cells were rinsed 3x with 1x PBS. All cells were imaged at room temperature with a Nikon Apo DIC 100X oil/-1.45-NA objective on an Eclipse Ti-E microscope (Nikon), driven by NIS Elements software (Nikon). Images were acquired with a CoolSNAP HQ cooled charge-coupled device camera (Roper Technologies). 9 Z-steps were acquired at 0.3 μm intervals.

3.4.3.2 Mitotic cell analysis

Cells were seeded onto Con-A coated with fresh Schneider's Media and allowed as detailed above and allowed to sit for 2 hours. Cells were fixed with MeoH as detailed above. Methanol was removed and cells were washes with PBS-T (1X PBS supplemented with 0.2% Triton X-100). Cells were blocked overnight with PBS-T with 2% BSA. Primary antibodies were added for 1 hour (see below for details). Anti-Asterless antibody addition was performed separately to prevent cross-reaction with antibodies. Cells were then washed 3 times with PBS-T and secondary antibodies and DAPI were added for 45 minutes. Cells were washed 3 times with PBS-T and left at 4° C with 1 mL of PBS prior to imaging. Primary antibodies used in this study were: anti-GFP (Living Colors), 1:1000; anti-tubulin (DM1 α; Sigma-Aldrich), 1:1000; anti-Asterless (Rusan Lab), 1:10,000. Secondary antibodies used in this study were: Cy2, Cy3, Cy5 (Jackson ImmunoResearch Laboratories), 1:500. Cells were

imaged at room temperature with a Nikon Apo DIC 100X oil/-1.45-NA objective on an Eclipse Ti-E microscope (Nikon), driven by NIS Elements software (Nikon). Images were acquired with a CoolSNAP HQ cooled charge-coupled device camera (Roper Technologies). Z-steps were acquired at 0.3 μm intervals. Images were used to determine mitotic spindle phenotypes as described in (Goshen 2006) and to determine spindle length, which was found by measuring the distance between centrosomes for cells classified as bipolar.

3.4.4 Live Cell microscopy

3.4.4.1 Total Internal Reflection Fluoresence (TIRF) microscopy

Treated *Drosophila* S2 cells were seeded on Con-A coated plates as detailed above for 2 hours prior to live-cell imaging Time-lapse movies were acquired with a 100x objective and numerical aperture 1.45 using the Nikon TIRF Microscope, captured with an Andor CCD camera. The Nikon TIRF was driven by Nikon Element Software. Images were acquired every second for 90-120 seconds.

3.4.5 Protein expression and purification

3.4.5.1 Protein expression

Msps TOG6 (1596-1852) both wildtype and mutants were transformed into BL21 DE3 (pLysS) *E. coli* cells and plated on KAN-resistance plates at 37°C overnight. The following day a 60 mL overnight growth for the wildtype protein and a 20 mL overnight growth for each of the mutants was started. The following day 10 ml of the starter culture was used to inoculate 6 L of selective LB for the native TOG6 and 2 L for mutant TOG6 the cultures were grown(1-50) at 37°C. until reaching OD at 600nm of 0.8 at which time protein expression was induced using 10 mM Isopropyl mopyranoside (IPTG).

3.4.5.2 Purification of native proteins

Ni^{2+}-NTA columns (Qiagen) were equilibrated with 100 mL of Buffer A (25 mM Tris pH 8.0, 10 mM imidazole, 300 mM NaCl, and 0.1% 2-Mercaptoethanol) then loaded with supernatant of from Msps 1596-1852 wildtype proteins onto the Ni^{2+}-NTA column (Qiagen). 100 mL of Buffer A was used to wash off any unbound protein from the column. The protein was eluted with 40 mL of Buffer B (25 mM Tris pH 8.0, 300 mM imidozole, 300 mM NaCl, and 0.1% 2-Mercaptoethanol). I cleaved the proteins using His-tagged PreScission protease while dialyzing the proteins for 36 hours into Buffer A. The cleaved protein was put back over the Ni^{2+}-NTA column and the flow through was collected and concentrated using a 10kDa molecular weight cut off concentrator (Millipore). To further purify wildtype Msps for crystallization trials a secondary purification was preformedusing an S column (INFO). The column was equilibrated with 100 mL of Buffer S (25 mM HEPES pH 7.0, 25 mM NaCl, 0.1 % 2-Mercaptoethanol). The concentrated protein was put onto the S column washed with buffer S and eluted with protein with HS buffer (25 mM HEPES pH 7.0, 1 M NaCl, 0.1 % 2-Mercaptoethanol) with a gradient of 0-100% HS buffer over 250 ml using the FPLC and collected 8ml fractions. Fraction contacting Msps TOG6 protein were pooled and concentrated using a 10 kDa molecular weight cut off concentrator and multiple rounds of centrifugation at 4000 rpm and 4°C while simultaneously exchanging the protein into storage buffer (100 mM NaCl, 25 mM HEPES, 0.1 % 2-Mercaptoethanol, pH 8.0). The protein was flash frozen and stored at -80°C.

3.4.5.3 Protein Purification of Msps 1596-1852 Mutants

To purify Msps TOG6 mutants the same primary Ni^{2+}-NTA purification was as detailed above. Mutant proteins (K1761E K1765E; R1808E K1811E T1812A) were then dialyzed into MES buffer pH 6 (25 mM NaCl, and 25 mM MES, 0.1 % 2-Mercaptoethanol)

for 36 hours after adding PreScission Protease to cleave the His-tag. I dialyzed K1725E the mutant into buffer A (pH 7.0). Meanwhile, I added PreScission protease and allowed it to cleave the His-tag for 36 hours. The mutant proteins were then put back over the Ni^{2+}-NTA column a second time to separate the cleaved protein from the uncleaved protein and PreScission protease. I utilized a 10kDa molecular weight cut off concentrator to concentrate each mutated protein. Mutant proteins were flash frozen and stored at -80 ℃.

3.4.6 Biochemical experiments

3.4.6.1 Circular dichroism

In a 1-mm-pathlength cuvette, Msps CTD constructs (1596-2042 and 1596-1852) and Msps 1596-1852 (K1761E K1765E; R1808E K1811E T1812A) were diluted to 0.10 mg/ml in CD buffer (10 mM sodium phosphate, pH 7.5, and 50 mM sodium fluoride). Spectra were acquired at 20°C from 260–185 nm with a step size of 0.5 nm every 1.25 s using a Chirascan-plus CD spectrometer (Applied Photophysics). Thermal melting data were obtained by monitoring CD signal at 208 and 222 nm while heating samples from 20°C to 94°C in a step size of 1°C. A CD buffer spectrum was subtracted from each domain spectrum, and the second derivative was taken for each melt curve to determine inflection points. All CD spectra were smoothed using Chirascan-plus software before analysis. CD data were completed on two separate experimental days with representative traces shown.

3.4.6.2 MT co-sedimenation

MT co-sedimentation experiments were performed with taxol-stabilized MTs. In brief, tubulin (20 μM final concentration) was diluted in BRB80 (80 mM Pipes, pH 6.8, 1 mM $MgCl_2$, and 1 mM EGTA) supplemented with 1 mM GTP and 1 mM DTT and allowed to sit on ice for 5 min. The solution was warmed to 37°C, and taxol was introduced stepwise

to generate long stable MT polymers. 1:100 dilutions of 20 μM, 200 μM, and 2 mM taxol were added with incubation times of 5, 5, and 15 min, respectively. Msps CTD (1596-2042) was cleared at 50,000 *g* at 4°C for 7 min and subsequently diluted to 50 μM in BRB80. Constructs were diluted to final concentrations of 50μM in BRB80, 10 μM taxol-stabilized MTs, 1 mM GTP, and 20 μM taxol. To determine the tubulin binding affinity constructs were diluted to final concentrations of 10μM in BRB80, 2.5 μM , 5 μM , 10 μM 0r 15 μM taxol-stabilized MTs, 1 mM GTP, and 20 μM taxol. All samples were and allowed to incubate for 20 min at RT. Reactions were layered on top of a glycerol cushion (BRB80, 40% glycerol, 1 mM GTP, and 20 μM taxol) and centrifuged at 70,000 *g* for 30 min at 25°C. The pellets were resuspended in equal volumes of BRB80, and SDS-PAGE was used to visualize the protein. The resulting gels were scanned, and densitometry was performed to determine the relative intensity.

3.4.6.3 Dynamic light scattering

TOG6 was expressed and purified as described earlier, including His-tag removal. Tubulin polymerization was monitored using a SPEX Fluorolog-3 spectrofluorometer (Horiba Jobin Yvon) in high-voltage (950 V) T-format mode using excitation and detection wavelengths of 350 nm. Excitation and emission slits were set at 0.5 and 0.75 nm, respectively. Clarified tubulin samples (18 μM final concentration) were incubated for 10 min at 4°C alone or with TOG6 (2 μM final concentration) in MES/glycerol polymerization buffer (50 mM MES, pH 6.6, 3.4 M glycerol, 5 mM DTT, 1 mM EGTA, 5 mM $MgSO_4$, and 1 mM GTP) to enhance proper MT structure formation. The cuvette holder was maintained at 37°C, and samples were injected into a 4-mm-pathlength cuvette. Scattering was recorded for 1,500 s at 1-s intervals.

3.4.7 Statistical analyses

eGFP comet velocity data were analyzed using a two-way unpaired Student's *t* test (GraphPad Prism). * $p<0.05$, ** $p<0.005$, ***$p<0.0005$, **** $p<0.0001$.

3.5 Supporting Information

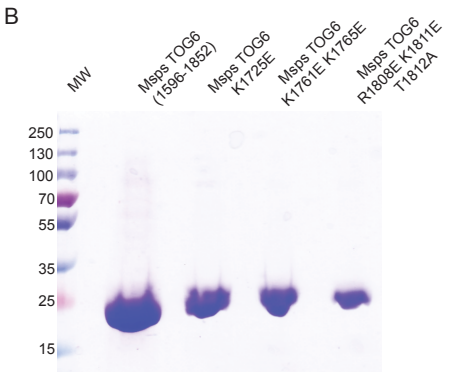

Supplemental Figure 3.1 Purified Msps TOG and Mutant constructs. (A) SDS gel of Msps TOG 6 (1596-2042), Msps TOG6 K1725E, Msps TOG6 K1761E/K1765E and Msps R1080E/K1811E /T1812A.

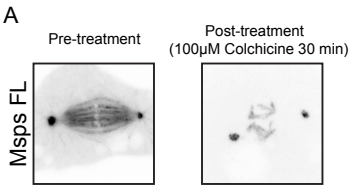

Supplemental Figure 3.2 Msps requires dynamic MTs to be enriched at the kinetochore. (A) Msps FL GFP is enriched at the kinetochore region. Post-treatment with colchicine Msps FL GFP remains at the centrosome and on k-fiber fragments that remain.

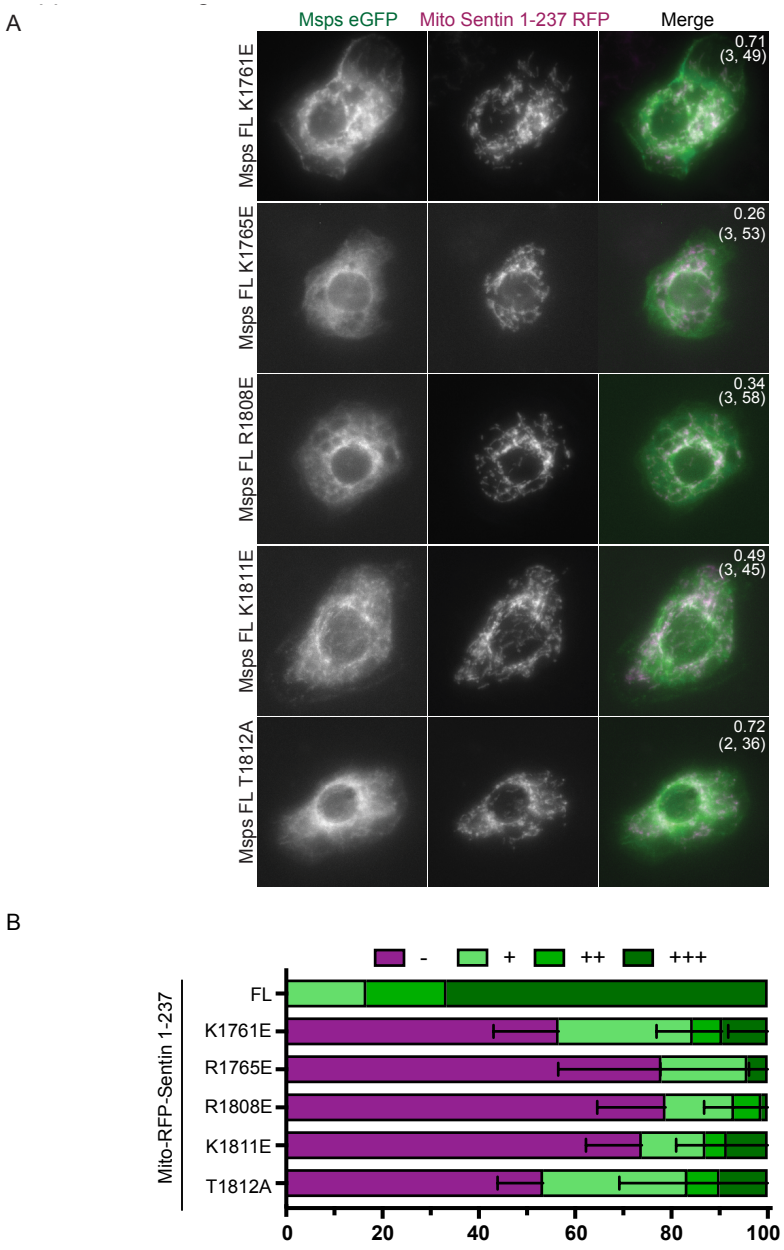

Supplemental Figure 3.3. Conserved residues within TOG6 are required to robustly interact with Sentin in a knocksideways assay. (A) Knocksideways assay with FL Msps mutations within TOG 6 with Mito-RFP-Sentin 1-237. All of the individually residues within TOG 6 show a decreased ability to knocksideways with Mito-RFP-Sentin 1-237.

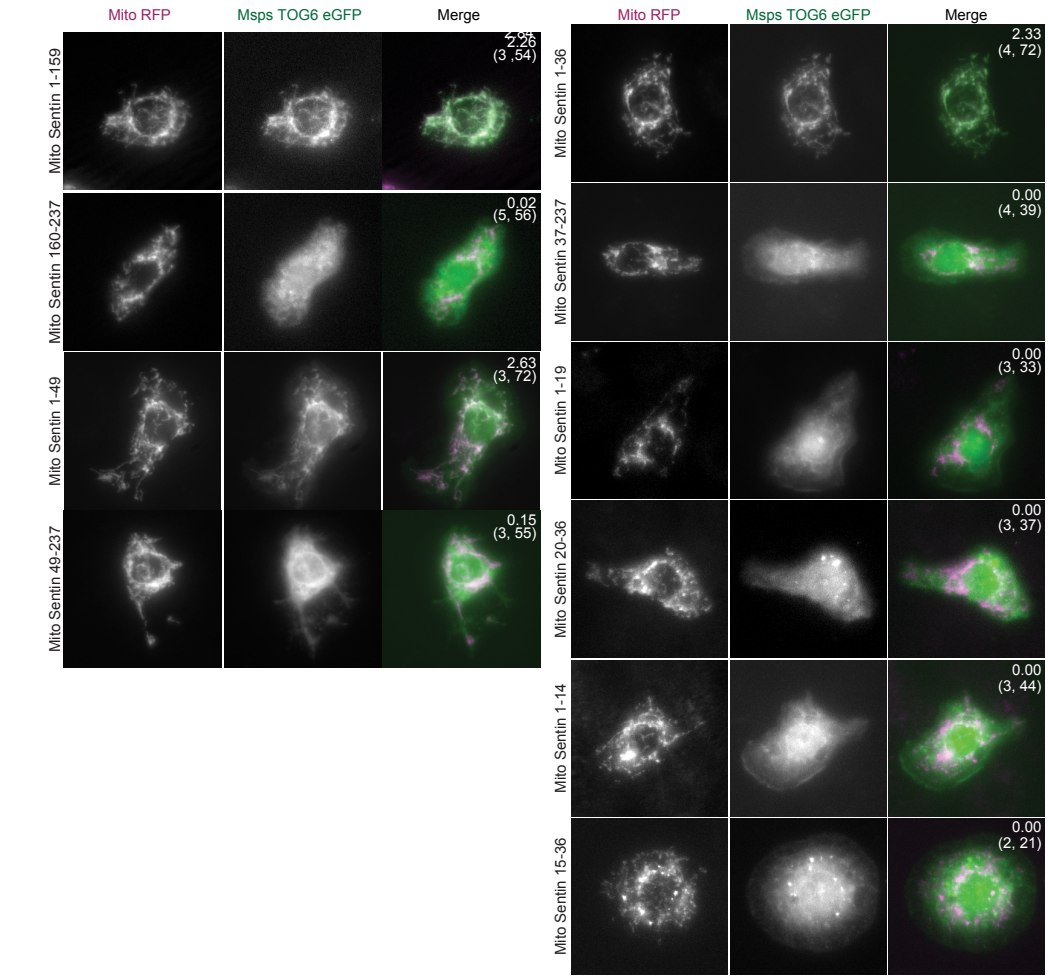

Supplemental Figure 3.4. Sentin 1-36 is the minimal region of Sentin that interacts with Msps in a knocksideways assay. (A) Representative images from analysis of Mito-RFP-Sentin fragments interacting with Msps TOG6 Fig. 9.

3.6 Acknowledgments

We thank the Rogers lab for Msps and EB1 cell expression constructs. We thank Karen Haase for comments regarding this chapter.

This work was supported by the National Institutes of Health grant RO1GM094415 and March of Dimes grant FY11-434 to K.C. Slep. R.C. Adikes was supported by National Institutes of Health grant F31-GM116476 for this work.

REFERENCES

Akhmanova A, Hoogenraad CC. Microtubule plus-end-tracking proteins: mechanisms and functions. Current opinion in cell biology. 2005;17(1):47-54. doi: 10.1016/j.ceb.2004.11.001. PubMed PMID: 15661518.

Akhmanova A, Steinmetz MO. Tracking the ends: a dynamic protein network controls the fate of microtubule tips. Nature reviews Molecular cell biology. 2008;9(4):309-22. doi: 10.1038/nrm2369. PubMed PMID: 18322465.

Al-Bassam J, van Breugel M, Harrison SC, Hyman A. Stu2p binds tubulin and undergoes an open-to-closed conformational change. The Journal of cell biology. 2006;172(7):1009-22. doi: 10.1083/jcb.200511010. PubMed PMID: 16567500; PubMed Central PMCID: PMC2063759.

Ayaz P, Ye X, Huddleston P, Brautigam CA, Rice LM. A TOG:alphabeta-tubulin complex structure reveals conformation-based mechanisms for a microtubule polymerase. Science. 2012;337(6096):857-60. doi: 10.1126/science.1221698. PubMed PMID: 22904013; PubMed Central PMCID: PMC3734851.

Bellanger JM, Gonczy P. TAC-1 and ZYG-9 form a complex that promotes microtubule assembly in C. elegans embryos. Current biology : CB. 2003;13(17):1488-98. PubMed PMID: 12956950.

Brittle AL, Ohkura H. Mini spindles, the XMAP215 homologue, suppresses pausing of interphase microtubules in Drosophila. The EMBO journal. 2005;24(7):1387-96. doi: 10.1038/sj.emboj.7600629. PubMed PMID: 15775959; PubMed Central PMCID: PMC1142550.

Brouhard GJ, Stear JH, Noetzel TL, Al-Bassam J, Kinoshita K, Harrison SC, et al. XMAP215 is a processive microtubule polymerase. Cell. 2008;132(1):79-88. doi: 10.1016/j.cell.2007.11.043. PubMed PMID: 18191222; PubMed Central PMCID: PMC2311386.

Burgess SG, Bayliss R, Pfuhl M. Solution NMR assignment of the cryptic sixth TOG domain of mini spindles. Biomolecular NMR assignments. 2015;9(2):411-3. doi: 10.1007/s12104-015-9620-4. PubMed PMID: 25971232.

Buster DW, Zhang D, Sharp DJ. Poleward tubulin flux in spindles: regulation and function in mitotic cells. Molecular biology of the cell. 2007;18(8):3094-104. doi: 10.1091/mbc.E06-11-0994. PubMed PMID: 17553931; PubMed Central PMCID: PMC1949370.

Cassimeris L, Becker B, Carney B. TOGp regulates microtubule assembly and density during mitosis and contributes to chromosome directional instability. Cell motility and the cytoskeleton. 2009;66(8):535-45. doi: 10.1002/cm.20359. PubMed PMID: 19373773.

Cassimeris L, Pryer NK, Salmon ED. Real-time observations of microtubule dynamic instability in living cells. The Journal of cell biology. 1988;107(6 Pt 1):2223-31. PubMed PMID: 3198684; PubMed Central PMCID: PMC2115680.

Charrasse S, Schroeder M, Gauthier-Rouviere C, Ango F, Cassimeris L, Gard DL, et al. The TOGp protein is a new human microtubule-associated protein homologous to the Xenopus XMAP215. Journal of cell science. 1998;111 (Pt 10):1371-83. PubMed PMID: 9570755.

Cullen CF, Deak P, Glover DM, Ohkura H. mini spindles: A gene encoding a conserved microtubule-associated protein required for the integrity of the mitotic spindle in Drosophila. The Journal of cell biology. 1999;146(5):1005-18. PubMed PMID: 10477755; PubMed Central PMCID: PMC2169485.

Currie JD, Stewman S, Schimizzi G, Slep KC, Ma A, Rogers SL. The microtubule lattice and plus-end association of Drosophila Mini spindles is spatially regulated to fine-tune microtubule dynamics. Molecular biology of the cell. 2011;22(22):4343-61. doi: 10.1091/mbc.E11-06-0520. PubMed PMID: 21965297; PubMed Central PMCID: PMC3216660.

Desai A, Mitchison TJ. Microtubule polymerization dynamics. Annual review of cell and developmental biology. 1997;13:83-117. doi: 10.1146/annurev.cellbio.13.1.83. PubMed PMID: 9442869.

Fox JC, Howard AE, Currie JD, Rogers SL, Slep KC. The XMAP215 family drives microtubule polymerization using a structurally diverse TOG array. Molecular biology of the cell. 2014;25(16):2375-92. doi: 10.1091/mbc.E13-08-0501. PubMed PMID: 24966168; PubMed Central PMCID: PMC4142611.

Gard DL, Kirschner MW. A microtubule-associated protein from Xenopus eggs that specifically promotes assembly at the plus-end. The Journal of cell biology. 1987;105(5):2203-15. PubMed PMID: 2890645; PubMed Central PMCID: PMC2114854.

Gergely F, Draviam VM, Raff JW. The ch-TOG/XMAP215 protein is essential for spindle pole organization in human somatic cells. Genes & development. 2003;17(3):336-41. doi: 10.1101/gad.245603. PubMed PMID: 12569123; PubMed Central PMCID: PMC195983.

Goshima G, Wollman R, Stuurman N, Scholey JM, Vale RD. Length control of the metaphase spindle. Current biology : CB. 2005;15(22):1979-88. doi: 10.1016/j.cub.2005.09.054. PubMed PMID: 16303556.

Grode KD, Rogers SL. The non-catalytic domains of Drosophila katanin regulate its abundance and microtubule-disassembly activity. PloS one. 2015;10(4):e0123912. doi: 10.1371/journal.pone.0123912. PubMed PMID: 25886649; PubMed Central PMCID: PMC4401518.

Haase KP, Fox JC, Byrnes AE, Adikes RC, Speed SK, Haase J, et al. Stu2 uses a 15-nm parallel coiled coil for kinetochore localization and concomitant regulation of the mitotic spindle. Molecular biology of the cell. 2018;29(3):285-94. doi: 10.1091/mbc.E17-01-0057. PubMed PMID: 29187574.

Hood FE, Williams SJ, Burgess SG, Richards MW, Roth D, Straube A, et al. Coordination of adjacent domains mediates TACC3-ch-TOG-clathrin assembly and mitotic spindle binding. The Journal of cell biology. 2013;202(3):463-78. doi: 10.1083/jcb.201211127. PubMed PMID: 23918938; PubMed Central PMCID: PMC3734082.

Howard J, Hyman AA. Dynamics and mechanics of the microtubule plus end. Nature. 2003;422(6933):753-8. doi: 10.1038/nature01600. PubMed PMID: 12700769.

Kawamura E, Wasteneys GO. MOR1, the Arabidopsis thaliana homologue of Xenopus MAP215, promotes rapid growth and shrinkage, and suppresses the pausing of microtubules in vivo. Journal of cell science. 2008;121(Pt 24):4114-23. doi: 10.1242/jcs.039065. PubMed PMID: 19033380.

Komarova YA, Akhmanova AS, Kojima S, Galjart N, Borisy GG. Cytoplasmic linker proteins promote microtubule rescue in vivo. The Journal of cell biology. 2002;159(4):589-99. doi: 10.1083/jcb.200208058. PubMed PMID: 12446741; PubMed Central PMCID: PMC2173097.

Kosco KA, Pearson CG, Maddox PS, Wang PJ, Adams IR, Salmon ED, et al. Control of microtubule dynamics by Stu2p is essential for spindle orientation and metaphase chromosome alignment in yeast. Molecular biology of the cell. 2001;12(9):2870-80. PubMed PMID: 11553724; PubMed Central PMCID: PMC59720.

Kronja I, Kruljac-Letunic A, Caudron-Herger M, Bieling P, Karsenti E. XMAP215-EB1 interaction is required for proper spindle assembly and chromosome segregation in Xenopus egg extract. Molecular biology of the cell. 2009;20(11):2684-96. doi: 10.1091/mbc.E08-10-1051. PubMed PMID: 19369422; PubMed Central PMCID: PMC2688548.

Lampert F, Hornung P, Westermann S. The Dam1 complex confers microtubule plus end-tracking activity to the Ndc80 kinetochore complex. The Journal of cell biology. 2010;189(4):641-9. doi: 10.1083/jcb.200912021. PubMed PMID: 20479465; PubMed Central PMCID: PMC2872915.

Li W, Miki T, Watanabe T, Kakeno M, Sugiyama I, Kaibuchi K, et al. EB1 promotes microtubule dynamics by recruiting Sentin in Drosophila cells. The Journal of cell biology. 2011;193(6):973-83. doi: 10.1083/jcb.201101108. PubMed PMID: 21646401; PubMed Central PMCID: PMC3115803.

Martinez-Campos M, Basto R, Baker J, Kernan M, Raff JW. The Drosophila pericentrin-like protein is essential for cilia/flagella function, but appears to be dispensable for mitosis. The

Journal of cell biology. 2004;165(5):673-83. doi: 10.1083/jcb.200402130. PubMed PMID: 15184400; PubMed Central PMCID: PMC2172389.

Matthews LR, Carter P, Thierry-Mieg D, Kemphues K. ZYG-9, a Caenorhabditis elegans protein required for microtubule organization and function, is a component of meiotic and mitotic spindle poles. The Journal of cell biology. 1998;141(5):1159-68. PubMed PMID: 9606208; PubMed Central PMCID: PMC2137183.

Miller MP, Asbury CL, Biggins S. A TOG Protein Confers Tension Sensitivity to Kinetochore-Microtubule Attachments. Cell. 2016;165(6):1428-39. doi: 10.1016/j.cell.2016.04.030. PubMed PMID: 27156448; PubMed Central PMCID: PMC4892958.

Mitchison T, Kirschner M. Dynamic instability of microtubule growth. Nature. 1984;312(5991):237-42. PubMed PMID: 6504138.

Mitchison T, Kirschner M. Microtubule assembly nucleated by isolated centrosomes. Nature. 1984;312(5991):232-7. PubMed PMID: 6504137.

Mortuza GB, Cavazza T, Garcia-Mayoral MF, Hermida D, Peset I, Pedrero JG, et al. XTACC3-XMAP215 association reveals an asymmetric interaction promoting microtubule elongation. Nature communications. 2014;5:5072. doi: 10.1038/ncomms6072. PubMed PMID: 25262927; PubMed Central PMCID: PMC4200520.

Rogers SL, Rogers GC, Sharp DJ, Vale RD. Drosophila EB1 is important for proper assembly, dynamics, and positioning of the mitotic spindle. The Journal of cell biology. 2002;158(5):873-84. doi: 10.1083/jcb.200202032. PubMed PMID: 12213835; PubMed Central PMCID: PMC2173155.

Schuyler SC, Pellman D. Microtubule "plus-end-tracking proteins": The end is just the beginning. Cell. 2001;105(4):421-4. PubMed PMID: 11371339.

Slep KC, Rogers SL, Elliott SL, Ohkura H, Kolodziej PA, Vale RD. Structural determinants for EB1-mediated recruitment of APC and spectraplakins to the microtubule plus end. The Journal of cell biology. 2005;168(4):587-98. doi: 10.1083/jcb.200410114. PubMed PMID: 15699215; PubMed Central PMCID: PMC2171753.

Slep KC, Vale RD. Structural basis of microtubule plus end tracking by XMAP215, CLIP-170, and EB1. Molecular cell. 2007;27(6):976-91. doi: 10.1016/j.molcel.2007.07.023. PubMed PMID: 17889670; PubMed Central PMCID: PMC2052927.

Srayko M, Quintin S, Schwager A, Hyman AA. Caenorhabditis elegans TAC-1 and ZYG-9 form a complex that is essential for long astral and spindle microtubules. Current biology : CB. 2003;13(17):1506-11. PubMed PMID: 12956952.

Steinmetz MO, Jelesarov I, Matousek WM, Honnappa S, Jahnke W, Missimer JH, et al. Molecular basis of coiled-coil formation. Proceedings of the National Academy of Sciences of the United States of America. 2007;104(17):7062-7. doi: 10.1073/pnas.0700321104. PubMed PMID: 17438295; PubMed Central PMCID: PMC1855353.

Tournebize R, Popov A, Kinoshita K, Ashford AJ, Rybina S, Pozniakovsky A, et al. Control of microtubule dynamics by the antagonistic activities of XMAP215 and XKCM1 in Xenopus egg extracts. Nature cell biology. 2000;2(1):13-9. doi: 10.1038/71330. PubMed PMID: 10620801.

Trogden KP, Rogers SL. TOG Proteins Are Spatially Regulated by Rac-GSK3beta to Control Interphase Microtubule Dynamics. PloS one. 2015;10(9):e0138966. doi: 10.1371/journal.pone.0138966. PubMed PMID: 26406596; PubMed Central PMCID: PMC4583408.

van der Vaart B, Franker MA, Kuijpers M, Hua S, Bouchet BP, Jiang K, et al. Microtubule plus-end tracking proteins SLAIN1/2 and ch-TOG promote axonal development. The Journal of neuroscience : the official journal of the Society for Neuroscience. 2012;32(42):14722-8. doi: 10.1523/JNEUROSCI.1240-12.2012. PubMed PMID: 23077057.

van der Vaart B, Manatschal C, Grigoriev I, Olieric V, Gouveia SM, Bjelic S, et al. SLAIN2 links microtubule plus end-tracking proteins and controls microtubule growth in interphase. The Journal of cell biology. 2011;193(6):1083-99. doi: 10.1083/jcb.201012179. PubMed PMID: 21646404; PubMed Central PMCID: PMC3115796.

Varga V, Helenius J, Tanaka K, Hyman AA, Tanaka TU, Howard J. Yeast kinesin-8 depolymerizes microtubules in a length-dependent manner. Nature cell biology. 2006;8(9):957-62. doi: 10.1038/ncb1462. PubMed PMID: 16906145.

Vasquez RJ, Gard DL, Cassimeris L. XMAP from Xenopus eggs promotes rapid plus end assembly of microtubules and rapid microtubule polymer turnover. The Journal of cell biology. 1994;127(4):985-93. PubMed PMID: 7962080; PubMed Central PMCID: PMC2200056.

Walker RA, O'Brien ET, Pryer NK, Soboeiro MF, Voter WA, Erickson HP, et al. Dynamic instability of individual microtubules analyzed by video light microscopy: rate constants and transition frequencies. The Journal of cell biology. 1988;107(4):1437-48. PubMed PMID: 3170635; PubMed Central PMCID: PMC2115242.

Wang PJ, Huffaker TC. Stu2p: A microtubule-binding protein that is an essential component of the yeast spindle pole body. The Journal of cell biology. 1997;139(5):1271-80. PubMed PMID: 9382872; PubMed Central PMCID: PMC2140218.

Widlund PO, Stear JH, Pozniakovsky A, Zanic M, Reber S, Brouhard GJ, et al. XMAP215 polymerase activity is built by combining multiple tubulin-binding TOG domains and a basic lattice-binding region. Proceedings of the National Academy of Sciences of the United States

of America. 2011;108(7):2741-6. doi: 10.1073/pnas.1016498108. PubMed PMID: 21282620; PubMed Central PMCID: PMC3041093.

CHAPTER 4: DISCUSSION AND FUTURE DIRECTIONS

4.1 How does spatial and temporal regulation affect cytoskeletal dynamics?

The highly dynamic nature of the actin and MT cytoskeleton is required for all basic cellular functions from cell migration to cell division. These networks must be remodeled constantly to perform a given cellular function, be it providing mechanical rigidity, sensing and responding to forces within and outside of the cell, or serving as force-generating machines. In addition to each network being independently reshaped over a cell's lifetime, the two networks must be properly integrated to ensure cellular outcomes such as proper cell migration or division. Extensive work has characterized the role of many regulators of the actin and MT cytoskeleton. Since the 1980s we have discovered and characterized hundreds of proteins that regulate actin and MT dynamics in vivo and in vitro. However, we still lack the finer resolution of the mechanistic role of these regulators in vivo (both at the cellular and organismal level). Additionally, we lack an understanding of how these regulators work in concert in vivo. These are technically and experimentally challenging question to probe. However, classical techniques paired with recent techniques and technologies allow us to begin to uncover these details. Spatiotemporal resolution down to the msec-nm time-space scale is just beginning to be uncovered using new techniques and technologies, including fast acting protein degradation, fast protein targeting (i.e. optogenetics) and nm spatial resolution (i.e. super resolution microscopy).

Here, we develop and employ methods to alter protein targeting a localization using a

novel optogenetic approach and classical structural/functional approaches. We developed and useded an optogenetic tool to gain insight into the msec/sec resolution time regime of MT-F-actin cross-linking. This allowed us to uncover key immediate down stream cellular events of cross-linking including decreased MT comet velocities on the sec time scale and an exclusion of MT from the cell periphery on the min-hr time scale. Additionally, using more classical structure/function based experiments, we were able to alter protein targeting using protein domains and through mutation of the protein sequence by just 1-3 amino acid. This enabled us to uncover that the XMAP215 family member Msps contains a very specific mechanism to allow for MT plus end targeting and thus proper function of the FL molecule. These results highlight the importance of precise protein positioning and interactions with binding partners to regulate cytoskeletal dynamics. Many questions remain to be addressed to fully understand the mechanisms underlying the spatiotemporal control of cytoskeletal dynamics. Some outstanding questions in regard to our studies are highlighted below.

4.2 Future Directions

4.2.1 Probing the subcellular resolution of MT dynamics

While our optogenetic studies allowed us to probe the temporal role of MT plus-end-F-actin cross-linking, the iLID/SspB system can also be used to spatially induce protein recruitment. Due to limitations of our current microscope system we were unable to probe the subcellar effect of cross-linking the MT and actin networks. We hypothesize that if cross-linking were induced in one region of the cell it would decrease MT comet velocities in that region and exclude MTs from that region. It is also possible that this could be propagated to other, non cross-linked cellular regions. These experiments would allow us to investigate regional effects of cross-linking and determine if there is any cross-talk to other

cellular regions. Furthermore, we were limited to studying the effects of cross-linking on non-motile cells. Expanding this work to cells which are able to migrate will allow us to determine if subcellar cross-linking and exclusion of MT can induce 1) lamellar protrusions and 2) induce migration.

Additionally, the tool we developed we induces MT plus-end-F-actin cross-linking. It will be interesting to investigate if there are different effects on MT dynamics and network architecture if the MT lattice ad F-actin are cross linked. Data from the Fuchs lab that show that the MT lattice spectraplakin (ACF7) interaction is regulated through GSK3β phosphorylation and this allows for directional migration (Wu et al., 2010). High levels GSK3β allow for a switch from MT lattice binding to plus-tip binding of spectraplakins. We can test the role of MT lattice-F-actin cross-linking by fusing the MT lattice binding GAR domain of Shot to iLID thus, targeting the optogenetic switch to the MT lattice.

4.2.2 Probing the spatiotemporal role of MT-F-Actin cross-linking in vivo

Probing the role of cross-linking of MT-F-Actin during development will be extremely exciting. Currently, we are working in collaboration with the Peifer lab to clone the SxIP-iLID system into *Drosophila* expression constructs and have these sent off for injection. Generation of *Drosophila* lines that contain SxIP-iLID and CH-CH-tRFP-SspB will allow use to probe the spatiotemporal role of cross-linking during key events in development, such as border cell migration and dorsal closure. Pervious studies have shown the optogenetic control of Rac (PA-Rac) can drive border cell migration (Wu et al., 2011). We hypothesize that activation of subcellular cross-linking could direct (or redirect) migration of the border cells. Another study showed that both the actin and MT binding domains of Shot are required to properly regulate dorsal cell closure and thus show the

importance of Shot engaging both networks and acting as a cross-linker in this process (Takács et al., 2017). We hypothesize that activation of cross-linking in the dorsal epithelial cells as they cell move, meet and zipper closed would alter MT and actin dynamics, could alter the lamella and filapodia protrusions in the cells and thus alter cellar dynamics of this process.

4.2.3 Recruitment of other proteins or protein domains to MT plus ends

Our work highlights the recruitment of one protein domain to the MT plus end. It will be exciting to see the spatiotemporal effect that other protein domains have on MT dynamics, network architecture, cell morphology and function.

4.2.4 Further probing the structure of the XMAP215 CTD

While cellular and biochemical data on the CTD are key to understanding the function of this domain, having a structure of the CTD would enable us to further understand and test the cellular function of this region. We are actively working to obtain crystals and structural data of the CTD and in particular TOG6 of Msps.

4.2.5 Biochemical and cellular analysis of the Msps:Sentin interaction

Our work on the CTD of the XMAP215 family member Msps, highlights potential role for the interaction of Msps CTD TOG6 with Sentin. We are currently investigating if this interaction is direct. Using purified of TOG6 and Sentin N-terminal constructs (1-36, 1-237) we will investigate the binding of these domains using size exclusion chromatography coupled with multi-angle light scattering (SEC-MALS) and isothermal titration calorimetry (ITC). To investigate the role of this interaction in cells, we will assay for the ability of Sentin fragments to rescue MT growth velocities. Previous data show that Sentin depletion decrease MT growth velocities and these can be rescue by expression of FL Sentin (Li et al.,

2011). We hypothesize that if the Sentin:Msps interaction is important for MT dynamics cells depleted of Sentin and transfected with a Sentin construct lacking the N-terminal region proposed to bind Msps will fail to rescue MT dynamics.

REFERENCES

Li W, Miki T, Watanabe T, Kakeno M, Sugiyama I, Kaibuchi K, et al. EB1 promotes microtubule dynamics by recruiting Sentin in Drosophila cells. J Cell Biol. 2011;193(6):973-83. doi: 10.1083/jcb.201101108. PubMed PMID: 21646401; PubMed Central PMCID: PMC3115803.

Takacs Z, Jankovics F, Vilmos P, Lenart P, Roper K, Erdelyi M. The spectraplakin Short stop is an essential microtubule regulator involved in epithelial closure in Drosophila. J Cell Sci. 2017;130(4):712-24. doi: 10.1242/jcs.193003. PubMed PMID: 28062848; PubMed Central PMCID: PMC5339884.

Wu X, Shen QT, Oristian DS, Lu CP, Zheng Q, Wang HW, et al. Skin stem cells orchestrate directional migration by regulating microtubule-ACF7 connections through GSK3beta. Cell. 2011;144(3):341-52. doi: 10.1016/j.cell.2010.12.033. PubMed PMID: 21295697; PubMed Central PMCID: PMC3050560.

Wu YI, Wang X, He L, Montell D, Hahn KM. Spatiotemporal control of small GTPases with light using the LOV domain. Methods Enzymol. 2011;497:393-407. doi: 10.1016/B978-0-12-385075-1.00016-0. PubMed PMID: 21601095; PubMed Central PMCID: PMC3407667.